Studying Duchenne Muscular Dystrophy and the Signaling Role of Dystrophin in *C. elegans*

by

Heather Hrach

A Dissertation Presented in Partial Fulfillment
of the Requirements for the Degree
Doctor of Philosophy

Approved April 2020 by the
Graduate Supervisory Committee:

Marco Mangone, Chair
Joshua LaBaer
Jason Newbern
Jeffery Rawls

ARIZONA STATE UNIVERSITY

May 2020

ABSTRACT

Duchenne muscular dystrophy (DMD) is a lethal, X-linked disease characterized by progressive muscle degeneration. The condition is driven by out-of-frame mutations in the dystrophin gene, and the absence of a functional dystrophin protein ultimately leads to instability of the sarcolemma, skeletal muscle necrosis, and atrophy. While the structural changes that occur in dystrophic muscle are well characterized, resulting changes in muscle-specific gene expression that take place in dystrophin's absence remain largely uncharacterized, as they are potentially obscured by the characteristic chronic inflammation in dystrophin deficient muscle.

The conservation of the dystrophin gene across metazoans suggests that both vertebrate and invertebrate model systems can provide valuable contributions to the understanding of DMD initiation and progression. Specifically, the invertebrate *C. elegans* possesses a dystrophin protein ortholog, *dys-1*, and a mild inflammatory response that is inactive in the muscle, allowing for the characterization of transcriptome rearrangements affecting disease progression independently of inflammation. Furthermore, *C. elegans* do not possess a satellite cell equivalent, meaning muscle regeneration does not occur. This makes *C. elegans* unique in that they allow for the study of dystrophin deficiencies without muscle regeneration that may obscure detection of subtle but consequential changes in gene expression.

I hypothesize that gaining a comprehensive definition of both the structural and signaling roles of dystrophin in *C. elegans* will improve the community's understanding of the progression of DMD as a whole. To address this hypothesis, I have performed a phylogenetic analysis on the conservation of each member of the dystrophin associated protein complex (DAPC) across 10 species, established an *in vivo* system to identify muscle-

specific changes in gene expression in the dystrophin-deficient *C. elegans,* and performed a functional analysis to test the biological significance of changes in gene expression identified in my sequencing results. The results from this study indicate that in *C. elegans*, dystrophin may have a signaling role early in development, and its absence may activate compensatory mechanisms that counteract disease progression. Furthermore, these findings allow for the identification of transcriptome changes that potentially serve as both independent drivers of disease and potential therapeutic targets for the treatment of DMD.

ACKNOWLEDGMENTS

To my P.I. and mentor Marco Mangone, thank you for all you have done for me. You have been consistently committed both to the success of my research and my success as an individual. You make sacrifices on a regular basis to support the students in your lab, and it has never gone unnoticed. I appreciate every RA, every high five over good data, and every hour spent helping me practice for my next talk. You have taught me confidence, discipline, and the importance of fundamental biology. You have taught me how to turn any mistake into a learning opportunity. You have taught me that if I think my experiment has enough controls, I should add one more. Most importantly, you have taught me what true passion looks like. I am leaving your lab with a new perspective on science and a set of skills I can be proud of because of your mentoring. Thank you.

To my advisor Dr. Josh LaBaer, I am so grateful for your support and advice. It's easy to get lost in the details of a PhD, and you have always reminded me to take a step back and look at the bigger picture. Your commitment to the greater purpose of my research has helped me recover from setbacks and stay focused on the end goal, even when it seemed out of reach. Your work ethic and dedication to your field inspire me to be and do better, and I will remember the example you have set for many years to come. I would not have made it to this point if you had not taken a personal interest in my success, and I am so thankful.

To my advisor Dr. Jason Newbern, thank you for your guidance and encouragement during this process. You have always been accessible, approachable, and committed to providing me with the tools I needed to drive my experiments forward. You have helped me to remain positive about experiments that seemed impossible. I have learned so much about trusting the process and remaining hopeful after difficult setbacks from having you as a

member of my committee. I have always felt that you prioritized my growth as a scientist and a professional, and I am so grateful to have had you as a member of my committee.

To my advisor Dr. Alan Rawls, I am truly grateful to have had your support. Your expertise in your field has not only proven essential in making my research successful, it has given me an incredible example of success that I can strive for in my own career. You have pushed me to do better as a scientist, and your support of my research has given me the confidence to believe that my work matters to the scientific community. I am also so grateful for the opportunity to work in your lab. The skills I gained in your lab have made me a more well-rounded scientist, and I would not be able to move forward to the next step of my career with confidence if you had not provided me with these fundamental skills.

The quality of my PhD has truly been determined by the friends I made along the way. To my friend, roommate, cheerleader, and support system Peach. I don't have the space or the words to properly thank you for being by my side. You are the best reason to come to lab every day, and this would have been impossible without you. Thank you. To my bonus advisor Dr. Jordan Yaron, I will never be able to thank you enough for your support. You set an incredible example for young scientists everywhere and I am lucky to have worked with you. To my peer and friend Kasuen Kotagama, I am so grateful for your friendship and training. Thank you for your patience, advice and positivity in the early years of my PhD. To my friend Gabby Richardson, you brought so much joy into my life when you joined our lab. I have never laughed harder than I did while sitting next to you, and I am so grateful for your friendship. Hannah Steber, I am so lucky to have met you. Working with you and being your friend has been a delight, and I'm thankful for the time we spent working together. Your courage and work ethic are inspiring. Shannon O'Brien and Christina Gallante, thank you for making the lab such a happy place to be. Watching both of you grow as people and

professionals has been a privilege; I am proud of you and grateful for your friendship. Alex Andre, thank you both for your friendship, and for the time sacrificed to train me. I am grateful to have had such a compassionate friend. To Ammar Tanveer, thank you for the years of friendship and humor- you have made school more fun. To the executive team at Biodesign: Kerri Robinson, Kathy Montalvo, and Dr. Stephen Munk, thank you for taking a genuine interest in my success. Working with you has been a privilege. To my mentor Dr. Jeanne Wilson Rawls, thank you for always being on my team. The students of MCB gain so much by having you advocating for us. To all of the friends I have made in MCB, SOLS, and Biodesign: Dr. Ching-Wen(Sandy) Hou, Dr. Meixuan Chen, Dr. Radwa Ewaisha, Alissa Lynch, Joanna Palade, Tanner Lamb, Cindy Xu, Kevin Klicki, Abigail Howell, Avina Naqvi, Jacqueline Carmona, Nolan Vale, Mark Knappenburger, Sarah Ellsworth, Dr. Justin Wolter, Dr. Stephen Blazie, Dr. Meryl Rodrigues, Sandhya Gangaraju, Dr. Femina Rauf, Eric Wilson, Anna Schorr, Wendi Simonson, Dominic Apodaca, Nicholas Jensen, Tony Pellum. Each of you have made my experience better and brighter, and I am thankful that we crossed paths. To every member of the Geissel and Hrach families who helped me get here: thank you. I would like to specifically thank my mother. I am certain that your resilience is hereditary, and it is the greatest gift you have given me.

Finally, I would like to thank my husband, Aaron. I will never be able to find adequate words to express my gratitude and love for you. I know this has not been easy, and you have made tremendous sacrifices so that I could pursue my degree. You have been an unwavering source of patience, positivity, and calmness. You have taken away all of the external stresses of life and given me the incredible privilege of focusing all of my efforts on my research. This would have been an impossible task without you by my side. I made it to the end because of you, and for you. Thank you, I love you.

TABLE OF CONTENTS

Page

LIST OF TABLES

LIST OF FIGURES

CHAPTER 1

INTRODUCTION

Duchenne muscular dystrophy: genetic basis, progression and treatment

Duchenne muscular dystrophy (DMD) is a lethal, X-linked recessive disease characterized by progressive muscle degeneration. The condition is driven by out of frame mutations in the dystrophin gene, which normally codes for a cytoplasmic protein that associates with the sarcolemma, or muscle cell membrane (Figure 1.1, Figure 1.2) [1]. The resulting loss of functional dystrophin protein leads to widespread instability of the sarcolemma, and ultimately to irreversible damage to the skeletal and cardiac muscles. DMD is the most commonly diagnosed form of muscular dystrophy, affecting approximately one in 5,000 live male births [2]. Because of the damage that occurs in cardiac and diaphragm muscles, among other symptoms, the life expectancy for those affected by the condition is on average less than 30 years of age [3].

Dystrophin's primary function was originally considered to be structural, as it forms a stabilizing connection between cytoskeletal F-actin and the transmembrane complex known as the dystrophin associated protein complex (DAPC) (Figure 1.2, Table 1.1)[4–6]. In its absence, the sarcolemma becomes susceptible to damage during contraction. The consequences of this are widespread, and include leakage of cytoplasmic contents and an influx of extracellular calcium to the muscle fibres [7]. In turn, dystrophin deficiency results in repeated cycles of necrosis, degeneration, and regeneration. Over time, this leads to fibrosis and increased deposits of fatty tissue in the muscle, ultimately contributing to impaired muscle function. Symptoms outside of skeletal muscle wasting and paralysis

include, but are not limited to, respiratory failure, pseudohypertrophy, and chronic inflammation of the muscle [7,8]. There are a number of shorter dystrophin isoforms that are expressed outside of the muscle, including a 71 kD dystrophin protein that is expressed in the brain (Figure 1.3)[9]. DMD patients that possess mutations within this isoform also exhibit non-progressive cognitive impairment [10–12]. This symptom is found in approximately one fifth of all DMD cases.

DMD patients are usually diagnosed before the age of five. The standard methods of diagnosis include testing for elevated serum creatine kinase, sequence analysis to test for mutation location and type, and evaluating a patient's performance in a number of standardized ambulatory tests [13–16]. There is typically apparent muscle weakness between the ages of two and seven, and loss of ambulation and dependence upon mobility devices by the time patients reach adolescence.

Patients with DMD can be distinguished from patients with other forms of dystrophinopathy by the nature of the mutation found in the dystrophin gene. Nearly all (90%) DMD patients share in the fact that they possess mutations that disrupt the open reading frame of the gene [17]. Interestingly, mutations are not evenly distributed throughout the dystrophin gene. Instead, dystrophin mutations are clustered within mutational hotspots, with the most common location being between exons 45 and 55 [18]. Within this hotspot, the most common mutation is a large deletion within exon 45 (Figure 1.1).

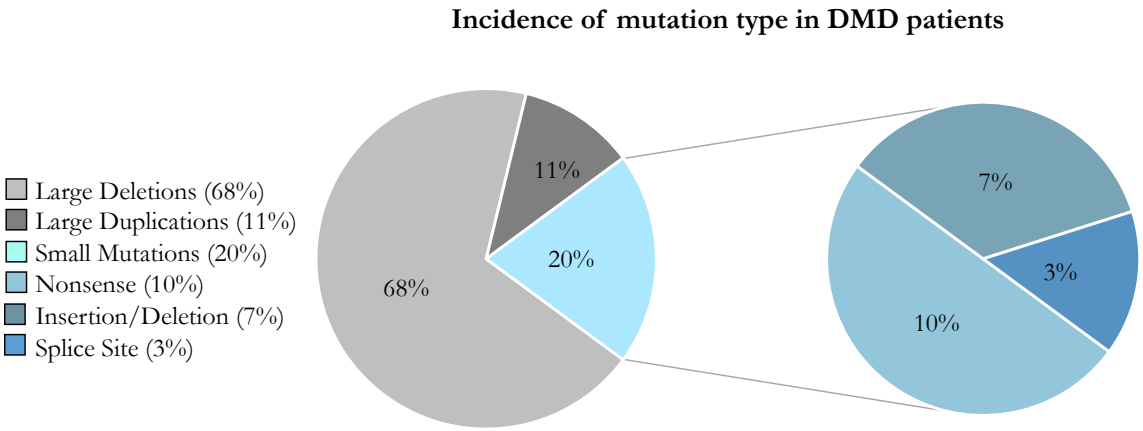

Figure 1.1: Summary of the average incidence of each mutation type recorded in patients with DMD. Large deletions that are one exon or greater account for an average of 68% of recorded mutations in DMD patients. Large duplications account for 11% of cases, and the remainder of mutations are small mutations that are either nonsense mutations (10%), small insertion or deletion (7%), and splice site mutations (3%).

Patients that possess mutations that retain the open reading frame of dystrophin present with symptoms that are usually mild in comparison to DMD, and are considered to have a different form of muscular dystrophy known as Becker muscular dystrophy (BMD)[19]. Patients with BMD present with a much wider range of variable symptoms [20,21]. Some patients remain ambulatory well into adulthood, and may even experience longevity like that of a person without any form of dystrophinopathy.

In both kinds of dystrophinopathy, the most commonly observed type of mutation is a deletion, specifically a large scale deletion of greater than 1 exon (Figure 1.1) [18,22]. When taking into account all mutations in the dystrophin gene that contribute to DMD, 68% of these mutations are deletions. Other types of mutations that have been recorded in patients with DMD include nonsense mutations, duplications, point mutations, and mutations in splice sites (Figure 1.1), [23]. The frame-shift mutations associated with DMD result in the presence of a premature stop codon that results in either the absence of a dystrophin protein or the production of a severely truncated version of dystrophin. In contrast, mutations that preserve the reading frame of the gene, which are found in BMD patients, allow for the complete translation of a dystrophin protein that is internally truncated, leading to a shortened, but still partially functional dystrophin protein. This hypomorphic version of the protein allows for some BMD patients to experience either mild or negligible symptoms when compared to DMD patients, as a stabilizing connection is still formed between cytoskeletal actin and the DAPC [6].

In the years following the discovery of DMD and its cause, significant progress has been made in our understanding of the condition on a genetic and molecular basis. Despite this, the method of treatment for DMD has not changed significantly in recent decades.

There is currently no readily available cure for the condition, and the goal for typical treatment of DMD is to slow down symptom progression and improve quality of life.

Treatment of dystrophic skeletal muscle typically includes the administration of glucorticoid steroids like prednisone and deflazacort as a means to temper the inflammatory response and slow down deterioration in muscles going through extensive cycles of necrosis and regeneration [24]. While this approach is relatively effective in managing symptoms and delaying muscle weakness, the long term use of glucorticoid steroids is associated with side effects that include atrophy and weakness of skeletal muscle, weight gain, osteoporosis, and high blood pressure [21,25,26]. The long term and short term use of glucorticoid steroids is still being optimized in DMD patients in order to balance the positive effects of these drugs with the side effects that can counterintuitively make symptoms in the muscle worse. In the second decade of life, treatment usually requires some form of ventilatory support as the function of the diaphragm becomes compromised [27]. Symptoms of cardiomyopathy are managed using ACE inhibitors and beta blockers [28,29].

Recent progress in genome editing techniques has resulted in the advent of a number of technologies that may one day be optimized to cure the condition. Perhaps the most potentially impactful of these is the discovery of the CRISPR/Cas9-mediated genome editing technology [30]. This system can be used to create targeted changes to a specific region of the genome, meaning it could potentially be used to correct frame disrupting mutations in the dystrophin gene. It has been shown in mouse models that CRISPR can be used to alleviate symptoms of DMD and restore wild type dystrophin expression in the skeletal muscle of mammalian muscle. Specifically, the AAV mediated delivery of CRISPR editing of the dystrophin gene in both *mdx* mice and in GRMD has results in long term

improvement of cardiac and skeletal muscle function [31–34]. Although this approach shows a great deal of promise, it has not yet been optimized for use in human patients, and may not be readily available to the general population in the near future. Alternative methods that have reached the clinical trial stage are exon skipping with antisense oligonucleotides, and the administration of a shorter version of dystrophin through an adenoviral vector (AAV) delivery system [35].

Because the majority of DMD patients possess mutations within the mutational hotspot between exons 45 and 55, this same group of patients could all benefit from a system that essentially skips this portion of the gene in order to restore the open reading frame. This is the principle behind drugs like eteplirson [36–38]. Eteplirson is a morpholino antisense oligomer that facilitates the skipping of exon 51, which is the most commonly mutated exon within this mutational hotspot. This results in a slightly shorter, but still functional form of the dystrophin protein that in theory alleviates the symptoms of DMD. This drug has been granted accelerated FDA approval following the release of further studies that definitively prove its efficacy and safety [39].

AAV-mediated delivery of minidystrophin has been designed with a similar goal in mind [40]. This system delivers a significantly shorter version of dystrophin that retains the N-terminal and C-terminal binding domains, but possesses a truncated rod region. This results in a partially functional version of the protein that would most likely result in patients with symptoms that reflect those seen in patients with BMD, as the dystrophin protein takes on a similar structure in patients with in-frame mutations within the rod region.

While all of these systems show great promise as potential cures for DMD, none have successfully made it through clinical trials to become readily available for all patients.

Furthermore, in their current state all three systems face their own unique set of limitations. The exon skipping therapy drug Eteplirson, while promising, does not offer a universal solution for all DMD patients. Approximately 40% of all DMD patients do not have mutations within exons 45 and 55, or a mutation within exon 51. This means that the drug treats only a subpopulation of DMD patients, and a universal and easily obtainable treatment is still necessary. Once administration of Eteplirson is optimized, the technology can certainly be adapted to cater to each unique mutation, but this requires a certain degree of personalized medicine that may not be attainable for all demographics. Until solutions for all mutations are available, this drug may not be the cure nearly half of all DMD patients are searching for.

The administration of mini-dystrophin using an AAV-mediated system has been met with a different obstacle. This system was first tested on a human patient in 2006, and the results were less than ideal [41,42]. The miniature form of dystrophin was found to be expressed at levels that were far too low to compensate for the widespread absence of functional dystrophin that is characteristic of DMD muscle. The current hypothesis used to explain supports the idea that the immune response was able to suppress the expression of mini-dystrophin [35]. Extensive research is currently being performed to temper the immune response towards mini-dystrophin protein in hopes of obtaining expression levels high enough to provide a convincing solution for DMD patients [43]

Significant work needs to be done in this field in order to move these treatment options forward. In the meantime, gaining a more comprehensive understanding of the disease is crucial to increase the number of known therapeutic targets and in turn increase the number of approaches that can be used to develop treatments for the condition.

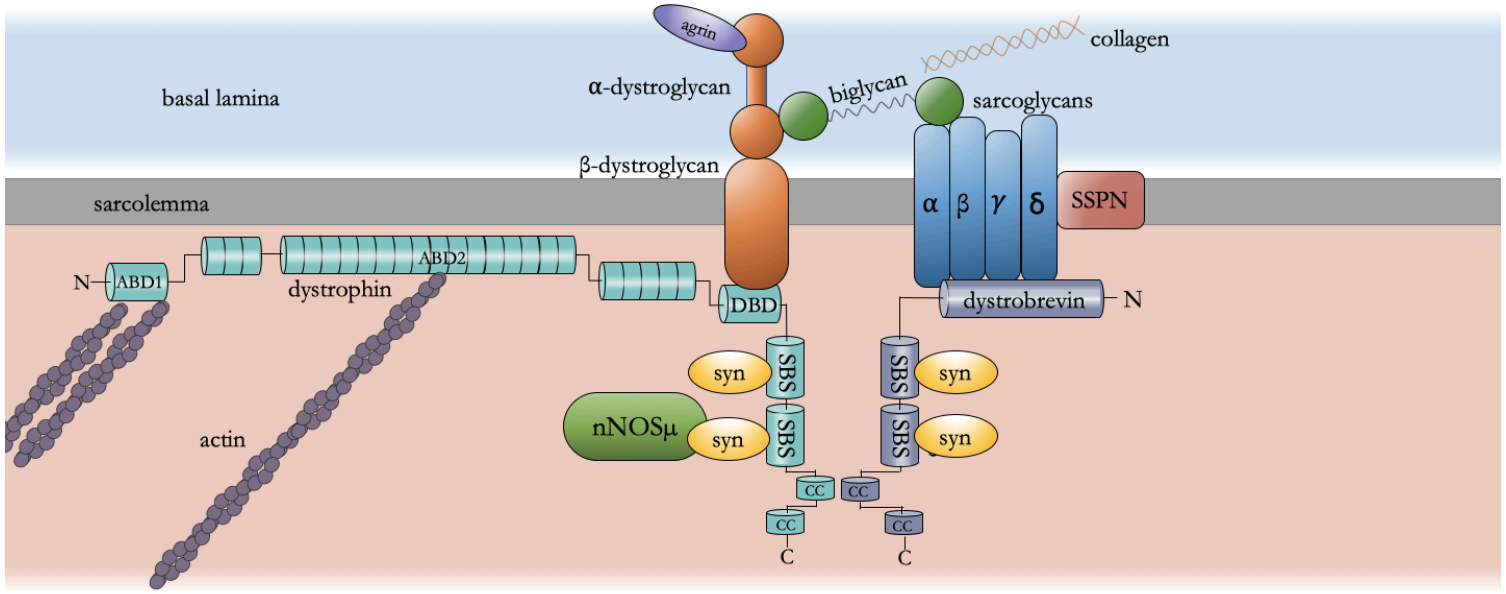

Figure 1.2: Dystrophin forms a stabilizing connection with the sarcolemma. Dystrophin binds to cytoskeletal actin through ABD1, found in the N-terminal region of the gene encoded for by exons 1-7, and ABD2 within the rod region of the gene within spectrin repeats 11-15. It binds to the dystrophin associated protein complex through its interaction with ß-dystroglycan through the C-terminal cysteine rich scaffolding region, thus stabilizing the cell membrane during contraction. SBS refers to syntrophin binding site, SSPN refers to the sarcospan, and DBD refers to dystroglycan binding domain. Adapted from Allen *et. al.,* 2015.

Dystrophin as a structural protein: functional domains and binding partners

The causative gene for DMD, dystrophin, codes for a structural protein found beneath the intracellular surface of the sarcolemma (Figure 1.2)[5]. Dystrophin is the longest gene in the human genome, and its full-length isoform spans 2.4 million base pairs and 79 exons (Figure 1.3). The genomic sequence for dystrophin composes nearly 1% of the genomic content located in the X-chromosome [44], and its longest isoform codes for a 427 kDa protein [45] in striated and cardiac muscle.

In healthy, wild type skeletal muscle, the full length 427 kDa isoform of the dystrophin protein forms a physical connection between the intracellular and extracellular environment through its connections with F-actin and ß-dystroglycan, and supports muscle contraction by connecting the sarcolemma with sarcomeres (Figure 1.2)[6].

The initial discovery of DMD was made in 1863 by the French neurologist Guillaume Benjamin Amand Duchenne, and was based on a case study including 13 children displaying similar symptoms. The causative gene, dystrophin was later discovered in 1987 [1]. Following the initial discovery and characterization of dystrophin several decades of research have been dedicated to the characterization of dystrophin and its function as a structural protein.

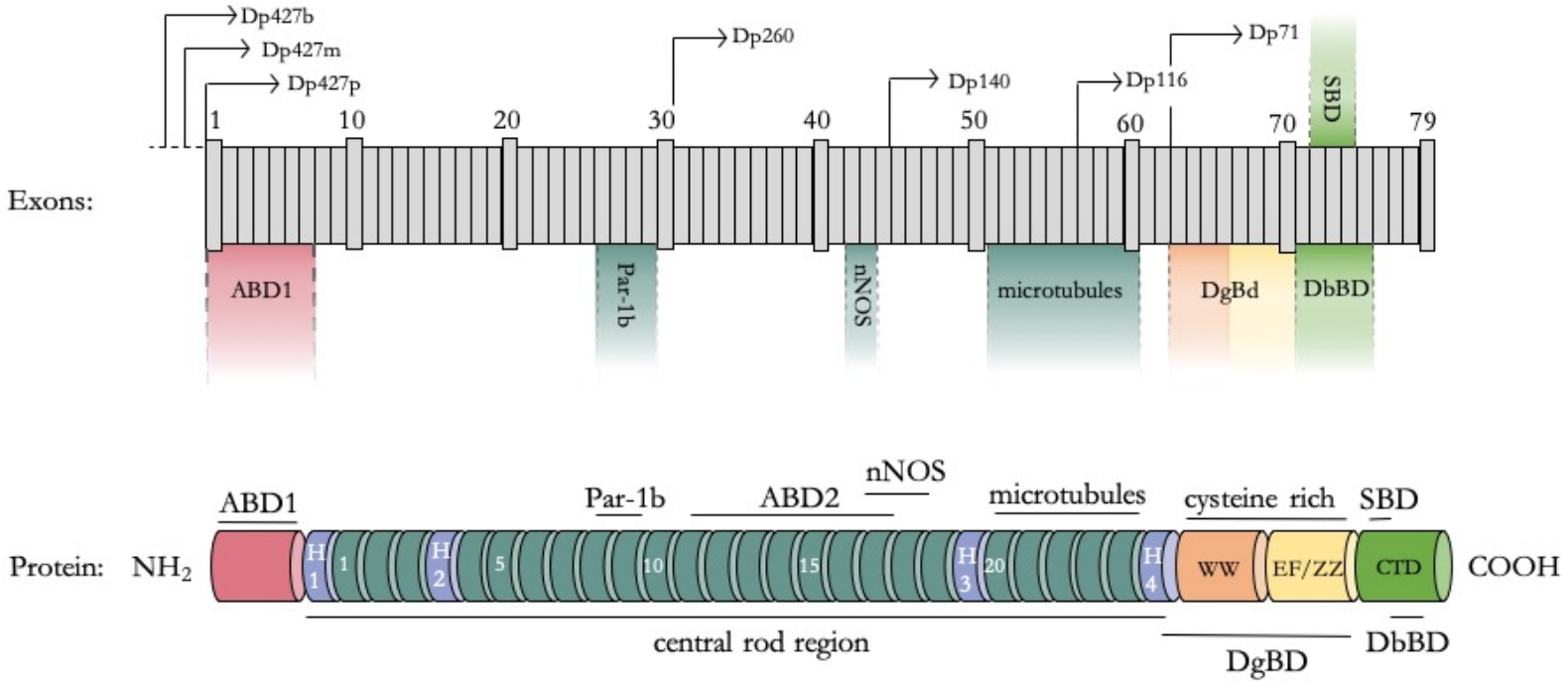

Figure 1.3: The four major functional domains of the Dystrophin gene. The top panel indicates the 79 exons which make up the full length dystrophin gene. The seven promoters controlling dystrophin expression are labeled above corresponding exons, with three tissue specific promoters controlling the expression of dystrophin in muscle, brain, and purkinje cells, and four internal promotes controlling dystrophin expression in various tissues outside of the muscle. The bottom panel represents the full length 427 kDa dystrophin protein with each of the four major functional domains labeled, as well as a number of binding sites for interacting proteins.

In order to gain a comprehensive understanding of dystrophin's role as a structural protein, the physical consequences of dystrophin's absence have been extensively characterized. It has been found both in human muscle biopsies and in the muscle of mammalian model systems that the effects of dystrophin's absence on the structural integrity of skeletal muscle are devastating and widespread. Some of the most notable cellular phenotypes include sarcolemma tear and rupture, myofibril damage, and elevated intracellular calcium. In effort to understand how the biochemical composition of the dystrophin protein effects the physical stabilization of the sarcolemma, a number of studies have thoroughly characterized the roles of the protein as a whole, and the role of each functional domain within the protein.

The dystrophin protein is thought to have four major functional domains (Figure 1.3). These four domains have been defined based on their essential role in the stabilization of the cell membrane, and are described as the actin binding domain, the central rod domain, the cysteine rich domain, and the C-terminal scaffolding domain. The first, the N-terminal actin binding domain (ABD1), is responsible for binding to cytoskeletal F-actin, and includes two calponin homology domains (CH) [46]. This region is also known to bind to the intermediate filament protein cytokeratin 19. Disrupting the interaction between ABD1 and cytokeratin 19 (K19) in K19 null mice results in skeletal myopathy, loss of contractile force, and disorganization of mitochondria in the muscle [47] (Figure 1.3).

The central rod region is composed of 24 helical spectrin repeats which are punctuated with four hinge domains, and together this region of the protein is responsible for the absorption of mechanical stress during contraction. Both structure and length of this

region likely make this domain of the protein particularly well suited to carry out this role. In fact, in a study that administered two different lengths of mini-dystrophin, it was discovered that a form of mini-dystrophin containing at least eight spectrin repeats was sufficient to restore a wild type phenotype in the *mdx* mouse, while a mini-dystrophin containing only four spectrin repeats was unable to do so [48]. Within the central rod region there is also is a second actin binding domain (ABD2) that spans from spectrin repeats 11-15 (Figure 1.3) [49,50]. Spectrin repeats 20-23 of the rod domain are responsible for binding microtubules. The functional loss of this region is implicated in DMD pathology as the skeletal muscle of *mdx* mice displays disorganization of the microtubule network (Figure 1.3) [51,52].

This is followed by a cysteine rich domain that is composed of two EF hand like domains and a WW and ZZ domain [53–55]. This cysteine rich region is required for the binding of ß-dystroglycan. The fourth recognized domain is the C-terminal domain, which associates with α-dystrobrevin and syntrophins [56,57]. The DAPC in turn binds to extracellular basal lamina through interactions with laminin (Figure 1.2, Figure 1.3, Table 1.1). In this way, the connection between dystrophin and the DAPC facilitates the stabilization of the sarcolemma during muscle contraction in skeletal, cardiac, and diaphragm muscles.

Members of the Dystrophin associated protein complex	
Cellular Localization	Protein
Extracellular	α-dystroglycan
	laminin-2
Transmembrane	β-dystroglycan
	α-sarcoglycan
	β-sarcoglycan
	γ -sarcoglycan
	δ -sarcoglycan
	sarcospan
Cytoplasmic	dystrophin
	α-dystrobrevin
	α1-syntrophin
	β1- syntrophin
	neuronal nitric oxide synthase

Table 1.1: Core members of the DAPC categorized by subcellular localization.

When all four of these domains are working in concert, dystrophin is able to stabilize the sarcolemma as it undergoes mechanical stress during contraction. In wild-type, mammalian muscle, after force has been generated by a single muscle fiber, this force is then transmitted laterally through the extracellular matrix (ECM) to the epimysium [58]. This phenomenon is made possible in part through the DAPC, which is primarily located between sarcomeres, or contractile units within the muscle [59]. It has been shown that in the absence of dystrophin, force is no longer transmitted laterally from sarcomere to the

ECM, suggesting that the connection between dystrophin and surrounding sarcomeres is essential for this to occur, and its absence is directly responsible for the contraction-induced injury seen in the muscle of DMD patients and mammalian models [58].

Dystrophin as a signaling protein

The structural role of the dystrophin protein, although complex, has been well characterized after several decades of research. Its anchoring connection to the DAPC plays a clear role in absorption and transmission of mechanical stress, thus stabilizing the sarcolemma. However, in forming this connection, dystrophin is also thought to facilitate the regulation of a number of signaling events whose transmission between the intracellular and extracellular environment is mediated by the DAPC. Furthermore, there is growing evidence that dystrophin alone is able to carry out a signaling role in the muscle through its numerous binding partners (Figure 1.2).

The absence of dystrophin is thought to broadly affect signaling pathways in the cell, including intracellular calcium signaling, production and localization of nitric oxide, and production of reactive oxygen species (ROS)[52,60–62]. It is important to note that changes in signaling can occur both as a direct result of contraction-induced damage to the sarcolemma, or independently and in parallel to structural changes within the muscle cell.

An alternative hypothesis to dystrophin's proposed role as a signaling protein is that the inability of dystrophin to facilitate the transmission of lateral force during contraction in turn leads to increased pressure on the cell membrane tearing, and finally an influx of components from the extracellular environment and release of cytoplasmic content. Although this hypothesis could feasibly explain a number of phenotypes, including elevated

intracellular calcium levels, it has not been conclusively shown. Despite the fact that this theory has persisted to some degree for many years in the DMD community, it is important to note that there is evidence to support the fact that force generated by muscle contraction is not actually required to increase membrane permeability in human DMD muscle [15,16,63]. The results of serum creatine kinase tests are often used as an indicator of increased membrane permeability in DMD patients, but the results of this test can be highly variable, and are typically elevated in the first year after birth, prior to exposure to years of repeated, high force muscle contraction [15]. This makes it highly likely that the absence of dystrophin alone, prior to muscle damage, is enough to induce widespread, deleterious effects on the muscle, further supporting the notion that dystrophin holds an essential signaling role in the muscle that affects nearly every aspect of a normal muscle cell's function. Current literature also supports the role of dystrophin in changes in miRNA expression, and altered activity of Wnt and Hippo pathways, although the exact mechanism behind these signaling changes is not well characterized [64–66]. Finally, the absence of dystrophin in *mdx* muscle reduces the amount of the calcium handling protein calsequestrin present, which directly reduces the levels of calcium released following the occurrence of an action potential [67]. This is one of a number of examples in which calcium signaling is significantly altered in dystrophic muscle. However, it has not yet been definitively determined if this phenotype is strictly a result of dystrophins inability to perform its signaling role, or if it is caused in part by damage to the sarcolemma.

The observed signaling changes in dystrophic muscle can potentially be explained by the disruption of dystrophin's interaction with the DAPC. There is an abundance of evidence to support the hypothesis that the DAPC is in fact essential for the transduction of extracellular signals to the intracellular environment, despite its initial characterization as a

structural complex [6,68]. There are several examples in which skeletal muscle signaling is disrupted in the case that one or more members of the DAPC fails to assemble and function normally in the absence of dystrophin [69,70]. One instance of this was highlighted by a study that evaluated the consequences of disrupting the connection between dystroglycan and laminin [71]. The major findings of this study were that interfering with the connection between dystroglycan and laminin is able to alter the P13K/AKT signaling pathway, which ultimately impacts cell survival [71]. It has also been shown that even when all members of the DAPC are present, mutations within these genes that cause functional changes to DAPC members can bring about changes in intracellular signaling [72,73]. This strongly suggests that the DAPC as a whole is not limited to a structural role through its connection with dystrophin.

Another classic example of the DAPC serving a signaling role in the muscle comes from the characterization of interactions between dystrophin, syntrophin, and calmodulin. Calmodulin, a calcium-binding signaling protein, associates with the DAPC through dystrophin and α-syntrophin to control calmodulin-mediated synthesis of nitric oxide (NO) [74]. There are a number of calmodulin-dependent cellular processes that are significantly reduced in dystrophic skeletal muscle, including the deregulation of calmodulin-regulated protein kinases whose activity is implicated in muscle cell survival [75–79]. Syntrophins, along with ß-dystroglycan, can also recruit the signaling protein GrB2 [80,81]. To address this phenomenon, a study performed in rabbit muscle has characterized an intricate series of interactions between the DAPC and signaling molecules within the cell. This group was able to demonstrate that when laminin is bound to an intact DAPC through α-dystroglycan, it enables intracellular syntrophin to form a complex with Grb2 and Sos1, thus allowing

syntrophin to recruit Rac1. This syntrophin-mediated recruitment of Rac1 then facilitates the binding Pak1 to Rac1, which results in the phosphorylation of c-Jun and JNK-p46 [82]. Although it was not directly characterized in this particular study, there is sufficient surrounding evidence supporting the idea that dystrophin's absence impairs the recruitment of and assembly of nearly all members of the DAPC to the sarcolemma at wild type levels[52,83], suggesting that this particular signaling cascade, and any others that depend on wild-type assembly of the DAPC would be directly interfered with should dystrophin be absent from the muscle [70,73,84]. While the disrupted signaling pathways described here do not provide a comprehensive definition of the DAPC's known signaling role, they certainly shed light on the complexity of the DAPC's as a signaling complex that is essential for typical muscle function.

It has been repeatedly demonstrated that in the absence of dystrophin, each of these members of the DAPC fails to assemble with the sarcolemma at wild type levels[83]. This suggests that the absence of dystrophin is able to indirectly bring about a cascade of signaling events within the muscle that are likely to be independent drivers of disease progression. However, dystrophin is capable of binding a number of essential signaling proteins itself, meaning it can be considered to be a critical signaling protein in the muscle, both independently and in cooperation with the DAPC [85]. This is evidenced both by the existence of functional domains that are known to bind to transiently interacting signaling proteins like neuronal nitric oxide synthase (nNOS), and by the existence of phenotypes like increased reactive oxygen species (ROS) signaling following the dystrophin-dependent disruption of microtubule networks [51,86,87]. More specifically, neuronal nitric oxide synthase (nNOS) is an enzyme responsible for synthesizing nitric oxide (NO), which is a

signaling molecule with an essential role in muscle physiology. nNOS is essential for normal muscle function, as the production of NO, and NO-mediated cGMP production are implicated in vasodilation, muscle metabolism, and the regulation of apoptotic and necrotic cell death [69,88–90]. nNOS is known to bind to SR16/17 of dystrophin's rod domain, and in dystrophin's absence there is a loss of localization of nNOS to the sarcolemma, and resulting impairment of NO signaling (Figure 1.3)[91,92]. It has also been found that by disrupting the connection between the rod domain of dystrophin and microtubules, disorganization of the intracellular microtubule network in turn causes an increase in ROS signaling. Microtubules control the stretch induced activation of NADPH oxidase 2, which is responsible for production of ROS, a process which is elevated in *mdx* muscle [62,86]. The signaling function of the polarity regulating kinase Par-1b is also altered in dystrophic muscle, as it typically binds to SR 8-9 within the rod domain (Figure 1.3) [93].

Perhaps some of the most intriguing demonstrations of dystrophin's signaling role in the muscle are performed in the context of deregulation of mitochondrial function. Impaired mitochondrial function is a universal phenotype of DMD. Dystrophic muscle exhibits drastic changes in cellular energy homeostasis. The consequences of this are widespread, and have detrimental effects on everything from muscle strength to impaired control of intracellular calcium homeostasis[94–96]. Although the downstream consequences of this phenotype are well characterized, the relationship between dystrophin deficiency and mitochondrial function remains difficult to define. The order of molecular events leading to the collapse of mitochondrial membrane potential and resulting cell death in dystrophic muscle is unclear. For this reason, one of the more elusive questions surrounding the progression of DMD remains unanswered. We do not yet know if dystrophin's absence from the cell membrane leads to an influx of calcium that overloads the mitochondria, or if

this phenotype begins prior to mechanical stress because of a metabolic deficiency brought about by dystrophin's unfulfilled signaling role within the cell.

In 2009, one group performed a series of experiments in undifferentiated *mdx* mouse myoblasts that strove to answer this question. Their observations were that undifferentiated *mdx* mouse myoblasts exhibit a compelling myriad of alterations to cellular metabolism, including increased formation of ROS and disorganization of mitochondria [97]. This finding is significant, as undifferentiated myoblasts have not yet fused, and dystrophin is not expressed and localized to the sarcolemma until after fusion. This strongly supports the hypothesis that dystrophin deficiencies are able to alter intracellular signaling and mitochondrial function long before dystrophin has assembled at the sarcolemma to carry out its traditional structural role. Collectively, all of these findings give weight to hypothesis that altered intracellular signaling in dystrophic muscle occurs before the incidence of contraction induced membrane damage, meaning dystrophin has dual roles in controlling the health and function of muscle.

The role of inflammation in DMD progression and bioinformatic studies of dystrophic muscle

Of the myriad of signaling changes that occur in dystrophin deficient muscle, the inflammatory response is among the strongest and most well characterized. The role of the immune response in the pathology of DMD has been characterized both in human muscle and in the muscle of mammalian model systems. It is also essential to consider the inflammatory response when evaluating dystrophin as a protein with dual signaling and structural roles in the muscle. Although contraction-induced membrane lesions contribute significantly to disease initiation and progression, in the earliest stages of DMD progression

there is evidence for aberrant intracellular signaling related to the immune response. One hypothesis is that these signaling changes related to the immune response occur before repeated contractions have damaged the cell membrane. In fact, some studies have confirmed that there is in fact significant activation of the innate immune response in fetal human muscle long before the appearance of clinical symptoms [98]. A number of studies focusing on the role of inflammation in disease progression have characterized the early upregulation of genes related to the inflammatory response that include chemokines, MHCs and cytokines, and the increased activation of immune cell infiltrates [99–101]. This phenomenon is in direct support of the idea that dystrophin's absence initiates a number of signaling cascades in the muscle prior to the occurrence of mechanical damage, further indicating that dystrophin serves as a signaling protein in the muscle.

Over time, our understanding of DMD initiation and progression has changed. The timeline of DMD onset no longer describes muscle that must first undergo repeated cycles of contraction to bring about damage, followed by the onset of chronic inflammation and signaling changes within the muscle. We now know that the inflammatory response and associated signaling changes are not necessarily a response to existing membrane damage, but instead may be contributing to this phenotype. In fact, it has been shown that there is significant activation of the innate immune response in fetal human muscle long before the appearance of clinical symptoms [98]. A number of factors contribute to cell death and muscle necrosis in DMD muscle. Although the immune response alone is not the primary cause of muscle fibre death, there are several pathways caused by the increased activation of immune cell infiltrates that are able to cause muscle fibre death [102].

In normal, wild type muscle, following rigorous contraction, there is minor leakage of ctyoplasmic content from myofibres into the extracellular environment, which triggers the activation of the innate immune response. When wild type dystrophin is present, the rate of membrane repair is rapid, the leakage of cytoplasmic contents is tempered, and the inflammatory response is resolved shortly after muscle injury. In stark contrast to this, dystrophic muscle is characterized by continual membrane instability. One theory is that the membrane instability caused by lack of dystrophin directly causes the release of cytoplasmic contents. Leakage of cytoplasmic contents into the extracellular environment is neither efficiently or completely resolved, and the activation of the innate immune response is constitutive as a result. Ideally, muscle should go through cycles of damage and repair in which the activation of the inflammatory response is resolved. This is not the case in DMD muscle, and the repetitive cycles of degeneration and repair without resolution sustains the chronic inflammation that affects DMD patients for the entire duration of the condition [103–107].

The abnormal constitutive activation of the immune response in dystrophic muscle includes an increased presence of activated macrophages. These macrophages are thought to produce nitric oxide at levels that promote the lysis of muscle fibres [103,108]. In fact, one study has shown that the preventative depletion of macrophages in *mdx* muscle early in development is able to reduce muscle injury [108]. Similarly, another study has shown that by depleting $CD4^+$ and $CD8^+$ T cells, there is significant reduction in *mdx* muscle fibre death and overall improvement in muscle pathology [109]. Taken together, this data supports the idea that the immune response is one factor inducing damage and cell death in dystrophic muscle.

Many of the questions surrounding dystrophin's role as a signaling molecule would ideally be answered using traditional sequencing approaches. Muscle biopsies taken from human skeletal muscle would reveal the overall trends in gene expression that occur in dystrophin's absence [110]. However, the repetitive cycles of muscle damage and repair that occur following muscle contraction illicit changes in gene expression that are primarily related to the chronic inflammatory response in the muscle. This response is consistently present in DMD muscle throughout the patient's life, albeit to a greater degree as symptoms progress. Although some of this response can be managed with corticosteroids, the strength of this inflammatory response typically dominates the results of an sequencing efforts [111,112]. In fact, a study that attempted to better characterize the signaling consequences of dystrophin deficiency in the muscle performed a series of transcriptomic analyses on the muscle of several dystrophin deficient mouse models. After categorizing their sequencing results based on function, they found that between 55-88% of their reads were associated with the inflammatory response, and bioinformatically filtered out these reads in order to assess the remaining trends in gene expression. [113]. Because of this challenge, it can be difficult to detect the subtler signaling changes that may occur independently from the structural damage and resulting inflammation that is characteristic of DMD muscle.

In order to contribute to the growing body of knowledge surrounding potential therapeutic targets that can be manipulated in the treatment of the disease, it is essential that there is a comprehensive definition of the dystrophin's signaling role in the muscle. This requires studying signaling changes in dystrophic muscle both in the presence of inflammation and independently from the inflammatory response.

Studying Duchenne muscular dystrophy in model systems

Due to the uncertainty surrounding the precise role of dystrophin in the initiation and progression of Duchenne muscular dystrophy, a number of model systems have emerged to address the most consequential questions in the field. The establishment of these systems have allowed the community to gain a better understanding of disease initiation and progression, identify a number of potential therapeutic targets, and ultimately test treatments like exon skipping as potential cures for future patients. The use of model systems has allowed for an increased rate of discovery while minimizing the number of invasive studies and tests performed on human patients affected by the condition.

Perhaps the most commonly used model system in DMD research is the *mdx* mouse [9]. This mouse strain was established in 1981 at the University of Leicester after the discovery of a C to T nonsense point mutation in exon 23 within a C57BL/10ScSn colony. [114]. This system quickly became the standard for performing *in vivo* studies on dystrophin deficient muscle. Studies conducted in the *mdx* mouse have contributed significantly towards our understanding of disease initiation and progression, the inflammatory response in the muscle, and the efficacy of the majority of proposed therapeutic strategies.

Like any model system, the *mdx* mouse faces a number of limitations in its ability to recapitulate the human version of DMD. Perhaps the most important of these limitations is the differential use of the protein utrophin. Utrophin is an autosomal homologue of the dystrophin protein that shares 85% identity with the amino acid sequence of dystrophin [115]. Despite this extensive sequence similarity, the two proteins do not have overlapping roles in human muscle. Although utrophin is widely expressed in fetal and adult muscle, it localizes to the neuromuscular junction rather than the sarcolemma [116,117]. Despite the

fact that utrophin expression is elevated in DMD patients, it is not able to alleviate symptom [118,119]. In contrast to this, mice are able to utilize utrophin compensatory pathways in the absence of dystrophin[120–123]. In this way, mice that possess only a null mutation in the dystrophin gene are able to prevent the progression of symptoms and maintain relatively normal muscle function.

Furthermore, mice do not display cardiac symptoms that are representative of the human version of the condition, they have enhanced regenerative capacity in the muscle, and do not exhibit shortened lifespan, further necessitating double mutants for clinically accurate studies. Because of this discrepancy between the two species, it is necessary to use double knockout mice, *mdx*/*utr*$^{-/-}$, in order to conduct more phenotypically accurate studies of DMD [124,125]. Although these systems have provided a number of indispensable insights in the field of DMD, their genetic complexity raises concerns about the accuracy and translational value of the results obtained with this system.

Another notable limitation associated with the use of the *mdx* mouse model is the speed at which genetic studies can be performed. The generation time for any given mouse strain is roughly 12 weeks [126], meaning that this model system cannot be realistically optimized for high throughput experiments designed to rapidly identify and test therapeutic targets *in vivo*.

The golden retriever muscular dystrophy (GRMD) dog is arguably the most phenotypically accurate model system available [127]. This system was discovered in the 1980s prior to the discovery of the dystrophin gene, based solely on presentation of symptoms and pattern of inheritance, and was later assigned as a model for DMD when a single point mutation in a splice site within the dystrophin gene was identified [128]. Phenotypic progression of the disease in the GRMD dog is notably more severe than what is

observed in the *mdx* mouse and recapitulates the human version of the disease much more accurately. Because of this, studies performed in this system have significant translational value. To date, this system has provided indispensable results, as in some cases, promising potential treatments generated in the *mdx* mouse have uncovered serious side effects when similarly tested in the GRMD dog.

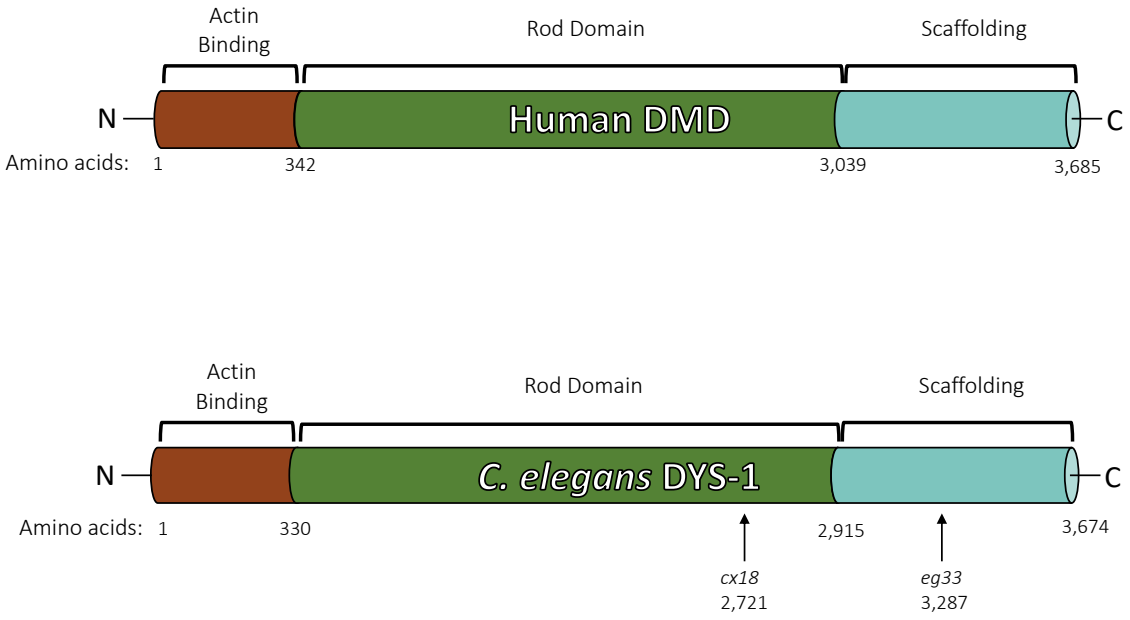

Figure 1.4: Conserved functional domains between human DMD and *C. elegans* DYS-1. The human and *C. elegans* version of the dystrophin protein is approximately the same size. The human dystrophin protein is 427 kDa, and the *C. elegans* ortholog is predicted to be 417.5 kDa. The major functional domains are conserved between the two species, with the N-terminal actin binding, the central rod, the cysteine rich, and the C-terminal scaffolding regions being present in both species. The *dys-1(cx18)* and *dys-1(eg33)* strains possess null mutations in the rod and scaffolding region respectively.

Interestingly, the dystrophin gene is conserved in both vertebrate and invertebrate species (Figure 1.4) [129,130]. One invertebrate in particular, the nematode *Caenorhabditis elegans* has been established as a promising model system for DMD. Similar to the *mdx* mouse, *C. elegans* do not exhibit progressive muscle degeneration and paralysis that is comparable to what is seen in humans. However, *C. elegans* strains possessing null mutations in the nematode dystrophin ortholog *dys-1* do exhibit a number of unique and progressive symptoms that indicate they may be a novel and informative tool for performing genetic studies that will have significant translational value [130–134]. Furthermore, they are particularly well suited to answer questions about dystrophin's signaling role, as their muscle cells are entirely post-mitotic, and they lack an inflammatory response in the muscle [135]. As a result, sequencing studies can be performed on muscle tissue in the absence of signaling responses associated with inflammatory or regenerative processes. *C. elegans* were established as a model system for DMD in 1998 [136] following the establishment of the *dys-1(cx18)* strain, which possesses a mutation that introduces a premature stop codon within the rod region (Figure 1.4). In subsequent years, a second strain was introduced, the *dys-1(eg33)*, in 2004 [137] which has routinely been used alongside the *dys-1(cx18)* strain to perform studies that have made a number of important contributions to our understanding of DMD.

The use of *C. elegans* as a model system for DMD is advantageous for a number of reasons. *C. elegans* have a short generation time of abut 48 hours, making them ideal for rapid genetic studies [138]. *C. elegans* are transparent, easy to culture, and perhaps most importantly, they lack both inflammation and regeneration in the muscle [135,139]. This has made them an attractive option for the study of dystrophin's complicated signaling role in the muscle independently from changes in gene expression that are associated with the

downstream consequences of dystrophin deficiency. Furthermore, the ease at which RNAi knockdown and overexpression experiments can be performed make them ideal for the identification of novel genetic partners of dystrophin. In this manner, this system complements systems with more apparent translational value, like the *mdx* mouse and GRMD by addressing limitations associated with long generation times, bioinformatic studies dominated by the inflammatory response, and a less than rapid rate of discovery.

Hypothesis and Specific Aims:

There is a wealth of information available characterizing the initiation and progression of DMD. Despite this, many aspects of the condition remain poorly understood. This is largely because the exact role of the causative protein, dystrophin, has not yet been elucidated. Each study that contributes to our understanding of the dystrophin protein also emphasizes the complexity of the dystrophin's role in the muscle.

The existence of both structural and signaling roles for dystrophin also suggests that there are independent drivers of disease progression that have yet to be defined. There is a need within the DMD community to explicitly define the consequences of dystrophin deficiencies in the muscle so that this information can be used in the pursuit of novel and effective therapeutic targets for the treatment of DMD.

I hypothesize that gaining a comprehensive definition of dystrophins structural and signaling roles in the muscle will improve our understanding of the progression of Duchenne muscular dystrophy as a whole. To address this hypothesis, I have performed a phylogenetic analysis on the conservation of the dystrophin protein across ten species, established an *in vivo* system to identify muscle-specific changes in gene expression in the

absence of dystrophin in the model organism *C. elegans,* and performed a functional analysis to test the biological significance of changes in gene expression identified in my sequencing results. The specific aims used to obtain each of these results are detailed below.

Aim 1: Perform a phylogenetic analysis on dystrophin and the surrounding members of the dystrophin associated protein complex across ten species.

This aim addresses a need for informative and complementary model organisms for the study of DMD. I hypothesize that gaining a clearer understanding of which members of the DAPC, and which functional domains within the dystrophin gene are conserved from one species to another reveals the extent to which each of these systems can be used to model the human version of the disease. To address this hypothesis, and to better understand the conservation of the dystrophin protein, I have aligned the sequence of the human dystrophin protein with dystrophin orthologs of 10 metazoan species. I have also repeated this analysis for each individual functional domain within the dystrophin protein, and for the core members of the DAPC for the invertebrate *C. elegans* and its respective orthologs.

The results from this analysis have emphasized the potential of both vertebrate and invertebrate model systems to serve as informative model systems for DMD based on the sequence conservation of essential members of the DAPC along with the major functional domains of the dystrophin protein.

Aim 2: Establish an in vivo system to isolate tissue-specific transcripts from the muscle of dystrophin deficient C. elegans strains.

The signaling changes that occur in dystrophin deficient muscle are not well characterized outside of those associated with the inflammatory response. The progression of DMD is complex and is driven forward by a number of cellular processes that are not necessarily caused by the inflammatory response. Despite this, inflammation in dystrophin deficient muscle is chronic, and gene signatures associated with the inflammatory response and signaling changes associated with muscle regeneration dominate the results of most bioinformatic studies.

To improve our understanding of the signaling consequences of dystrophin deficiencies, I have optimized the PAT-Seq system using an approach that captures signaling changes in dystrophic *C. elegans* muscle at distinct stages of disease progression. The results from this aim directly address this issue by revealing the tissue-specific changes in gene expression that occur in *C. elegans* muscle independently from the inflammatory and regenerative signaling responses.

Aim 3: Perform a functional analysis on trends in gene expression identified in PAT-Seq results.

The changes in gene expression observed in dystrophic *C. elegans* muscle suggest two distinct roles for dystrophin in the muscle. They also shed light on the order in which the molecular events contributing to disease pathology occur. The trends in gene expression identified here support the notion that there are metabolic deficiencies within dystrophic cells early in development, and this phenotype is followed by significant structural changes to the muscle later in disease progression.

To verify the biological significance of the changes in gene expression identified in my sequencing results, I have performed a series of experiments that confirm there are observable phenotypes resulting from these signaling changes. This includes the establishment and analysis of dystrophin deficient mitochondrial reporter strains, an RNAi screen that confirms the importance of upregulated genes implicated in muscle structure, and qPCR experiments that reveal a subset of genes found to be overexpressed in my datasets are also upregulated at the RNA level in mammalian satellite cells, thus confirming the translational value of these findings.

CHAPTER 2

PHYLOGENETIC ANALYSIS OF DYSTROPHIN AND ESSENTIAL MEMBERS OF THE DAPC

Overview

Dystrophin-like proteins have been relatively well characterized in mouse, canine, drosophila, and *C. elegans* [140]. Outside of the better characterized model organisms, dystrophin is known to be conserved to some degree throughout metazoans. Based on predicted protein sequences, there is a highly conserved dystrophin like protein in nearly all metazoans [141–143]. There is also the presence of a dystrobrevin-like protein in nearly all metazoans, which suggests these two genes were derived from an early duplication event in a single ancestral gene for the DAPC protein family [129]. The presence of orthologs for the dystrophin protein along with a number of its essential DAPC binding partners suggests

there is also a conserved functional role for this protein in both vertebrate and invertebrate muscle[141,143].

The devastating nature of DMD necessitates the establishment of as many informative and efficient model systems as possible, and the characterization of these systems begins at the sequence conservation level. with comparing muscle structure and function between organisms, specifically with respect to dystrophin and its role in the muscle. In order to do so, it must first be confirmed that each of these species possesses an ortholog of the dystrophin gene that shares both sequence and functional similarities with the human dystrophin gene. Previous phylogenetic studies focusing on the dystrophin gene have revealed that the dystrophin protein family is highly conserved, as is its overall structure and protein size in both vertebrates and invertebrates (Figure 1.4)[129,143]. This knowledge has provided important insights about the translational value of a number of animal models used for the study of DMD.

Evaluating the presence or absence of orthologs for essential DAPC members within each species, and then assessing the extent to which these proteins are conserved can provide valuable insights to the translational value for each system, and the limitations for each system based on functional differences in predicted protein sequences. Furthermore, evaluating the extent to which each functional domain within these dystrophin orthologs is conserved can provide a more clear understanding of how each dystrophin like protein interacts with the DAPC and cytoskeletal actin in the muscle of each organism.

Orthologs of the Dystrophin Protein Across Eight Metazoan Species

Orthologs of the dystrophin protein have been evaluated in eight species, four of which have been adapted for use as a model system and have made significant contributions towards our understanding of DMD. This analysis has uncovered a wide range of sequence conservation, with this highest being *Canis lupus familiaris* at 94.7%, and the lowest being *Caenorhabditis elegans* at 21.2%. Among vertebrates, percent similarity is 78% or above, with the lowest percent identities being the invertebrates drosophila and *C. elegans* (Table 2.1). Despite significant differences in sequence similarity between vertebrates and invertebrates, the presence of dystrophin like proteins in all of these organisms suggests that dystrophin plays a crucial and fundamental role in muscle biology.

All of these proteins appear to share the same overall structure, size, and pattern of expression. The human dystrophin protein is 3,685 amino acids in length, and the protein size is 427 kDa for its full-length isoform found in the muscle. For the eight species evaluated, orthologs of the dystrophin protein ranged from 3,497 to 3,678 amino acids (Table 2.1). It is also important to note that certain domains are more highly conserved between species than the protein as a whole. The extensive sequence conservation of the N and C-terminal regions again suggest a conserved structural role as a scaffolding molecule at the muscle cell membrane. Furthermore, the dystrophin protein family can be characterized by a number of elements that appear to always be present in the C-terminal scaffolding region of the protein. This includes two EF domains, a ZZ domain, and two coiled-coil domains. Interestingly, this structure can be found in all species examined here from the highly similar canine dystrophin to the dystrophin ortholog found in the invertebrate

C. elegans (Figure 2.1). This information can be used to infer that all members of the dystrophin protein family form a DAPC at the sarcolemma that interacts with dystrophin in a similar manner through the C-terminal scaffolding region.

Organism	Length (aa)	Percent identity
Homo sapiens	3685	-
Canis lupus familiaris (Dog)	3678	94.7%
Sus scrofa (Pig)	3674	93.9%
Rattus norvegicus (Rat)	3677	91.6%
Mus musculus (Mouse)	3678	91.0%
Ceanorhabditis elegans (Worm)	3674	21.2%
Gallus gallus (chicken)	3660	78.3%
Danio rerio (Zebrafish)	3609	56.9%
Drosophila Melanogaster (Fruit fly)	3497	27.7%

Table 2.1: Conservation of dystrophin orthologs across eight metazoan species based on percent identity.

Comparison of the DAPC and individual functional domains within the dystrophin protein in C. elegans

The conservation of dystrophin in both vertebrate and invertebrate species raises a number of questions regarding the function and purpose of the dystrophin protein in human skeletal muscle. Although the percent identity between human dystrophin and the

invertebrate *C. elegans* dystrophin ortholog *dys-1* is low, analyzing the conservation of each of the functional domains of dystrophin individually reveals that there is ≥37% similarity between the two proteins, with the N-terminal actin binding domain sharing 40% identity with ABD1 within the human dystrophin protein (Table 2.2). The region with the lowest percent conservation between these two species is the C-terminal scaffolding region, with percent identity between the two species being 37% (Table 2.2).

Protein		***C. elegans ortholog***	**Percent identity**
dystrophin		DYS-1	21.2%
	ABD1	-	40%
	rod region	-	44%
	C-terminal scaffolding	-	37%
dystroglycan		DGN-1	17.2%
dystrobrevin		DYB-1	32.4%
α-sarcoglycan		SGN-1	18.8%
β-sarcoglycan		SGN-1	20.2%
α1-syntrophin		STN-1	35.4%
β1- syntrophin		STN-1	35.0%

Table 2.2: Alignment of each member of the human DAPC with *C. elegans* orthologs. Percent identities between protein sequences were calculated with Mview. Percent identity for dystrophin is shown for the protein as a whole, and for each functional domain. The cysteine rich domain and dystroglycan binding domain were combined as "C-terminal scaffolding" domain for alignments.

The *C. elegans* DYS-1 protein possesses 23 spectrin repeats rather than 24 within the rod region. This could potentially explain why the two proteins are very similar in size, but the rod domains share a relatively low shared sequence identity when compared with other

vertebrate species. The *C. elegans* DYS-1 protein also possesses a WW domain, two EF domains, two coiled coil domains, a ZZ domain, and predicted dystroglycan, dystrobrevin and syntrophin binding domains in the C-terminal region based on sequence similarity with the human binding domains for each of these proteins (Figure 2.1).

Interestingly, a number of studies have shown that although *C. elegans* have a single orthologous protein for the human dystroglycans, DGN-1, this protein does not appear to be expressed or have function in the muscle [144]. Instead, DGN-1 appears to be expressed primarily in the neurons of *C. elegans*, has a relatively well characterized role in neuronal migration, and does not appear to localize with the other members of the invertebrate DAPC [144–147]. This raises a number of questions regarding why the binding domain for this protein has been retained within the DYS-1 protein, and what the relationship is between these two proteins *in vivo* (Figure 2.1).

After performing a phylogenetic analysis on the essential members of the DAPC surrounding dystrophin, it was found that not only do *C. elegans* possess orthologs for at least 6 of these crucial members, the percent similarity between these proteins ranges from 17.2% to 35% (Table 2.2). Interestingly, the alignment of dystroglycan shows the lowest percent identity among all members of the DAPC (Table 2.2). In humans, dystroglycan is cleaved after translation into α- and ß-subunits, and dystrophin binds directly to the ß-subunit within the DAPC [148]. In *C. elegans* this does not occur, and *dgn-1* remains as a single protein. This difference could potentially shed light on the functional differences and discrepancies in patter in expression between the two species. In this light, it is reasonable to suggest that the DAPC member with the lowest percent identity would be dystroglycan, as there appears to be an evolutionary divergence that has affected both sequence and function between the two species.

In contrast, the alignment of human dystrobrevin with the *C. elegans dyb-1* has revealed a percent identity that is significantly higher at 32.4% (Table 2.2). This is not surprising, as it has been shown that in *C. elegans* strains with null mutations in *dyb-1* show identical head bending phenotypes to those seen in *cx18(dys-1)* and *eg33(dys-1)* strains. It has been hypothesized that the DYS-1 protein likely binds directly to the dystrobrevin ortholog DYB-1 within the DAPC. The observed head bending phenotypes along with the high percent identity supports the idea that dystrobrevin assembles and functions within the DAPC in *C. elegans* similarly to the human version of the protein.

Finally, the single syntrophin ortholog within *C. elegans, stn-1* has been aligned to the human sequences for both α1 and ß1 syntrophins. The percent identity between these proteins is high for both paralogs of the protein at 35.4 % and 35% respectively (Table 2.2). *C. elegans* knockout strains do not have a recorded phenotype for null mutations in *stn-1*, but the high percent identity between these proteins suggests that these proteins are likely to function similarly between human and nematode, and that STN-1 plays an important role within the DAPC.

The presence and conservation of these proteins supports the idea that the invertebrate dystrophin protein functions similarly to the human version, and likely interacts with one or more of the orthologs of these DAPC members to stabilize the sarcolemma in invertebrate muscle.

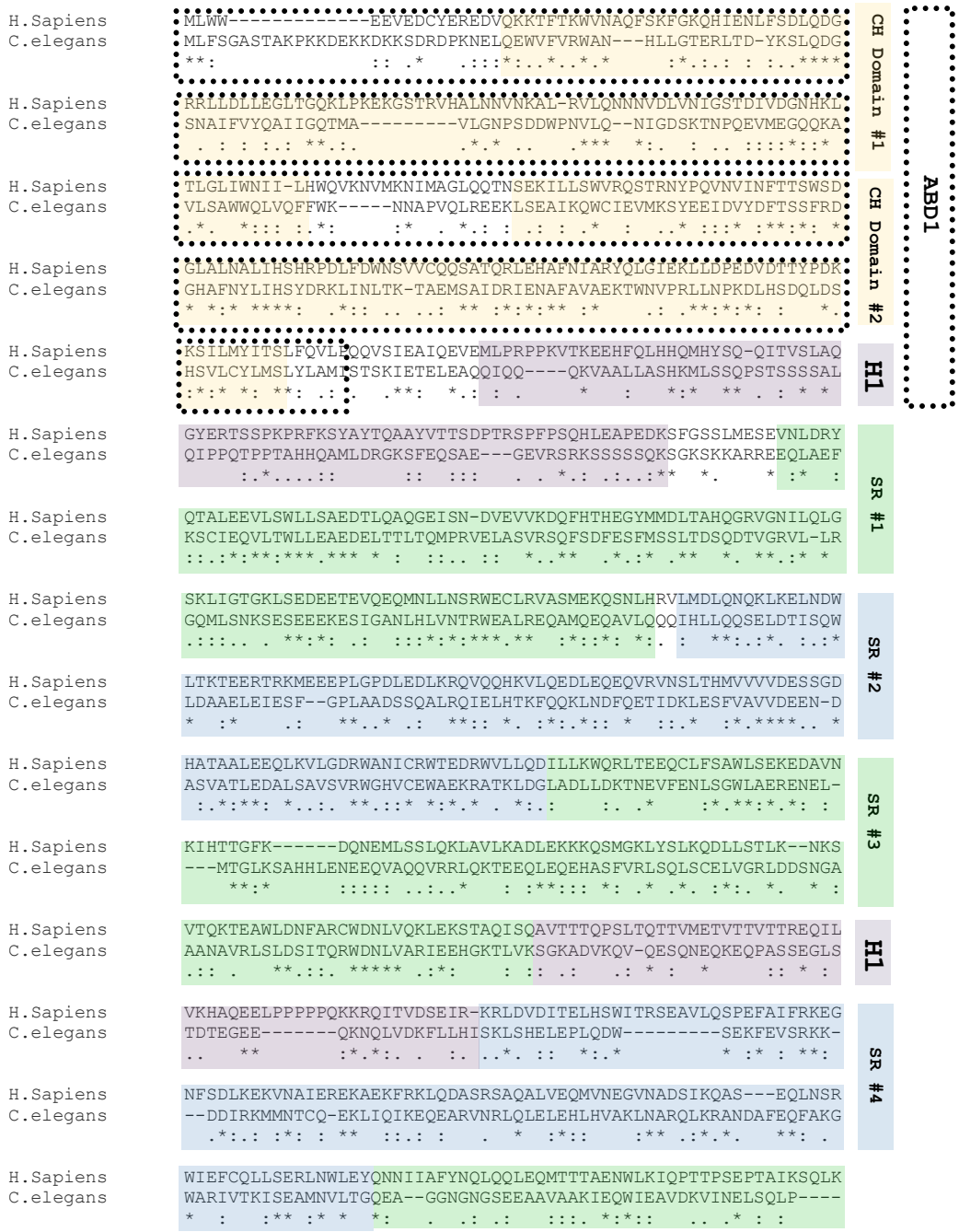
H.Sapiens
C.elegans
CH Domain #1
CH Domain #2
ABD1
H1
SR #1
SR #2
SR #3
SR #4

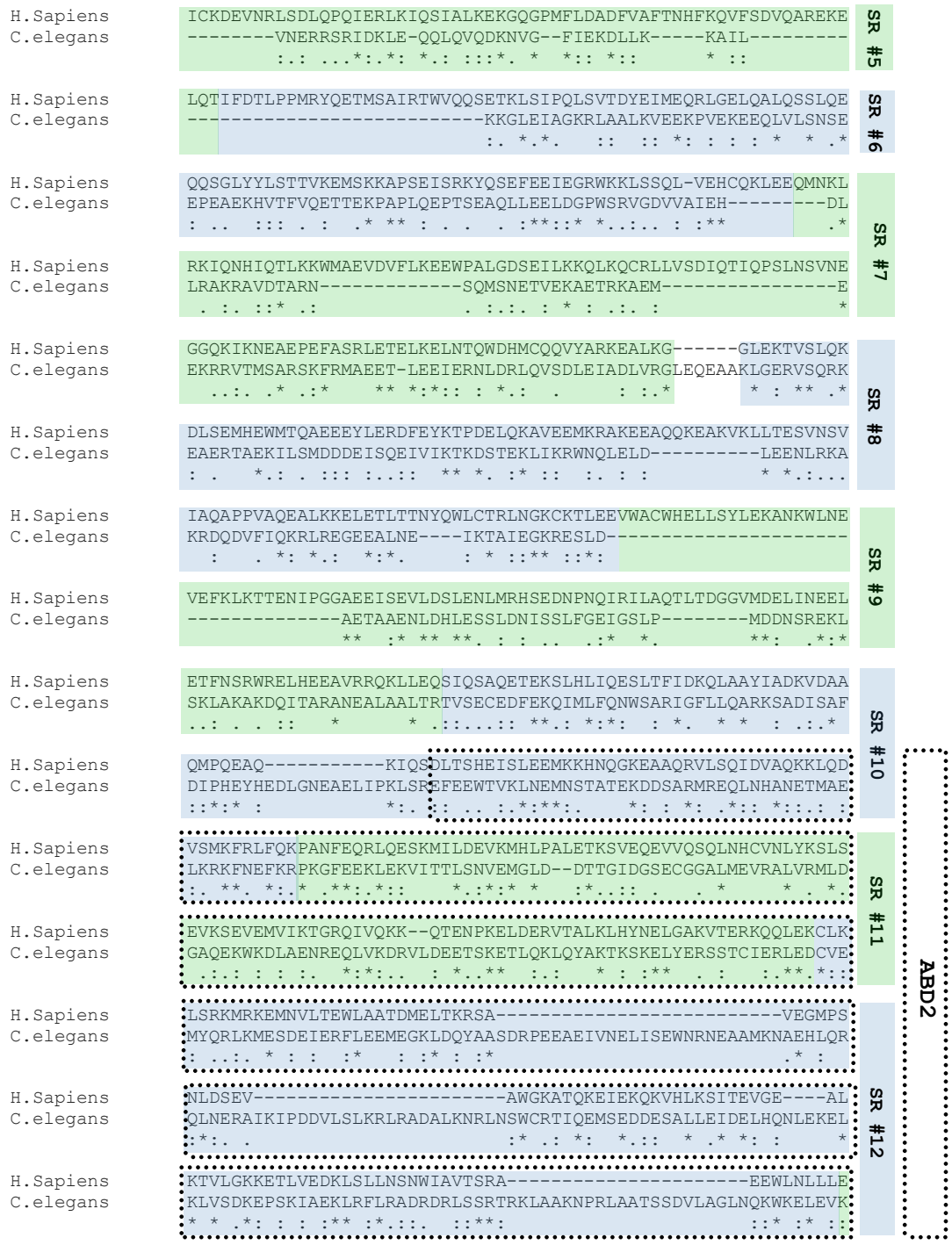
H.Sapiens
C.elegans
SR #5
SR #6
SR #7
SR #8
SR #9
SR #10
SR #11
SR #12
ABD2

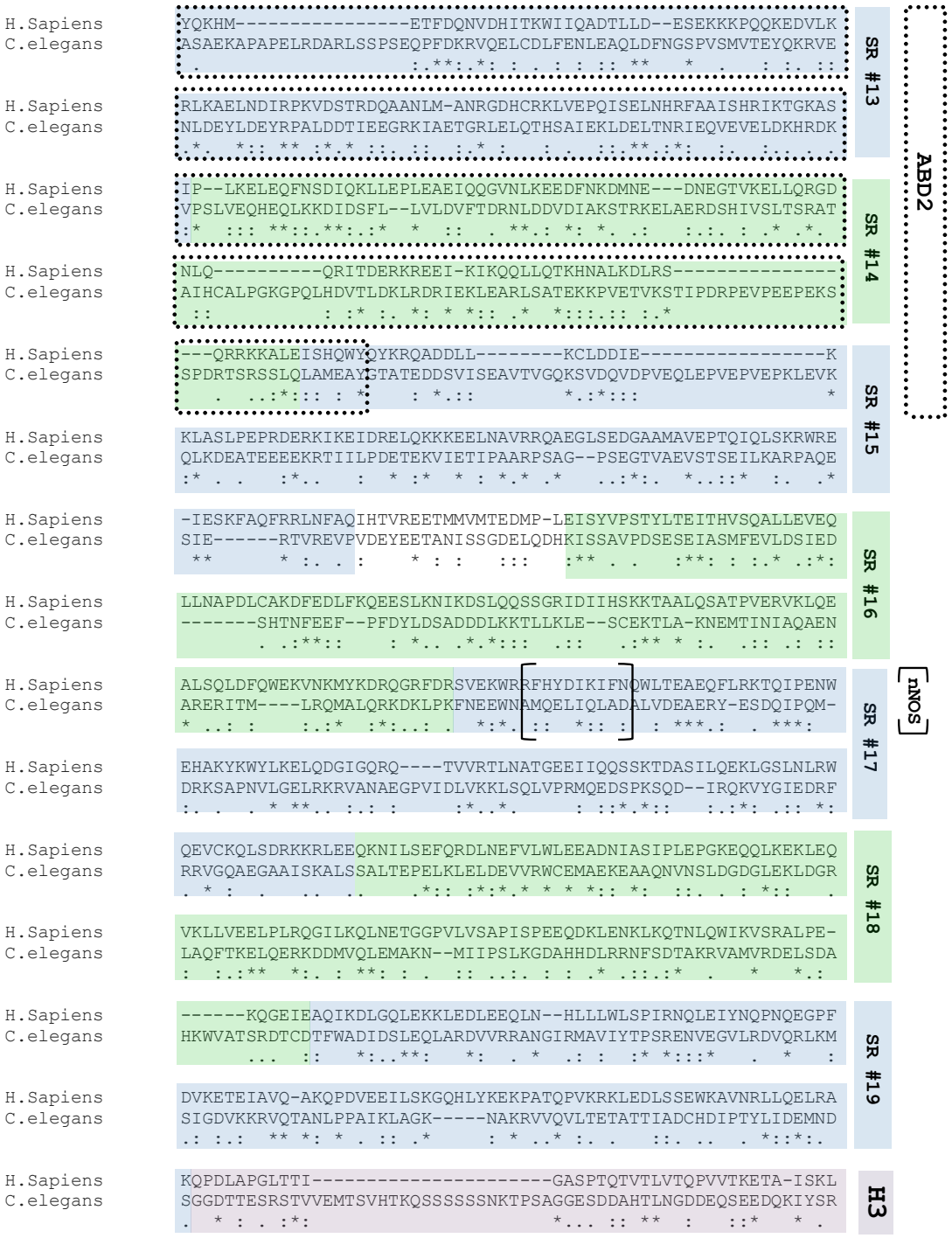
H.Sapiens
C.elegans
SR #13
SR #14
SR #15
SR #16
SR #17
SR #18
SR #19
H3
ABD2
nNOS

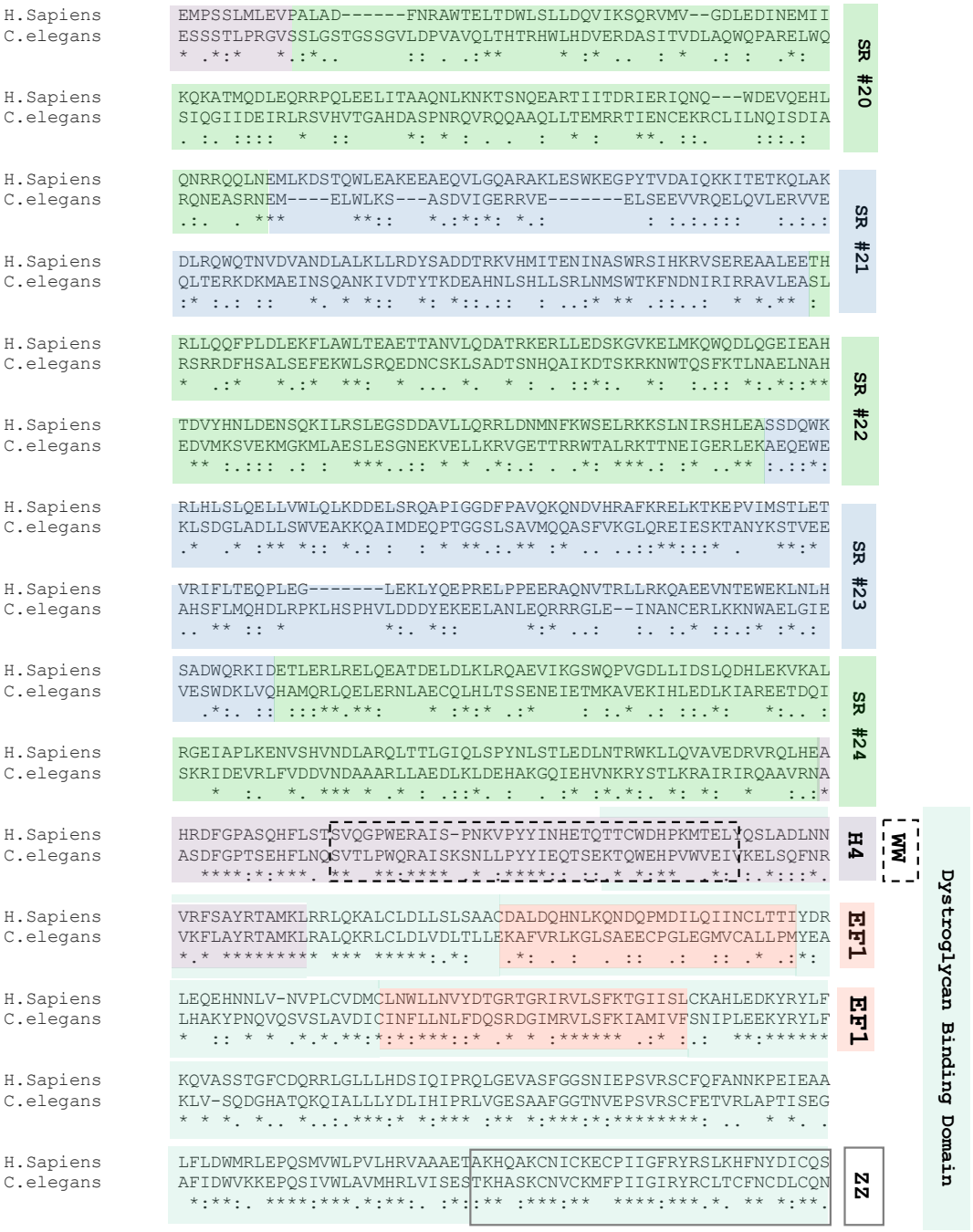
H.Sapiens
C.elegans
EMPSSLMLEVPALAD------FNRAWTELTDWLSLLDQVIKSQRVMV--GDLEDINEMII
ESSSTLPRGVSSLGSTGSSGVLDPVAVQLTHTRHWLHDVERDASITVDLAQWQPARELWQ
SR #20
KQKATMQDLEQRRPQLEELITAAQNLKNKTSNQEARTIITDRIERIQNQ---WDEVQEHL
SIQGIIDEIRLRSVHVTGAHDASPNRQVRQQAAQLLTEMRRTIENCEKRCLILNQISDIA
QNRRQQLNEMLKDSTQWLEAKEEAEQVLGQARAKLESWKEGPYTVDAIQKKITETKQLAK
RQNEASRNEM----ELWLKS---ASDVIGERRVE-------ELSEEVVRQELQVLERVVE
SR #21
DLRQWQTNVDVANDLALKLLRDYSADDTRKVHMITENINASWRSIHKRVSEREAALEETH
QLTERKDKMAEINSQANKIVDTYTKDEAHNLSHLLSRLNMSWTKFNDNIRIRRAVLEASL
SR #22
RLLQQFPLDLEKFLAWLTEAETTANVLQDATRKERLLEDSKGVKELMKQWQDLQGEIEAH
RSRRDFHSALSEFEKWLSRQEDNCSKLSADTSNHQAIKDTSKRKNWTQSFKTLNAELNAH
TDVYHNLDENSQKILRSLEGSDDAVLLQRRLDNMNFKWSELRKKSLNIRSHLEASSDQWK
EDVMKSVEKMGKMLAESLESGNEKVELLKRVGETTRRWTALRKTTNEIGERLEKAEQEWE
SR #23
RLHLSLQELLVWLQLKDDELSRQAPIGGDFPAVQKQNDVHRAFKRELKTKEPVIMSTLET
KLSDGLADLLSWVEAKKQAIMDEQPTGGSLSAVMQQASFVKGLQREIESKTANYKSTVEE
SR #24
VRIFLTEQPLEG-------LEKLYQEPRELPPEERAQNVTRLLRKQAEEVNTEWEKLNLH
AHSFLMQHDLRPKLHSPHVLDDDYEKEELANLEQRRRGLE--INANCERLKKNWAELGIE
SADWQRKIDETLERLRELQEATDELDLKLRQAEVIKGSWQPVGDLLIDSLQDHLEKVKAL
VESWDKLVQHAMQRLQELERNLAECQLHLTSSENEIETMKAVEKIHLEDLKIAREETDQI
RGEIAPLKENVSHVNDLARQLTTLGIQLSPYNLSTLEDLNTRWKLLQVAVEDRVRQLHEA
SKRIDEVRLFVDDVNDAAARLLAEDLKLDEHAKGQIEHVNKRYSTLKRAIRIRQAAVRNA
WW
H4
HRDFGPASQHFLSTSVQGPWERAIS-PNKVPYYINHETQTTCWDHPKMTELYQSLADLNN
ASDFGPTSEHFLNQSVTLPWQRAISKSNLLPYYIEQTSEKTQWEHPVWVEIVKELSQFNR
EF1
VRFSAYRTAMKLRRLQKALCLDLLSLSAACDALDQHNLKQNDQPMDILQIINCLTTIYDR
VKFLAYRTAMKLRALQKRLCLDLVDLTLLEKAFVRLKGLSAEECPGLEGMVCALLPMYEA
EF1
LEQEHNNLV-NVPLCVDMCLNWLLNVYDTGRTGRIRVLSFKTGIISLCKAHLEDKYRYLF
LHAKYPNQVQSVSLAVDICINFLLNLFDQSRDGIMRVLSFKIAMIVFSNIPLEEKYRYLF
KQVASSTGFCDQRRLGLLLHDSIQIPRQLGEVASFGGSNIEPSVRSCFQFANNKPEIEAA
KLV-SQDGHATQKQIALLLYDLIHIPRLVGESAAFGGTNVEPSVRSCFETVRLAPTISEG
ZZ
LFLDWMRLEPQSMVWLPVLHRVAAAETAKHQAKCNICKECPIIGFRYRSLKHFNYDICQS
AFIDWVKKEPQSIVWLAVMHRLVISESTKHASKCNVCKMFPIIGIRYRCLTCFNCDLCQN
Dystroglycan Binding Domain

Figure 2.1: Alignment of human dystrophin protein and C. elegans dystrophin like protein *dys-1*. The actin binding domains in the N-terminal regions and rod region are outlined with dotted lines and labeled as ABD1 and ABD2. Spectrin repeats within the rod domain are labeled SR #1-SR #24 with alternating green and blue boxes. Hinge regions are labeled as H1-H4 and are outlined with purple boxes. Syntrophin binding domains for syntrophin-α1 and syntrophin-ß1 are labeled as SNTA1 and SNTB1 and are highlighted in grey with solid and dashed lines respectively. The WW domain within hinge region 4 is outlined with a dashed line. The binding site for neuronal nitric oxide synthase within spectrin repeat 17 is outlined with brackets.

Tissue specific expression of dystrophin isoforms in human and C. elegans

In humans, the dystrophin gene has seven tissue specific promoters, four of which are internal and drive the expression of smaller dystrophin isoforms containing only some of the major functional domains [149,150]. Among these, there are promoters that drive the expression of dystrophin isoforms in the brain, the retina, and the peripheral nerves,

although the expression and function of these isoforms is not nearly as well characterized as the full length isoform present in the muscle (Figure 1.3) [150–154]

The expression of full-length dystrophin in humans is controlled by three different tissue specific promoters, all of which are located upstream of the first exon. These promoters are all known as DP427 promoters and are distinguished by their tissue type: dp427m (muscle), Dp427c (brain), and Dp427p (purkinje) [149,155,156]. The muscle isoform dp427m controls expression of full-length dystrophin in skeletal muscle, cardiac muscle, and glial cells. Dp427c controls the expression of a 427 kDa dystrophin protein in the brain and the retina[156]. The dp427p promoter drives expression of a full-length dystrophin protein in both purkinje cells and the muscle. The remaining four internal promoters drive expression of shorter isoforms in a number of tissues and have been named according to the molecular weight of the protein they produce. The promoters dp260, dp140, and dp116 drive expression in the retina, kidney, brain, and Schwann cells respectively. The promoter dp71 is able to drive expression of dystrophin in nearly all tissues except the skeletal muscle, and dp71 transcripts have been found in the brain, liver, kidney, lungs and heart (Figure 1.3).

Although only one promoter has been characterized for the *C, elegans dys-1* gene, there are seven different isoforms that have been genomically annotated [142]. The longest of these isoforms, F15D3.1a, is expressed in the body wall muscle of *C. elegans*. The expression of *dys-1* has been detected outside of the body muscle as well, in vulval, pharyngeal, and neuronal tissues, although the presence and function of DYS-1 in these tissues has not been further characterized.

CHAPTER 3

CHARACTERIZING TISSUE SPECIFIC CHANGES IN GENE EXPRESSION IN DYSTROPHIC C. ELEGANS MUSCLE

Publication Note

The research reported in this chapter has been submitted for publication in *Human Molecular Genetics*. Shannon O'Brien, Hannah S. Steber, and Marco Mangone. All co-authors have granted permission for this work to be included in this dissertation.

OVERVIEW

Duchenne muscular dystrophy (DMD) is an X-linked, recessive disease caused by out of frame mutations in the dystrophin gene [19]. The dystrophin gene codes for a structural protein found beneath the sarcolemma, where it is anchored both to the dystrophin associated protein complex (DAPC) and cytoskeletal actin, thus stabilizing the protein complex and the integrity of the cell membrane [157]. In humans, the absence of functional dystrophin results in progressive degeneration of the skeletal and cardiac muscles. The hallmark symptoms of DMD extend beyond muscle degeneration to include respiratory failure, cardiomyopathy, pseudohypertrophy, and chronic, widespread inflammation of the muscle. The condition remains the most commonly diagnosed type of muscular dystrophy, affecting approximately 1 in 3,500 live male births globally.

While the role of dystrophin in forming a physical connection between the extracellular matrix (ECM) and cytoskeleton has been well characterized [158], a comprehensive molecular definition of dystrophin's function is not fully understood. Outside of dystrophin's structural role, decades of research have led to the proposal that

dystrophin has an essential signaling role in the muscle as well, and its absence may induce a myriad of changes in gene expression that in turn influence the progression of DMD symptoms. Dystrophin deficiencies have been implicated in changes in nNOS localization [87,91,159], miRNA expression [160,161], and alterations to the Wnt, and Hippo signaling pathways [65,162]. Despite all the progress made in elucidating the signaling role of dystrophin, we still do not have an all-encompassing definition of the signaling consequences of dystrophin deficiencies. This issue is due in part to the fact that chronic inflammation of mammalian muscle has the ability to obscure more subtle changes in gene expression outside of the inflammatory pathway.

Vertebrate models of DMD include the *mdx* mouse [163] and the golden retriever muscular dystrophy canine [128]. Both models have contributed significantly towards our understanding of dystrophin's function [164], but face limitations when studying the cell autonomous effects of dystrophin deficiencies on skeletal muscle, independently of the myolysis and fibrosis associated with chronic inflammation observed in mammals. In addition, *mdx* mice are challenging to use for the study of molecular mechanisms using high-throughput approaches such as genome-wide screens and other large-scale studies [165].

Mitochondrial dysfunction and systemic deregulation of cellular energy homeostasis have been observed in DMD patients, *mdx* mice and the invertebrate *C. elegans* [166–170]. Mitochondria play an important role in both healthy and dystrophic muscle function, as a steady-state flux of ATP, Ca+ and other components of energy metabolism are required for muscle contraction. A recent study identified a significant increase in enzymes that are major consumers of NAD+ in dystrophic muscle tissues, and its replenishment was shown to ameliorate symptoms in *mdx* mice and *C. elegans* [168].

Mitochondria also play a pivotal role in disease progression, but it is still not clear if its dysfunction is induced by the loss of muscle fibres, which in turn induce muscle paralysis and necrosis, or if it occurs in early stages of the disease when paralysis and loss of muscle tissue have not yet been initiated [171]. The field of DMD research has yet to reach a comprehensive definition of the exact role mitochondrial function plays in the initiation and progression of DMD.

The invertebrate model *C. elegans* has the potential to address these questions and serve as an informative model system for DMD. These nematodes possess a singular ortholog of the dystrophin gene (*dys-1*), which is similar in protein size to the human dystrophin gene and contains similar actin-binding and scaffolding regions [136]. Additionally, several essential members of the DAPC are conserved between humans and nematodes [172,173]. The *C. elegans* DAPC is comparable to the human complex and includes key proteins such as dystrobrevin (DYB-1), sarcoglycans (SGCA-1, SGCB-1 and SGN-1), and the syntrophins (STN-1 and STN-2) [174]. This predicts strong selective pressure for functional conservation of the DAPC from *C. elegans* to humans.

The *C. elegans* mutant strains *dys-1(cx18) and dys-1(eg33)* represent a novel tool to study DMD *in vivo* [175]. These mutant strains contain different nonsense mutations causing a premature stop codon in different portions of the gene. *dys-1* has been well characterized for its function in the worm body wall and vulva muscles, and its expression has been detected in a number of tissues outside of the muscle, including the gonad and pharynx [176]. Mimicking the human condition, early reports have shown that loss of *dys-1* does not result in dramatic muscular degeneration phenotypes. Instead, they display defects in motility that are phenotypically distinct from humans, but are still the direct result of a loss of functional

dys-1. This includes anomalous bending of the head, hyperactivity, impaired burrowing ability, hyper contraction of the body wall muscle, and age-dependent, progressive loss of locomotor function [177]. In later stages, *dys-1* worm strains also exhibit partial muscle cell death with shorter lifespans than *wt* worms [178] and momentary lack of forward progression in dystrophic worms cultivated within agar pipettes [177].

Both *dys-1* worm strains display similar disease phenotypes, suggesting that both mutations, although in different portions of the *dys-1* gene, affect similar pathways. The introduction of human *dystrophin* cDNA in these mutant worms rescues these phenotypes [178], suggesting they are indeed a highly appropriate disease model. Of note, *dys-1*(*eg33*) and *dys-1*(*cx18*) strains have been recently found to respond differently to stress and to pharmacological treatment [170], with the *dys-1(eg33)* strain being more phenotypically severe.

C. elegans possess an innate immune response; the adaptive immunity is primitive and cell-mediated immunity is absent [179]. The absence of chronic inflammation and muscle regeneration, which are normally implicated in the progression of myofiber necrosis and fibrosis in human DMD patients and mammalian models, may be one component that allows these worm strains to move somewhat similarly to *wt* worms. Changes in motility are subtle, localized to specific areas, and become most apparent in adult worms. Because the muscle tissue in these strains is not being actively damaged by chronic inflammation as in patients with DMD and *mdx* mice, there are no major changes in muscle structure between *wt* and dystrophic muscles in *C. elegans*. This lack of extensive muscle damage or paralysis allows for the study of cell autonomous contributions to the progression of DMD symptoms and resulting changes in gene expression in the absence of inflammation.

Our lab has previously adapted an established technique named PAT-Seq, which optimizes tissue-specific RNA isolation from intact organisms [180], allowing the identification of tissue-specific transcriptomes at single-base resolution [181–183]. This method, named PAT-Seq, takes advantage of the binding affinity and specificity of the cytoplasmic PolyA Binding Protein (PABPC1) to polyA tails of mRNAs [184] by fusing the worm ortholog of PABPC1 (*pab-1)* to a 3XFLAG tag and a fluorescent marker (GFP::*pab-1*::3xFLAG), and placing this cassette under the control of a tissue-specific promoter of choice. UV crosslinking and immunoprecipitation using α-FLAG antibodies in worms expressing this cassette allows the isolation and sequencing of tissue specific polyA+ RNA. The result is a high-quality tissue-specific transcriptome that is depleted of contaminating transcripts from outside tissues. Using this technique, our lab recently profiled *C. elegans* intestine, pharynx and body muscle tissues [181]. This study allowed us to define and analyze body muscle transcriptome at an unprecedented resolution [181].

In order to identify muscle-specific transcriptome changes occurring throughout DMD progression, we crossed the *dys-1(cx18)* and *dys-1(eg33)* mutant strains with our *myo-3p*::GFP::*pab-1*::3xFLAG, or PolyA-Pull (*wt* PAP) worm strain [181], producing two novel strains named DP1 and DP2 respectively. These two strains were then used to isolate and sequence muscle-specific transcriptomes in worms lacking the dystrophin protein at different stages of the disease, allowing us to fully define the dynamic transcriptome changes occurring in the absence of inflammation at controlled time points, during early and late stages of symptom progression. Furthermore, we have examined changes in gene expression that are unique to each of the dystrophin-deficient strains in order to better understand functional differences between the two mutant strains. We have also performed targeted

genetic experiments to study the contribution of selected genes towards symptom progression identified by our approach.

We have found that that the two different truncated versions of the dystrophin gene in *dys-1*(*cx18*) and *dys-1*(*eg33*) strains are both stably transcribed and drive distinct differences in gene expression pattern. Our transcriptome analyses have found that the absence of *wt* dystrophin in *C. elegans* lead to widespread splicing errors, and initiate deregulation of mitochondrial function in the earliest stages of development. This impairment leads to differential expression of genes involved in muscle function and differentiation during later stages of development and adulthood, perhaps as a part of a compensatory mechanism that is able to impede dystrophin-dependent muscle degeneration.

RESULTS

Pat-Seq from the muscle of mutant dys-1 C. elegans strains produced high-quality muscle-specific mRNAs

In order to sequence *C. elegans* dystrophin-deficient muscle tissue, we have taken advantage of the PAT-Seq assay used in our previous studies [181,182]. The original *wt* PAP strain expresses the gene *pab-1* fused to GFP (N-terminus) and a 3xFLAG tag (C-terminus) restricted to the muscle by the tissue-specific promoter *Pmyo-3* [181,182] (Figure 3.1). *pab-1* is the *C. elegans* ortholog of the human cytoplasmic polyA binding protein (PABPC1), which typically binds the polyA track of mature mRNAs in the cytoplasm and is required for translation [185].

Since *dys-1*(*cx18*) and *dys-1*(*eg33*) strains possess nonsense mutations in different portions of the gene (Figure 1.4), we decided to cross our worm strain *myo-3p*::GFP::*pab-*

1::3xFLAG (*wt* PAP) with both of these strains (Figure 3.1, Figure 3.2). The two new strains were named DP1 (*dys-1*(*eg33*;PAP) and DP2 (*dys-1*(*cx18*);PAP).

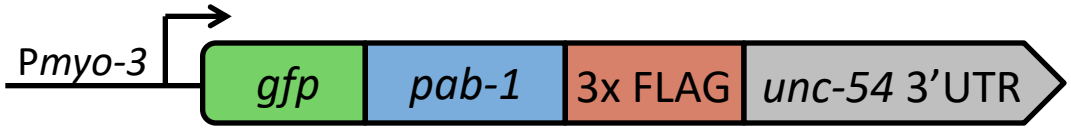

Figure 3.1: PolyA-Pull Expression construct. The worm ortholog of cytoplasmic polyA binding protein (PABC1), or *pab-1* in worms is fused to GFP on the 3' end as a marker of expression, and a 3X FLAG tag on the 5' end for isolation of the protein using anti-FLAG beads. The 3' UTR of unc-54 is used to ensure that the expression of the PAP construct is not inhibited by miRNA targeting. The PAP cassette is placed under the control of the *myo-3* promoter. *myo-3* is the *C. elegans* ortholog of myosin heavy chain types 6 and 7 in humans and drives the expression of the PAP cassette exclusively in the body wall muscle.

To confirm the presence of the nonsense mutations in the *dys-1* gene in the crossed F1 worms that were GFP-positive in the muscle, we sequenced these mutations using Sanger sequencing (Figure 3.2). We also used a PCR approach to confirm the genomic integration of the PAP construct in the MosSCI locus [186] in both DP1 and DP2 strains (Figure 3.2). In order to further validate our cross, we subjected these worm strains to a Kaplan-Meier survival analysis (Figure 3.3). The average lifespan of N2 worms in this experiment is approximately 21 days, and both new strains behave similarly to their reciprocal pre-crossed strain, with their lifespan drastically declining at day 18, an overall increase in lethality when compared to *wt* worms (Figure 3.3). These two new strains also retain the head bending phenotype (Figure 3.4). Taken together these results suggest that we successfully crossed both dystrophin-deficient strains with our *wt* PAP strain and that the DP1 and DP2 strains

reflect the phenotypes already characterized in the literature before and after our crosses, suggesting our PAP construct did not interfere with the *dys-1* phenotype.

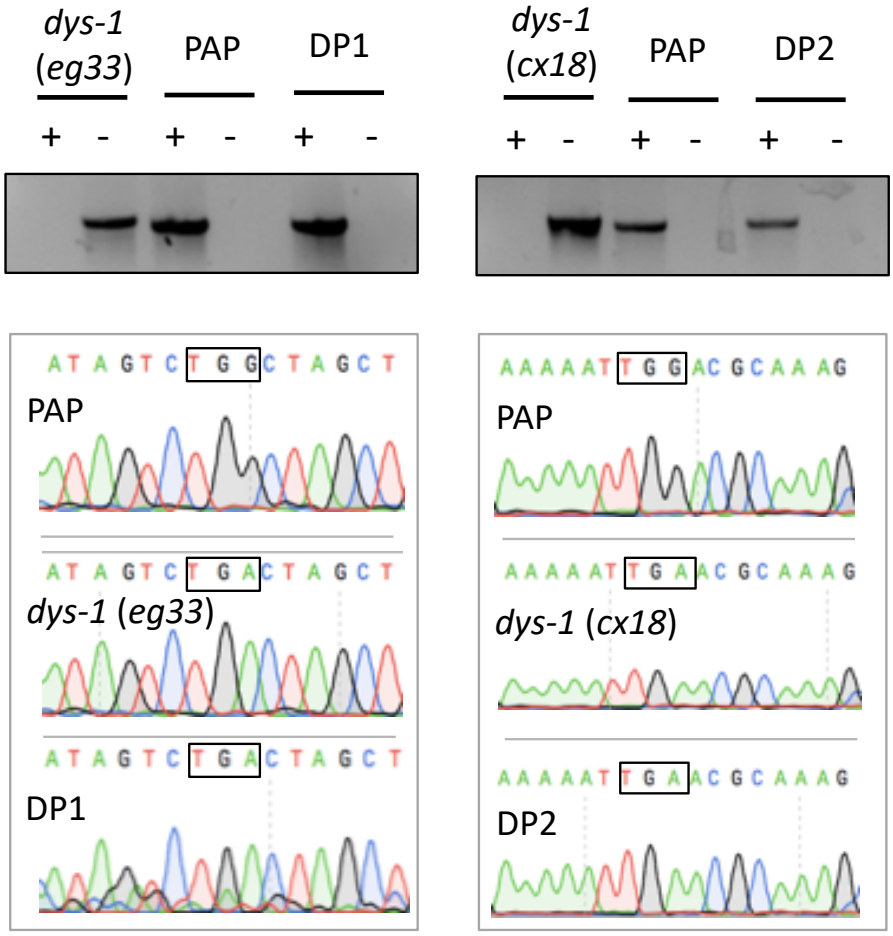

Figure 3.2: Confirmation of establishment of DP1 and DP2 transgenic strains. DP1 and DP2 strains retain *cx18* and *eg33* mutations after being crossed with our *wt* PAP strain. Top Panel: PCR analysis from genomic DNA extracted from *dys-1*(*eg33*), *dys-1*(*cx18*), DP1, DP2, and *wt* PAP strains. "+" denotes primers pairs that confirmed the presence of a single copy integrated construct, and "-" denotes primers pairs that confirmed the absence of an integrated PAP construct (red asterisks mark the presence of the integrated construct). Bottom Panel: trace files produced from the sequencing of the *dys-1* locus confirmed the presence of the nonsense mutation in both DP1 and DP2 strains (black squares).

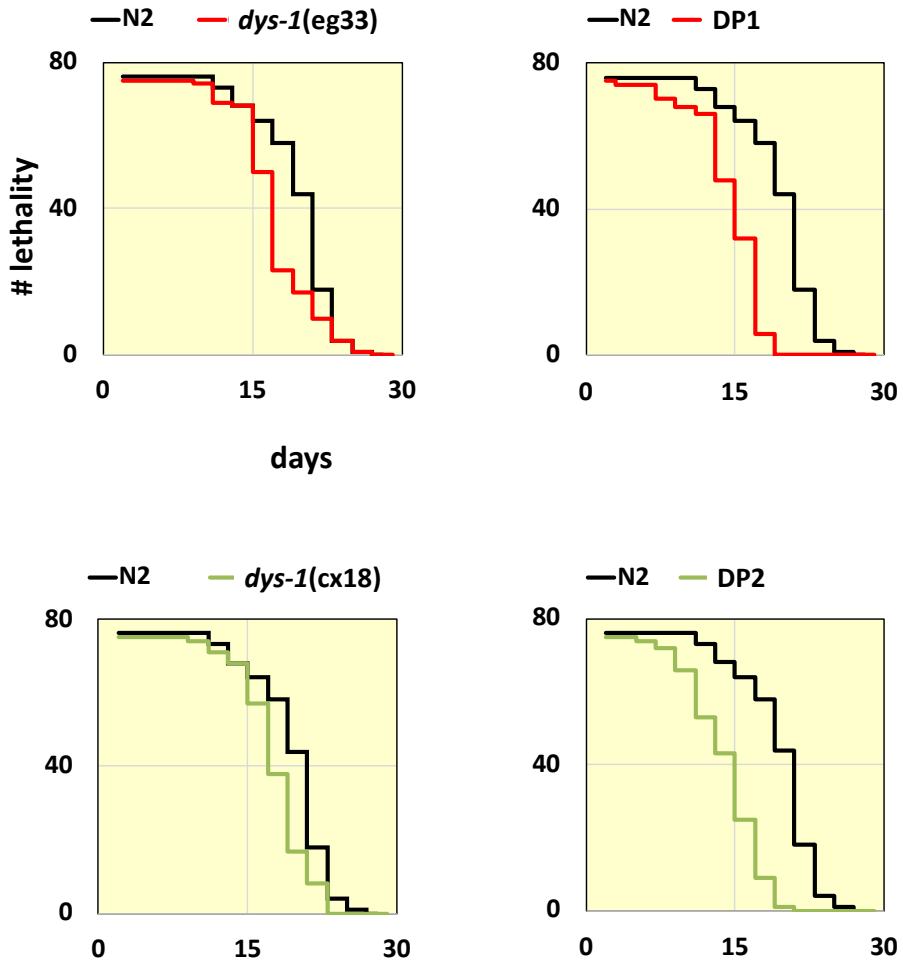

Figure 3.3: Kaplan Meier survival analysis. Survival curves were performed on *dys-1(cx18)*, *dys-1(eg33)*, DP1, and DP2 to confirm the effects of dystrophin deficiencies and the PAP cassette on lifespan. Each graph represents the average percent lethality for 75 worms per control and experimental strain. Left Panels compare both *dys-1* strains to *wt* strains. Right Panels compare both *dys-1* strains after crossing with *wt* strains containing our PolyA-pull (PAP) constructs.

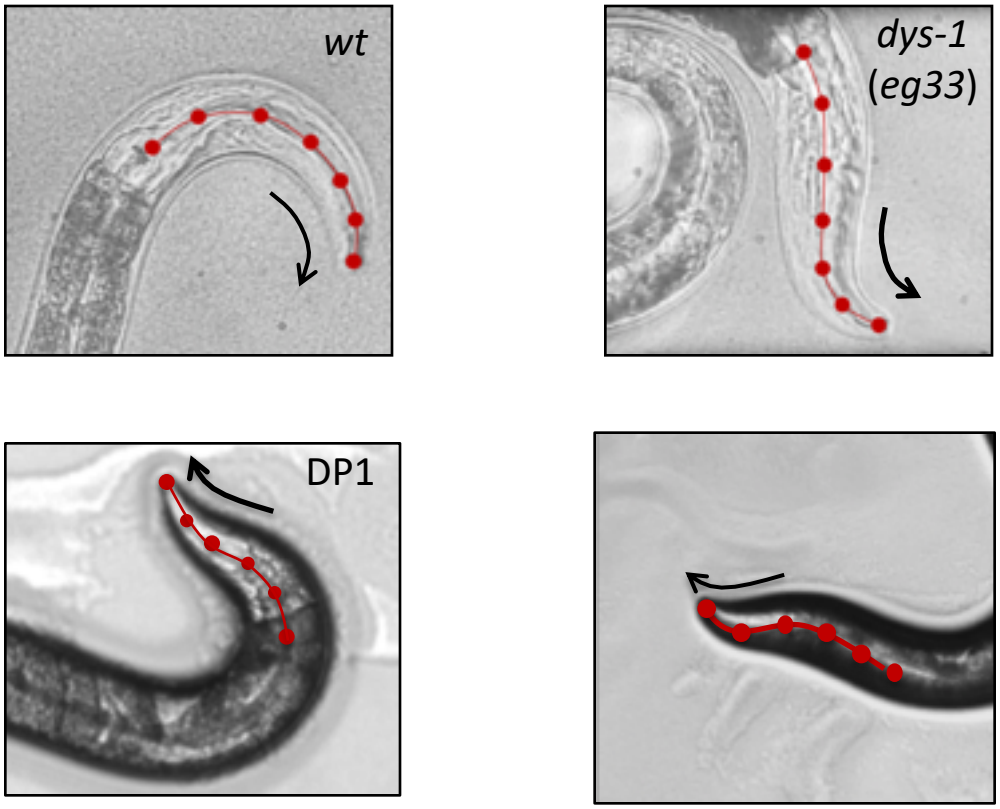

Figure 3.4: DP1 and DP2 strains retain head bending phenotype. *dys-1* strains *dys-1(cx18) and dys-1(eg33)* exhibit a head bending phenotype. *wt* head bending coincides with direction of movement (black arrows), while *dys-1* head bending opposes direction of movement. This head bending phenotype is retained in DP1 and DP2 strains after crossing the *dys-1*(*eg33*) and *dys-1*(*cx18*) strains with the *wt* PAP strain.

We next performed the PAT-Seq experiments, isolating and sequencing muscle-specific mRNAs from DP1 and DP2 strains (Figure 3.5). We wanted to detect precise changes in gene expression, not only in later developmental stages but also before the onset of the disease was initiated, to have a more comprehensive overview of the dynamic gene changes occurring during the initiation and the progression of the disease. In addition, we wanted to reduce our sample number to simplify the data analysis and increase the depth of our sequencing results. Therefore, we grew large mixed populations of our DP1, DP2 and

control *wt* PAP and *dys-1* strains, and then performed sequential mechanical filtrations by size, which led to the isolation of two pools of worms for each strain: one containing embryo-L2 worms, which we labeled 'pre-symptomatic' (PRE), and another containing L3-adult worms, which we labeled 'post-symptomatic' (POST) (Figure 3.5).

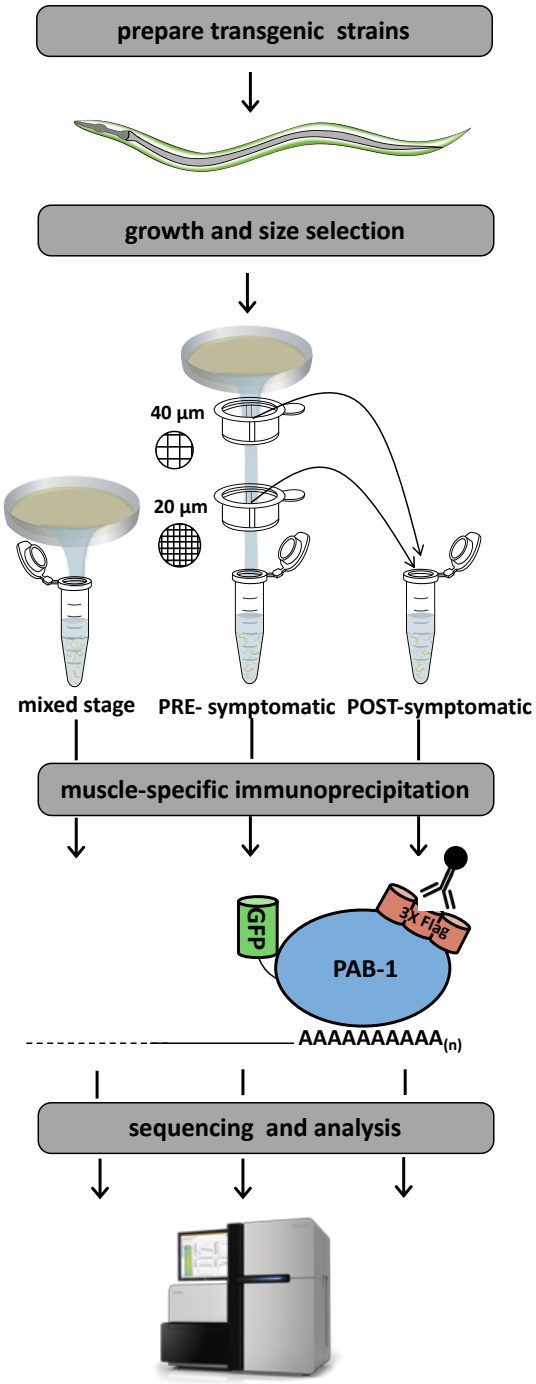

Figure 3.5: Experimental pipeline used to isolate PRE and POST symptomatic muscle-specific transcriptomes. Transgenic strains expressing the PAP cassette in a *dys-1* genetic background were established. These strains were subjected to mechanical filtration to obtain PRE and POST symptomatic populations. These populations were crosslinked, and immunoprecipitations were performed using α-FLAG beads. mRNA transcripts were released from bound, flag-tagged PAB-1 protein and sequenced.

We immunoprecipitated, sequenced and analyzed mRNA from mixed stage populations, PRE and POST symptomatic populations from DP1 and DP2 mutant strains, and PRE and POST symptomatic populations from our *wt* PAP strain (16 immunoprecipitations total, see Experimental). To confirm the specificity of our immunoprecipitations, cDNA was synthesized from RNA obtained from one of our mixed-stage samples. PCRs were then performed using three primer sets that bound within tissue specific genes in the muscle *(myo-3)*, intestine (*ges-1*), and cuticle (*dpy-7)*. In control cDNA samples, all three genes were detected. In cDNA from our tissue specific RNA-IP, there is detection of the muscle specific gene and depletion of the non-muscle genes (Figure 3.6).

We obtained approximately 900M reads across all our sequenced samples, with approximately 50M reads for each dataset (Table 3.1). Within these samples, we were able to map an average of 42% of all the obtained reads to the *C. elegans* genome (WS250) (Table 3.1). Both experimental and biological replicates in each dataset correlate well with each other (Figure 3.7), with ~2,000 shared protein-coding genes within each group (Table 3.2).

Sample			Total reads	Mapped (%)	Not mapped
dys-1(eg33)	PRE	experiment	61,331,245	16,458,692 (27)	44,872,553
		replicate	46,677,723	17,812,390 (38.1)	28,865,333
	POST	experiment	60,617,365	55,397,232 (91.39)	5,220,133
		replicate	45,052,554	40,638,981 (90.2)	4,413,573
PAP	PRE	experiment	60,136,874	25,824,737 (43)	34,312,137
		replicate	38,934,890	15,628,961 (40)	23,305,929
	POST	experiment	47,138,436	13,403,525 (28.5)	33,734,911
		replicate	35,399,372	15,437,939 (44)	19,961,433
DP1	PRE	experiment	74,708,361	6,519,607 (9)	68,188,754
		replicate	80,851,313	8,513,602 (10.5)	72,337,711
	POST	experiment	85,543,247	60,585,159 (70.8)	24,958,088
		replicate	76,252,221	49,950,579 (65.5)	26,301,642
DP2	PRE	experiment	86,493,693	16,895,535 (19.5)	69,598,158
		replicate	27,624,484	2,174,470 (8)	25,450,014
	POST	experiment	36,061,335	23,851,357 (66.1)	12,209,978
		replicate	29,015,306	17,706,345 (61)	11,308,961

Table 3.1: Summary of results from PAT-Seq after deep sequencing.

Sample			Genes	
dys-1(eg33)	PRE	experiment	3,394	2,603*
		replicate	3,416	
	POST	experiment	2,951	1,738*
		replicate	2,957	
PAP	PRE	experiment	2,864	1,712*
		replicate	2,996	
	POST	experiment	3,487	2,187*
		replicate	3,353	
DP1	PRE	experiment	2,078	1,100*
		replicate	2,176	
	POST	experiment	3,020	1,950*
		replicate	2,636	
DP2	PRE	experiment	2,415	1,640*
		replicate	2,454	
	POST	experiment	3,005	2,266*
		replicate	2,885	

Table 3.2: Summary of genes detected in this study. Raw reads derived from the mRNA libraries on the Illumina Hi-Seq Instrument, mapped to the C. elegans WS250 genome annotation. Genes marked with an asterisk correspond to genes detected in both biological replicates (fpkm>=4)

Our sequencing efforts detected 3,747 genes across all datasets (Table 3.2). Within these datasets, we were able to identify uniquely expressed genes in either PRE or POST datasets, or genes with an increase or decrease of at least 2-folds when compared with their respective negative controls (Figure 3.10).

47% of the total genes identified in this study have been previously mapped by our group in the *C. elegans* body muscle tissue (Figure 3.8) [182]. When we repeated this analysis

separately in either our PRE or POST datasets, this percentage increases to ~60% similarity, with >85% identity in our top 250 genes in all our datasets (Figure 3.8).

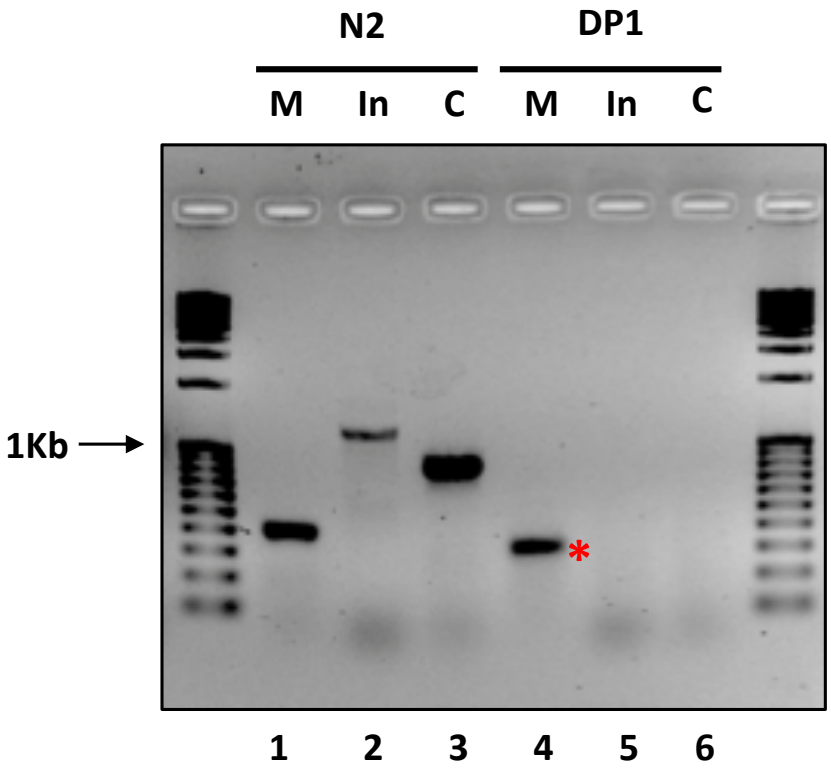

Figure 3.6: There is a depletion of non-muscle transcripts in cDNA synthesized from RNA extracted in PAT-Seq RNA precipitations. Quantification of the specificity and sensitivity of the pull-down experiments using genomic PCR (lanes 1, 2, and 3) and RT-PCR (lanes 4, 5 and 6). Using immunoprecipitation, we successfully isolate the muscle specific gene *myo-3* (lane 4) (*) from RNA from our DP1 strain, but not the intestine specific gene *ges-1* (lane 5) and the cuticle specific gene *dpy-7* (lane 6). Lanes 1, 2 and 3 show the expected band sizes of the genes tested.

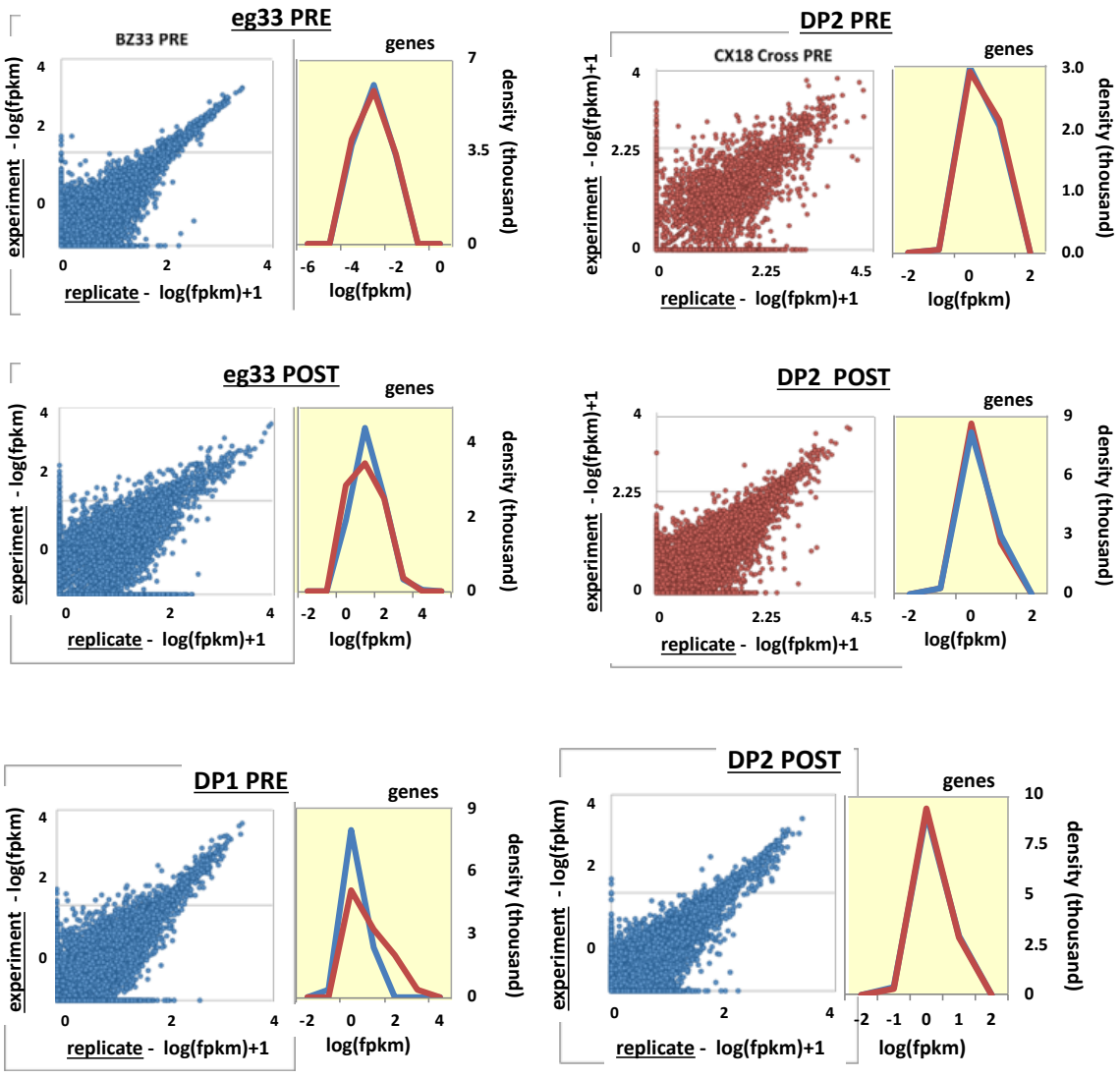

Figure 3.7: Correlation of biological replicates for each RNA-IP sample. Left panels: Scatter plot of mapped genes from eg33 PRE and POST, DP1 PRE and POST and DP2 PRE and POST datasets displayed by fpkm value detected in each replicate on a logarithmic (log10) scale, to highlight the similarity of detection between replicates. Right panels: The distribution of the fpkm values in experiment (red) and replicate (blue) samples for each dataset. The plots were generated using the cummeRbund package v. 2.0.

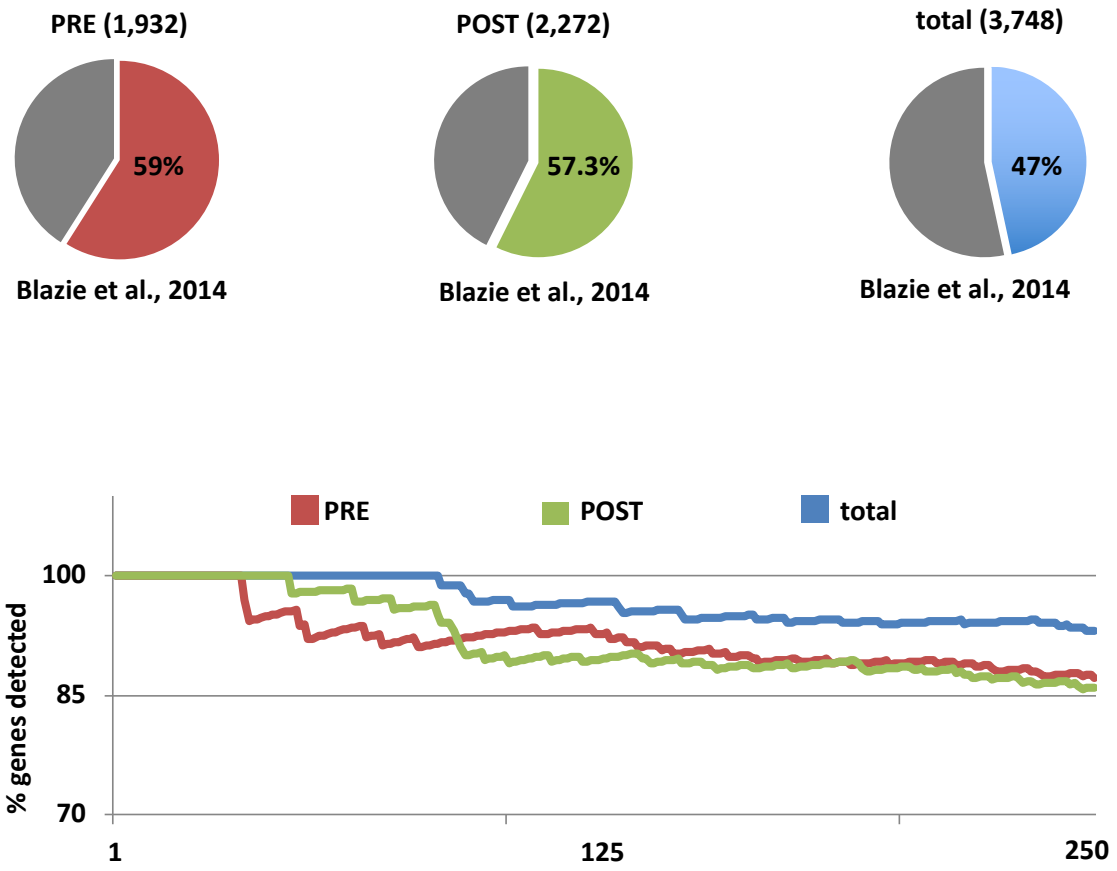

Figure 3.8: Comparative analysis of genes detected in our study versus body muscle-specific datasets from Blazie et al., 2014. The number of genes overlapping our PRE, POST, and a combined dataset (total) are summarized in the top panel. Genes identified in this study and the muscle-specific dataset from Blazie et al., are ranked by fpkm value, and the top 250 genes from both datasets are compared in the bottom panel.

Mitochondrial response is implicated in the initiation of symptoms in PRE datasets

Our PRE symptomatic dataset is primarily composed of embryo to L2 worms (Figure 3.5). We obtained 1,931 protein-coding genes expressed in this group, with 173 unique genes not expressed elsewhere. Within this group 957 genes have a human ortholog (49.5%) [187]. In order to identify changes in gene expression that occur in a *dys-1* background early in development, we compared our DP1 and DP2 PRE symptomatic datasets to corresponding *wt* PAP PRE symptomatic datasets. There are very few genes that change drastically in expression level between the *wt* PAP control and PRE dataset (Figure 3.9). A GO term analysis on the top 50 genes identified enrichment in genes involved in nematode larval development (Figure 3.11).

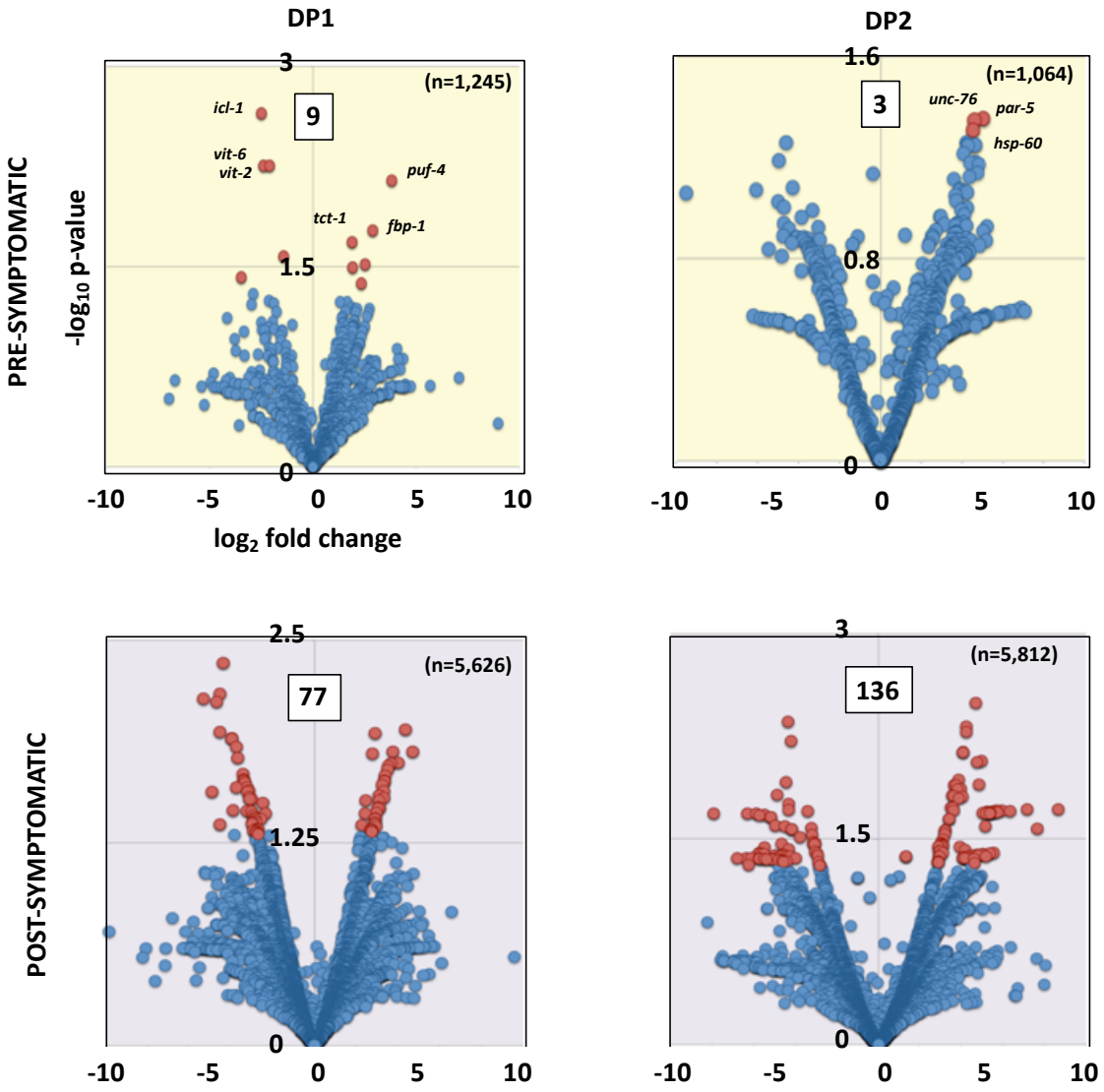

Figure 3.9: Differential gene expression analysis in PRE- and POST- symptomatic strains. We have studied the changes in gene expression for genes detected in both *wt* PAP, DP1, and DP2 strains. The volcano plots show the changes of gene expression between each strain (p-value versus fold-change). The total number of genes that significantly switch between PRE and POST symptomatic ($p<0.05$) are shown in red and boxed. The top genes identified in our PRE dataset are named in the chart. The density for the genes detected in the POST dataset prevents individual labeling. This analysis has been performed using the SAMtools suite (Li et al., 2009). The complete list of genes produced by this software is shown in Supplemental Table S4.

We detected an unusual abundance of mitochondrial genes involved in ATP production and regulation of apoptotic processes within the top hits identified in our DP1 and DP2 PRE datasets when compared to *wt* PAP PRE datasets (Figure 3.10, Figure 3.12). *ant-1.1* is an ADP/ATP translocase with a three-fold increase over the median between DP1 and DP2 datasets (when compared with the wild type PRE dataset) (Figure 3.12). This mitochondrial membrane receptor is responsible for transporting ATP synthesized from oxidative phosphorylation into the cytoplasm and absorbs back ADP in a 1:1 molar ratio [188,189].

In addition to this gene, we also detected gene expression changes in the genes Y69A2AR.18 (5-fold), F58F12.1 (3-fold), *icd-1* (2.5-fold), H28O16.1 (2-fold), *atp-3* (2-fold), which are all mitochondrial ATP synthase subunits involved in the synthesis of ATP from ADP and inorganic phosphate (Figure 3.10).

~200 genes are instead downregulated in both our DP1 and DP2 PRE datasets (Figure 3.10). Many of these genes are also mitochondrial genes, including *Icl-1*, *nduo-4*, *nduo-5*, *cytb-5.2*, *mev-1*, *rad-8*, *atp-4* and Y82E9BR.3 (Figure 3.9, Figure 3.10, Figure 3.12).

Importantly, our approach detected only 173 genes present in the PRE dataset and absent in its *wt* PRE control dataset. 43% of these genes have a human homolog [187]. These genes most likely reflect the initiation of the disease, but most of them have an unknown function. When aligned to the human proteome, many of them show significant matches to known human genes. *smo-1* is among those significantly abundant. *smo-1* is the *C. elegans* homolog of SUMO, a small ubiquitin-like signaling modifier that is attached to proteins dictating localization and function.

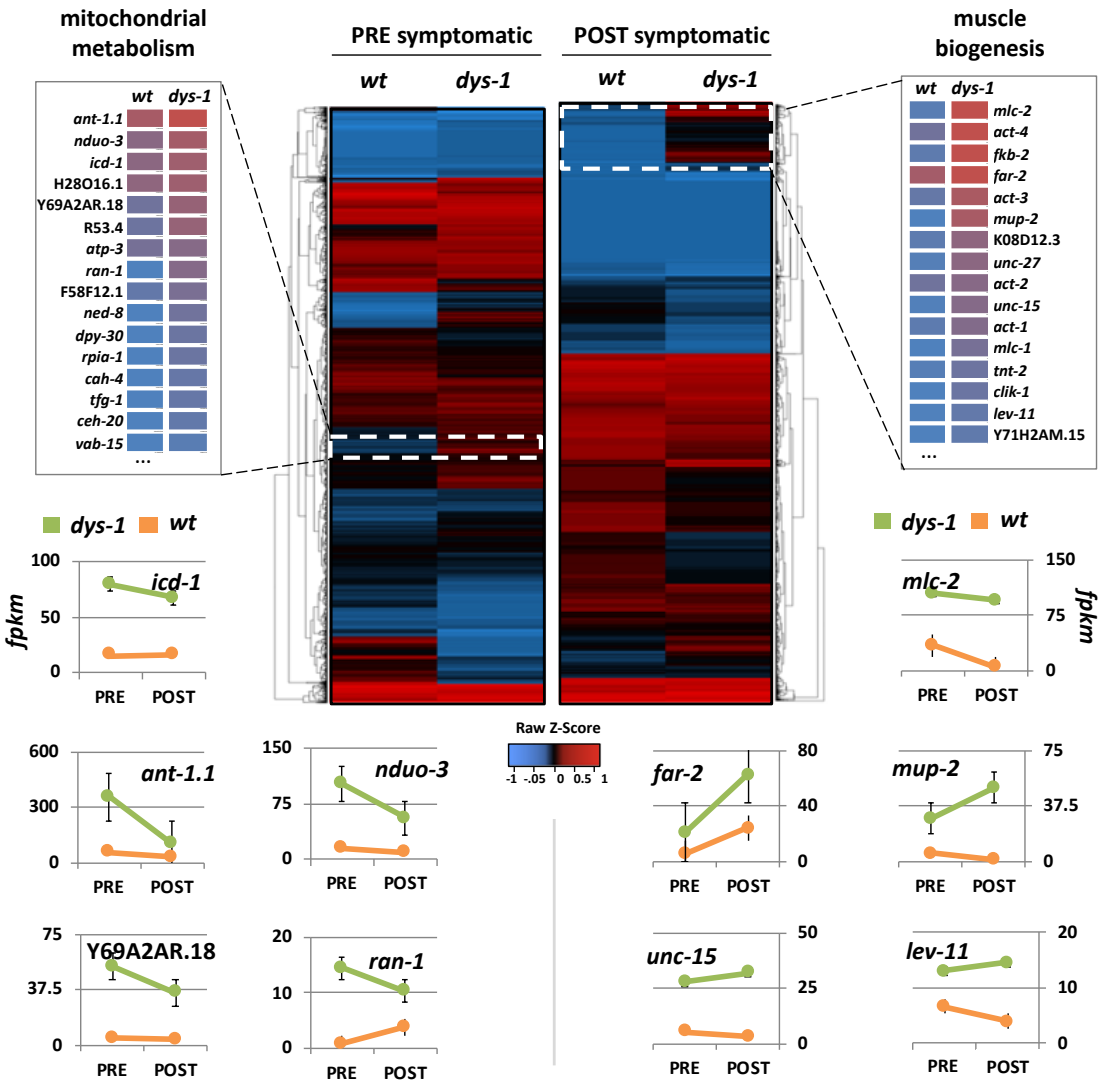

Figure 3.10: Heat map summarizing the average change in gene expression of DP1 and DP2 strains as compared to the *wt* PAP strain. White boxes in the heat map mark genes that were upregulated in DP1 and DP2 strains in PRE and POST datasets. The framed gene-lists highlight the change in expression level for selected genes based on function (mitochondrial metabolism or muscle biogenesis) and their rank in our datasets. Below the heat maps, the change in expression level (FPKM) between PRE and POST symptomatic stages of selected genes are graphed linearly (green: median between DP1 and DP2; orange: wild type). "*wt*" refers to *wt* PAP, "*dys-1*" refers to an average of DP1 and DP2 scores.

PRE symptomatic

id	description	q-value	hits	total
GO:0005739	mitochondrion	6.96E-10	20	136
GO:0015992	proton transport	1.85E-03	5	11
GO:0044281	small molecule metabolic process	2.24E-03	16	229
GO:0006818	hydrogen transport	2.24E-03	5	12
GO:0003012	muscle system process	5.76E-03	7	42
GO:0006937	regulation of muscle contraction	1.05E-02	5	20
GO:0010941	regulation of cell death	1.44E-02	7	56
GO:0046034	ATP metabolic process	1.51E-02	5	24
GO:0015672	monovalent inorganic cation transport	1.51E-02	6	39
GO:0042981	regulation of apoptotic process	2.69-E02	5	29

POST symptomatic

id	description	q-value	hits	total
GO:0005856	cytoskeleton	1.29E-07	18	153
GO:0043292	contractile fiber	2.50E-05	5	11
GO:0046034	ATP metabolic process	4.90E-05	5	20
GO:0046034	ATP metabolic process	4.90E-05	7	24
GO:0005739	mitochondrion	1.27E-04	7	56
GO:0030239	myofibril assembly	1.67E-04	16	229
GO:0055001	muscle cell development	2.07E-04	5	12
GO:0051146	striated muscle cell differentiation	2.07E-04	13	145
GO:0061061	muscle structure development	3.34E-04	14	178
GO:0042692	muscle cell differentiation	4.44E-04	13	158

Figure 3.11: Different signaling pathways are affected in PRE and POST symptomatic samples. GO term analysis of the top 50 genes uniquely present either in our PRE or POST datasets showed enrichment in genes involved in mitochondria metabolism (PRE) and muscle biogenesis (POST).

		PRE			POST		
		WT	*dys-1*	Fold Increase	WT	*dys-1*	Fold Increase
NADH-coenzyme Q Oxidoreductase (complex I)							
F31D4.9	NDUFA1	0.19	1.545	**8.13**	-	-	-
C33A12.1	NDUFA5	0.36	1.93	**5.36**	-	-	-
nuo-3	NDUFA6	1.46	3.14	**2.15**	2.55	2.44	**0.96**
F45H10.3	NDUFA7	-	-	-	0.71	1.115	**1.57**
Y54F10AM.5	NDUFA8	0.78	1.71	**2.19**	-	-	-
F37C12.3	NDUFAB1	-	-	-	0.46	1.15	**2.5**
B0334.5	NDUFAF6	-	-	-	0.11	1.255	**11.41**
F59C6.5	NDUFB10	0.55	1.23	**2.24**	1.22	1.06	**0.87**
F42G8.10	NDUFB11	0.62	2.165	**3.49**	-	-	-
F44G4.2	NDUFB2	-	-	-	0.16	1.425	**8.91**
C18E9.4	NDUFB3	-	-	-	1.04	0.47	**0.45**
nuo-6	NDUFB4	0.18	1.22	**6.78**	0.21	1.465	**6.98**
D2030.4	NDUFB7	-	-	-	0.15	1.495	**9.97**
C16A3.5	NDUFB9	0.85	1.725	**2.03**	0.52	1.78	**3.42**
Succinate Dehydrogenase (complex II)							
mev-1	Cytochrome b560 subunit	5.22	2.17	**0.42**	2.33	3.195	**1.37**
sdha-1	Subunit A, Flavoprotein	-	-	-	0.29	1.005	**3.47**
sdhb-1	Subunit D, Flavoprotein	1.12	1.025	**0.92**	0.36	1.11	**3.08**
sdhd-1	Subunit B, Flavoprotein	0.67	4.305	**6.43**	1.01	2.725	**2.7**
Q-Cytochrome c oxidoreductase (complex III)							
Y71H2AM.5	COX6B2	0.89	6.15	**6.91**	0.14	3.045	**21.75**
F26E4.6	COX7C	2.05	7.825	**3.82**	0.1	2.02	**20.2**
cyc-1	Cyc-1	1.18	0.745	**0.63**	0.52	2.205	**4.24**
cyc-2.1	Cyc-2.1	15.09	11.975	**0.79**	1.31	6.855	**5.23**
Cytochrome C Oxidase (Complex IV)							
W09C5.8	COX IV	12	19.68	**0.79**	1.31	6.855	**5.23**
ATP Synthase (Complex V)							
H29O16.1	Alpha subunit	18.73	37.57	**2.01**	8.4	47.64	**5.67**
atp-2	Beta subunit	8.89	12.3	**1.38**	4.49	13.02	**2.9**
F58F12.1	Delta subunit	2.56	7.205	**2.81**	0.93	5.135	**5.52**
ASG-2	Gamma subunit	1.11	3.945	**3.55**	0.6	1.18	**1.97**
atp-3	ATP50	5.99	12.32	**2.06**	2.89	10.43	**3.61**
Y82E9BR.3	ATP5G1	72.31	67.215	**0.93**	12.94	37.875	**2.93**
atp-5	ATP5H	1.78	3.885	**2.18**	1.9	5.9	**3.11**
Y69A2AR.18	ATP5C1	4.62	26.625	**5.76**	3.91	17.74	**4.54**
ATPase Translocase							
ant-1.1	Adenine nucleotide transporter	57.36	178	**3.1**	29.29	51.02	**1.74**

Figure 3.12: Summary of Trends in Mitochondrial Gene Expression

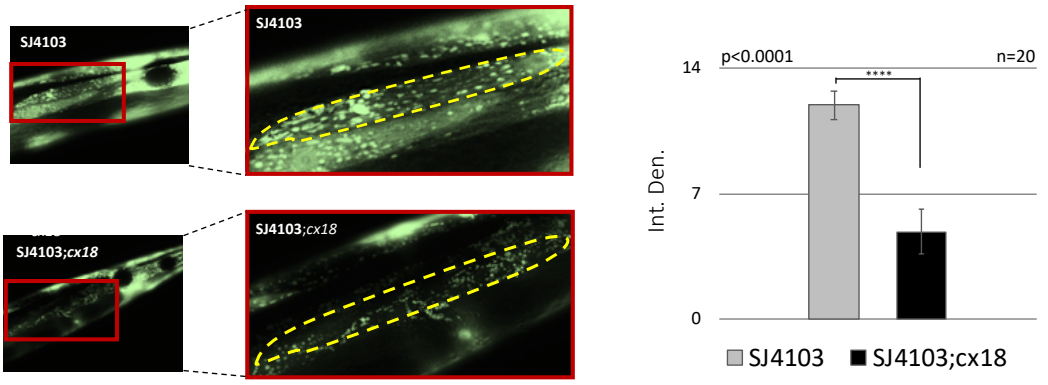

Figure 3.13: Loss of DYS-1 induces decreased mitochondria localization in the muscle. Left panel: Fluorescent of body muscle specific mitochondrial fluorescence in SJ4103 strains in *wt* and *dys-1(cx18)* genetic backgrounds. Enlargements expand the single muscle cell at the base of the pharynx (yellow). Right Panel: quantification of the average brightness (integrated density) of body muscle specific mitochondria in SJ4103 strains in *wt* and *dys-1(cx18)* genetic backgrounds.

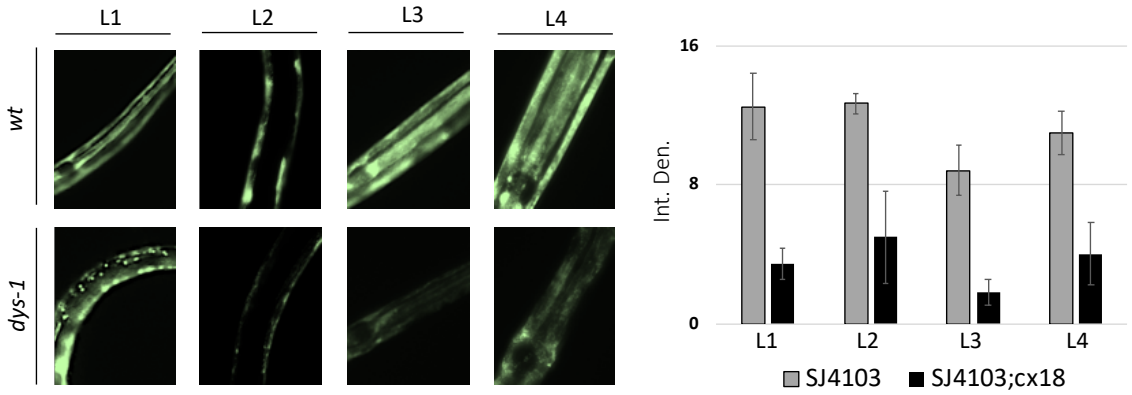

Figure 3.14: Loss of DYS-1 induces decreased mitochondria localization throughout development. Left Panel: Body muscle specific mitochondrial fluorescence in each developmental stage decreases in the *dys-1(cx18)* strain. Right Panel: Quantification of the relative brightness. n=27

Mitochondrial abundance is disrupted in the absence of functional dystrophin

We were intrigued by the presence of a large number of genes involved in apoptosis and mitochondria metabolism in both our DP1 and DP2 PRE and POST datasets as compared to their corresponding *wt* PRE and POST datasets (Figure 3.12), and decided to further study and validate these findings using a different genetic approach. We crossed the *dys-1*(*cx18*) strains with the SJ4103 strain, which restricts the expression of GFP in mitochondria of body muscle tissue [190] and used the resultant new strain to study if the loss of *dys-1* alters the abundance of muscle mitochondria throughout development. This new strain (SJ4103;*cx18*) is still hyperactive, presents the same head bending phenotype observed in the *dys-1*(*cx18*), and displays significantly less mitochondria localized in the body muscle cells (Figure 3.13). Loss of mitochondria in the body wall muscle was also detected throughout development (Figure 3.14). Importantly, the loss of muscle mitochondria is DAPC-dependent, as it can be recapitulated through the silencing of *dys-1* or other members of the dystrophin complex using RNA interference (Figure 3.15). Interestingly, the knockdown of these same members of the *C. elegans* DAPC with RNA interference did not induce a head bending phenotype in all cases (Figure 3.16). Instead, a head bending phenotype was observed only for the knock down of *dys-1* and *dyb-1*. This suggests that each of these proteins plays an important role within the muscle and the DAPC, but *dyb-1* and *dys-1* likely play closely related roles in the muscle. One hypothesis to explain this is result is that the DYS-1 protein potentially binds directly to DYB-1, similar to the manner in which the human dystrophin protein binds to ß-dystroglycan in the human DAPC. In this light, the knockdown of either *dys-1* or *dyb-1* would sever the connection between the two proteins and induce a head bending phenotype.

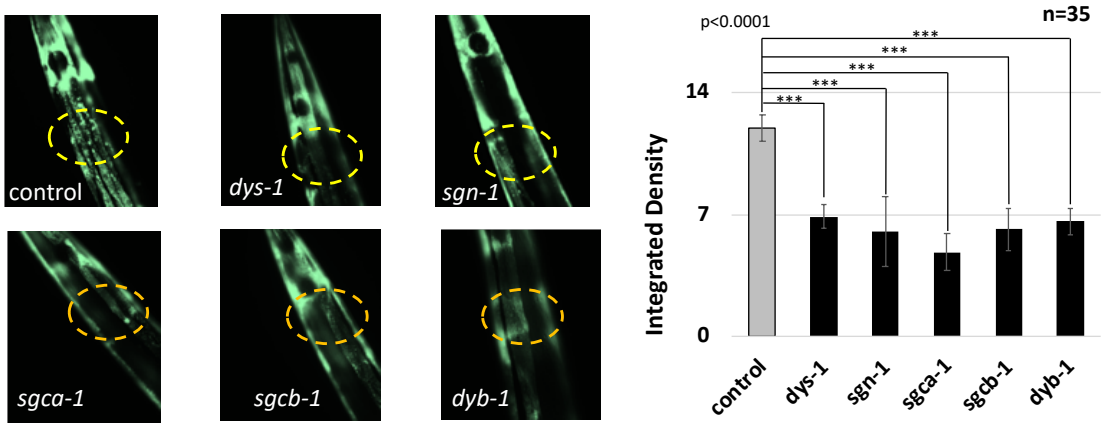

Figure 3.15: Knockdown of five core members of the *C. elegans* DAPC is able to induce decreased mitochondrial abundance in the body muscle. Known members of the DAPC were knocked down using RNAi in SJ4103 strains, and brightness of mitochondrial fluorescence was quantified as average integrated density using ImageJ analysis. Representative images for each gene knockdown are pictured in the left panel and the quantification is displayed in the right panel ($p<.0001$ t-test).

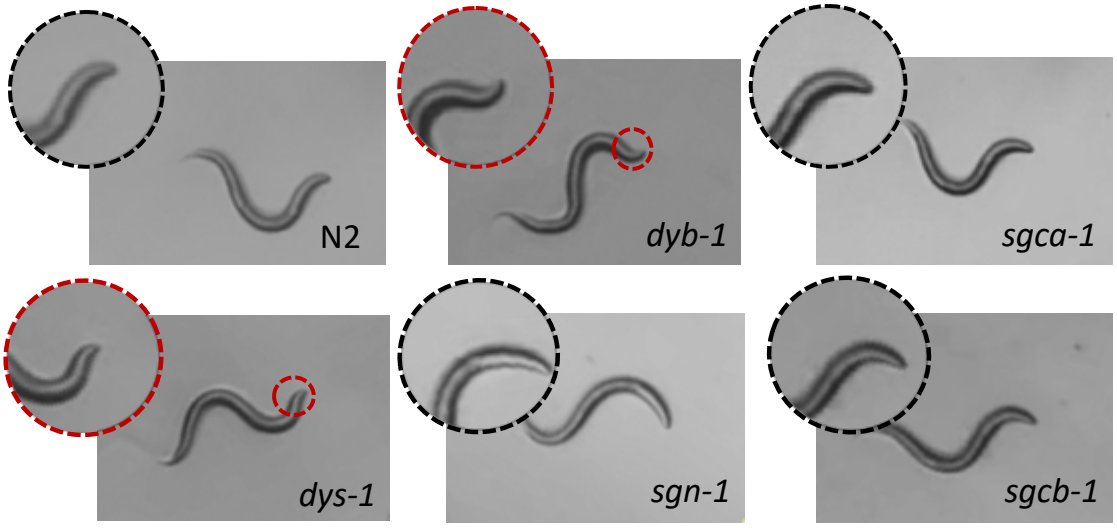

gene name	aberrant head bending	*wt* head bending
RNAi control	-	✓
dys-1	✓	-
dyb-1	✓	-
sgn-1	-	✓
sgca-1	-	✓
sgcb-1	-	✓

Figure 3.16: The knockdown of some, but not all members of the *C. elegans* DAPC is able to induce head bending phenotypes. Performing RNAi on five members of the DAPC, including *dys-1*, revealed that only two members of the DAPC, dystrophin (*dys-1*) and dystrobrevin (*dyb-1*) is able to induce a head bending phenotype.

Genes involved in myogenesis and muscle contraction are abundant in the POST dataset

In order to identify trends in gene expression that occur later in development in a *dys-1* background, we compared our DP1 and DP2 POST datasets to the corresponding *wt* POST datasets. In our POST dataset we detected 2,273 protein-coding genes across both DP1 and DP2 strains. Within this group 1,148 genes have a human ortholog (50%) [187]. Only 58% of genes are shared with the PRE dataset (Figure 3.10). This discrepancy is

probably consistent with the progressive nature of the disease, and the associated destructive changes in muscle structure and overall health.

Essential constituents of the mitochondrial metabolism are also overexpressed at this stage, although at lower levels than in our PRE dataset. They include the mitochondria ATP synthase *Icd-1*, *ant-1.1*, H28O16.1, Y69A2AR.18, *atp-2* and *atp-3*, *nduo-1* (NADH-ubiquinone oxidoreductase), W09C5.8 (cytochrome c oxidase) (Figure 3.10).

The most abundant class of genes in this stage are involved in myogenesis. This includes *mlc-1* and *mlc-2* (myosin light chain), *mup-2* (troponin), *act-1* (actin), *unc-27* (troponin), *lev-11* (tropomyosin), and *unc-15* (paramyosin) (Figure 3.10, Figure 3.11). This result is consistent with muscle hypertrophy or active replacement of muscle in humans and is in line with previous studies in worms which show marked hypertrophy and increased myofibril diameter following high intensity muscle exertion through burrowing [191]. In this context, the increase in transcription we observed may suggest a hidden compensatory signaling pathway activated in the absence of *dys-1* that precedes cell death. We chose to explore this trend in our sequencing results in detail, as changes in muscle structure have been reported as the mostly likely contributor to the *dys-1* phenotype in surrounding literature [131].

To further validate the translational value of these findings, the expression level of orthologs of some of the most significantly upregulated genes evaluated in wild-type and *mdx/utr* $^{-/-}$ satellite cells. Cells were cultured first in growth medium and then differentiation medium (see Experimental). After the formation of multinucleated myotubes, total RNA was extracted and used for cDNA synthesis. cDNA was used as a template for RT-qPCR analysis of mRNA expression levels for cardiac troponin T (TNNT2), myosin regulatory light chain 2 (MYLPF), and α-actin (ACTA1). It was found that expression levels of ACTA1

did not coincide with our results, and was significantly downregulated in *mdx/utr*$^{-/-}$ satellite cells when compared to wild-type satellite cells (Figure 3.17). However, the expression levels of TNNT2 and MYLPF reflect the trends identified in our PAT-Seq results and were significantly upregulated in *mdx/utr*$^{-/-}$ satellite cells when compared with wild-type satellite cells (Figure 3.17).

Previous works have shown that interactions between DYS-1 and other structural proteins at the dense body including DYC-1 are essential in muscle adhesion and structure, and severing this interaction potentially leads to degradation of the sarcomere and muscle structure [131]. Of note, when we overexpressed the *C. elegans* homolog dystrobrevin (*dyb-1*) in *dys-1*(*cx18*), we detected an intact DAPC in the body muscle in our POST symptomatic worms (Figure 3.18), suggesting that in *C. elegans*, the presence of a full length DYS-1 protein may be dispensable for the assembly of the DAPC.

Collectively, ~250 genes were significantly downregulated in our DP1 and DP2 POST datasets (Figure 3.10). *Unc-22* encodes "twitchin", a protein required for proper assembly of thick filaments into A-bands, and regulation of myosin activity [192,193] and is 2-times less abundant in our POST datasets when compared with our negative control. B0336.3, an ortholog of human RBM26/27 involved in body morphogenesis and striated muscle myosin thick filament assembly, is 3-times less abundant in our POST datasets when compared with our negative control. The muscle genes *ins-14*, *aex-5* and *ttn-1* were also found downregulated in this analysis (Figure 3.10).

Only 38 genes are uniquely present in our POST dataset. The majority of these genes have unknown functions. 11 of these genes (29%) have a human ortholog [187].

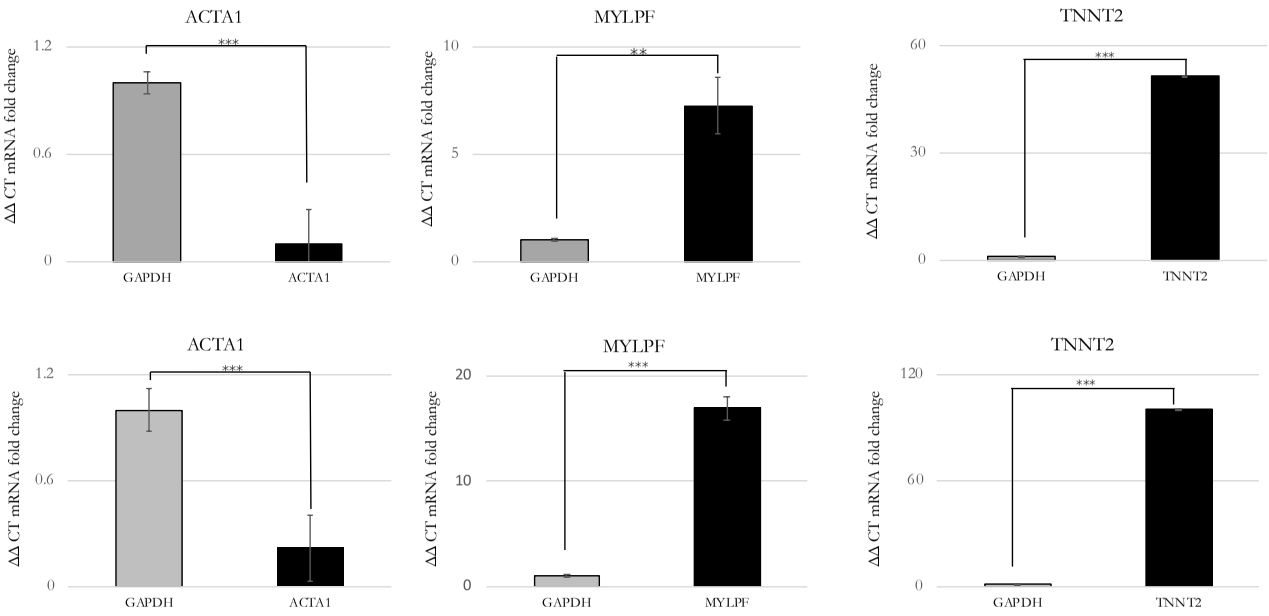

Figure 3.17: qPCR to measure relative fold increase of mRNA in *mdx-/-utr-/-* mice. The relative changes in mRNA expression levels for mouse orthologs of three genes that were significantly upregulated in POST symptomatic sequencing results were measured using RT-qPCR. Top and bottom panels represent two biological replicates. Displayed values represent the average of three technical replicates. All samples were normalized to GAPDH. The genes targeted were alpha-actin1 (ACTA1), myosin light chain. Phosphorylated (MYLPF), and troponin T (TNNT2).

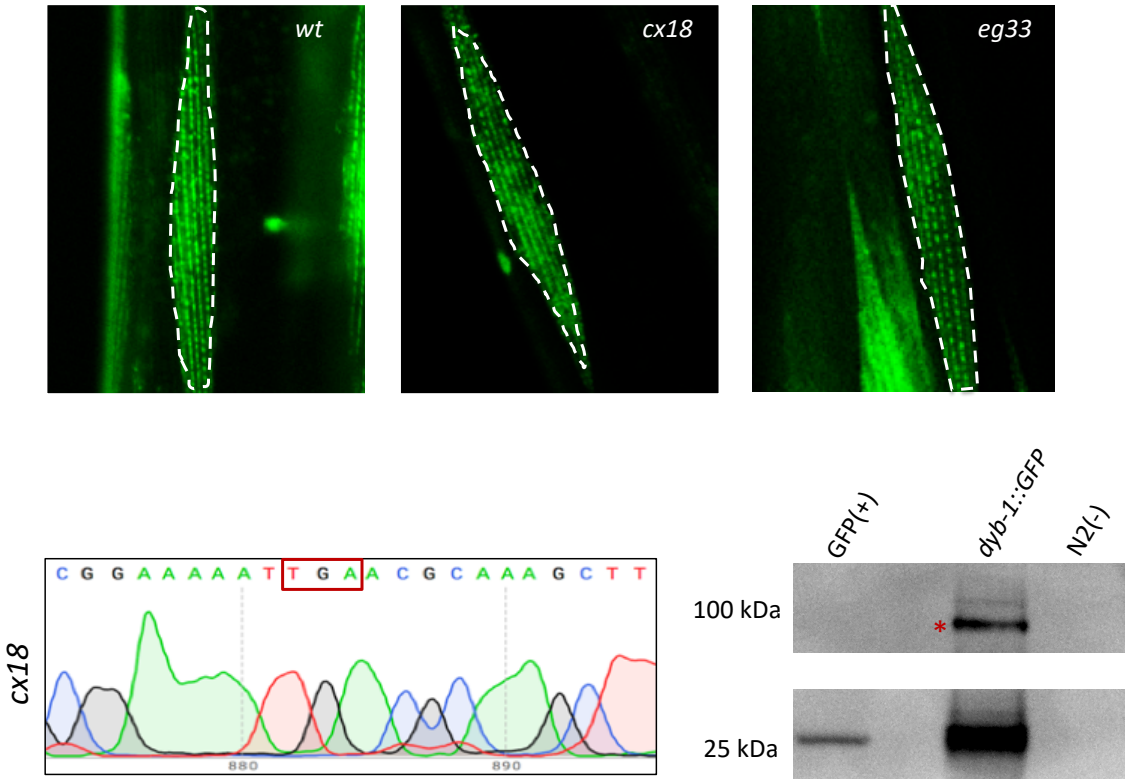

Figure 3.18: *dyb-1* assembles within the DAPC in the absence of *dys-1*. Top panel: Fluorescent images showing localization pattern of *dyb-1::GFP* along muscle fibres in *wt* and *dys-1*(cx18) genetic backgrounds. A single muscle cell in each strain is outlined in white to indicate regions being compared between images. Bottom panel: trace file in bottom left panel depicts the presence of the expected premature stop codon in the *cx18; dyb-1::GFP* strain. Western blot results in bottom right panel show predicted protein size of *dyb-1::GFP* fusion at 96 kDa (highlighted with a red asterisk).

Aberrant splicing events are pervasive in the POST symptomatic dys-1(eg33) strain

A recent study identified alternative splicing defects in transcriptomes from myotonic dystrophy skeletal muscle and heart [193]. To investigate whether this phenomenon may be present in DMD as well, we first examined our *dys-1(eg33)* POST datasets for changes in expression of genes related to splicing. Several SR proteins (*SRP-1*,

SRP-2, *SRP-3*, and *SRP-5*) and snRNPs (*SNR-1*, *SNR-2*, *SNR-5* and *SNR-6*) showed at least 2-fold increase or decrease in expression levels in our PRE and POST datasets, when compared to their respective wild type controls (Figure 3.19). SR proteins and snRNPs are splicing factors involved in both constitutive and alternative RNA splicing and function in a dosage-dependent manner, meaning that their relative abundance dictates different splicing events [194]. Since the expression levels of these genes were particularly altered in our PRE and POST datasets, we decided to test if defects in RNA splicing were also present in these stages. For this analysis, we focused on our *dys-1*(eg33) strain.

We mapped 26,692 changes in splicing junction usage in this mutant strain in both our PRE and POST muscle transcriptomes when compared to our PRE and POST control datasets respectively (Figure 3.19). Within this pool we detected extensive differences in splice junction usage in our DP1 strain (Figure 3.19). 10% of these identified RNA splicing junctions (1,413) used novel acceptors and donors, and many of these occur with more than 2-fold-change in our PRE and POST datasets (Figure 3.19).

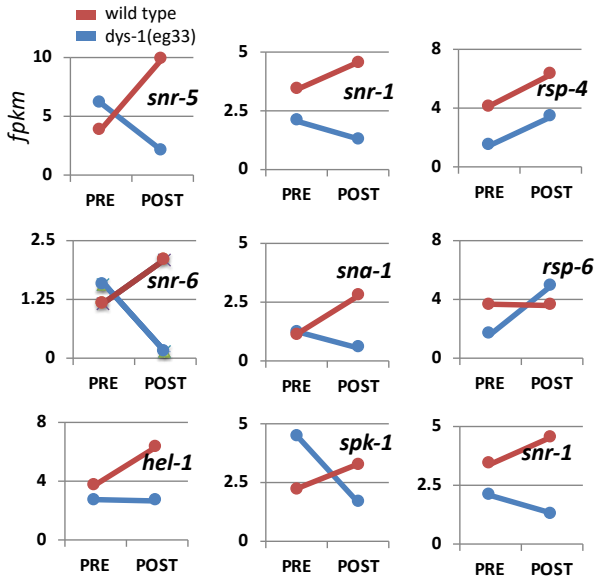

n=26,692

# of novel splice junctions				
	known	novel		
		inclusion	exclusion	aberrant
PRE	14,131	192	73	474
POST	11,040	241	127	939
total	25,171	433	200	1,413

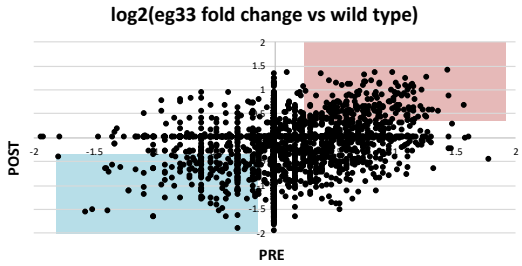

Figure 3.19: PAT-Seq results uncover splicing defects in the *dys-1(eg33)* strain. Top panel: change in gene expression identified in 9 snRNPs and SR genes from our PRE and POST datasets. Middle panel: total number of novel splice junction identified in this study. Bottom panel: Analysis of splice junction usage in the DP1 dataset. The graph illustrates the changes in splice junction abundance. The x-axis represents the fold-change of the number of reads for each splice junction comparing the PRE dataset to wild type, while the y-axis represents the fold change obtained when comparing DP1 POST dataset to wild type. Splice junctions with more than 2-fold enrichment in both datasets are highlighted in red, while splice junctions with 2-fold depletion in both datasets are highlighted in blue.

Transcriptomes of dys-1(eg33) and dys-1(cx18) are similar but not identical

We then decided to study the variability in gene expression present between the two *dys-1* strains. A recent study [170] found that the *dys-1*(*eg33*) strain is more clinically relevant than *dys-1*(*cx18*) for muscular dystrophy studies in *C. elegans*. The *dys-1*(*eg33*) strain is weaker than *dys-1*(*cx18*) strain and its wild-type counterparts [170]. This mutant strain exhibits impaired thrashing in liquid and strong mitochondrial network fragmentation in the body wall muscles [170]. Although the molecular mechanisms responsible for these phenotypic

differences are not yet known, it is possible that the difference in location of the mutation in the *dys-1* gene could be a contributor. These differences could be explained by the presence of different genetic programs executed in the muscles of these two strains driven by specific protein domains which are present in the *dys-1*(*eg33*) mutant strain and lost in the *dys-1*(*cx18*) mutant strain. Our transcriptome results in DP1 and DP2 strains and their two biological replicates support this hypothesis. Although they are very similar, the presence and the expression levels of the genes we mapped in these two mutant strains revealed subtle differences (Figure 3.9, Figure 3.21).

We decided to test if *dys-1* mRNA was indeed present in the muscle tissue of these two strains and is perhaps responsible for the phenotypic differences detected between these two mutant strains. Using an RT-PCR approach we consistently detected the presence of the *dys-1* transcript in both *dys-1*(*cx18*) and *dys-1(eg33*) strains, with no obvious degradation, suggesting that at least at mRNA level, these two transcripts are stably present in dystrophic muscle (Figure 3.20). We then compared the gene population shared between our DP1 and DP2 mutant strains in the POST datasets. As expected, the majority of genes are shared between both datasets, but we also detected unique gene populations expressed only in our DP1 and DP2 strains (Figure 3.9, Figure 3.21). ~30% of the total genes identified in DP2 dataset (*dys-1*(*eg33*)) were not detected in our DP1 (*dys-1*(*eg33*)) mutant strain (Figure 3.21). Most of these genes are involved in signaling pathways, such as the MAPK and the Wnt pathways, which are known to be involved in muscle formation [195]. Some of the genes, including *gsk-3* and *unc-62* were also detected in the DP1 (*dys-1*(*eg33*)) strain but show a striking increase in fold change in the DP2 (*dys-1*(*cx18*)) strain (Figure 3.21).

We then aligned the protein sequences of human dystrophin and worm *dys-1* and mapped the location of the *dys-1* mutation in both *dys-1*(*eg33*) and *dys-1*(*cx18*) strains. We found that the last two spectrin-like (SR) repeats, the WW domain and the β-dystroglycan binding domain are present in the *dys-1*(*eg33*) strain but missing in the *dys-1*(*cx18*) (Figure 3.22). These elements are critical for binding β-dystroglycan, and in humans anchor the dystrophin complex to the sarcolemma. This portion of the protein is overall the most conserved region between the human dystrophin and DYS-1 (Figure 3.23).

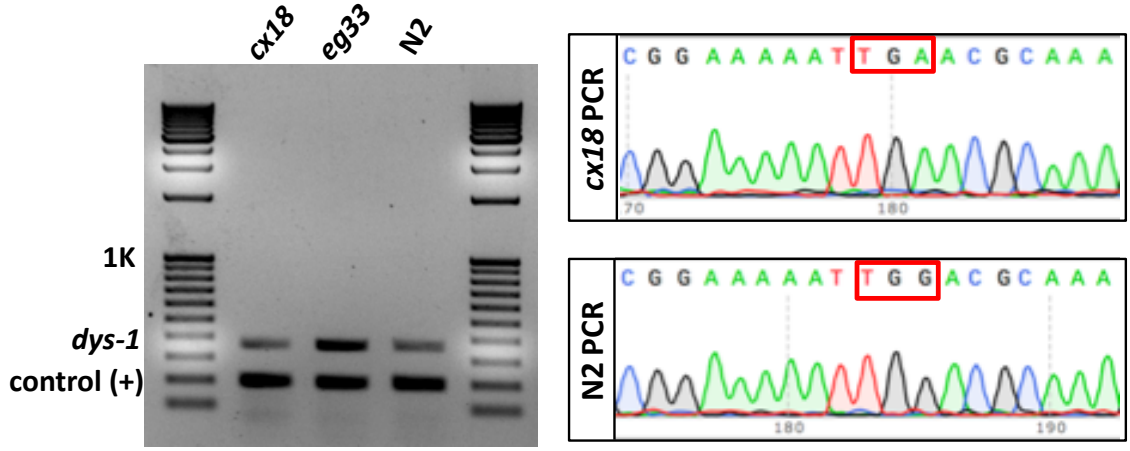

Figure 3.20*: dys-1 is expressed in dys-1(eg33) and dys-1(cx18) strains.* Top Panel: Detection of *dys-1* transcript *in dys-1*(*eg33*) and *dys-1*(*cx18*) mutant. RT-PCR analysis was performed on total RNA using primers that anneal on either side of the *cx18* mutation in the *dys-1* transcript, mixed with primers which anneal to the *myo-2* gene within exons 5 and 6 (control +). Bottom Panel: The amplicon corresponding to the bands observed in the *dys-1(cx18)* and N2 lanes in the top panel were purified and sequenced using primers surrounding the region containing the *cx18* mutation. The red box shows the location of the nonsense mutation in *dys-1*(*cx18*) mutant.

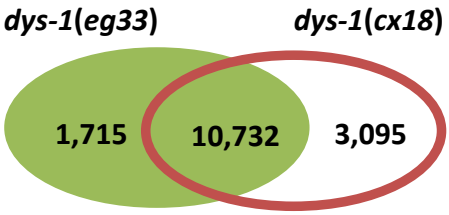

	adj.Pval	nGenes	Pathways
1	9.70E-09	6	Endocytosis
2	5.00E-04	3	MAPK signaling pathway
3	5.00E-04	3	Wnt signaling pathway
4	1.20E-03	2	Hedgehog signaling pathway
5	3.30E-03	3	Protein processing in endoplasmic reticulum
6	3.30E-03	2	Cysteine and methionine metabolism
7	4.70E-03	2	Glycolysis / Gluconeogenesis
8	4.70E-03	5	Metabolic pathways

	adj.Pval	nGenes	Pathways
1	3.50E-07	5	Oxidative phosphorylation
2	2.80E-06	7	Metabolic pathways
3	2.00E-03	2	ErbB signaling pathway
4	6.40E-03	2	Lysosome
5	6.40E-03	2	Endocytosis

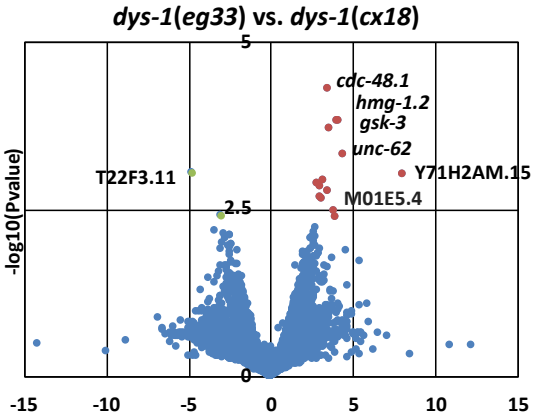

Figure 3.21: Different signaling pathways are affected in *dys-1(eg33)* and *dys-1(c18)* genetic backgrounds. Left Panel: Venn diagram comparing the number of genes detected in DP1 and DP2 strains in their respective POST datasets. Top list of a GO Term analysis performed using the unique genes detected in the DP1 or DP2 strains. Right Panel: Volcano plot depicting gene expression changes in common genes between DP1 and DP2 strains. Significantly overexpressed genes in the DP1 strain are shown as a red dot (p<=.005).

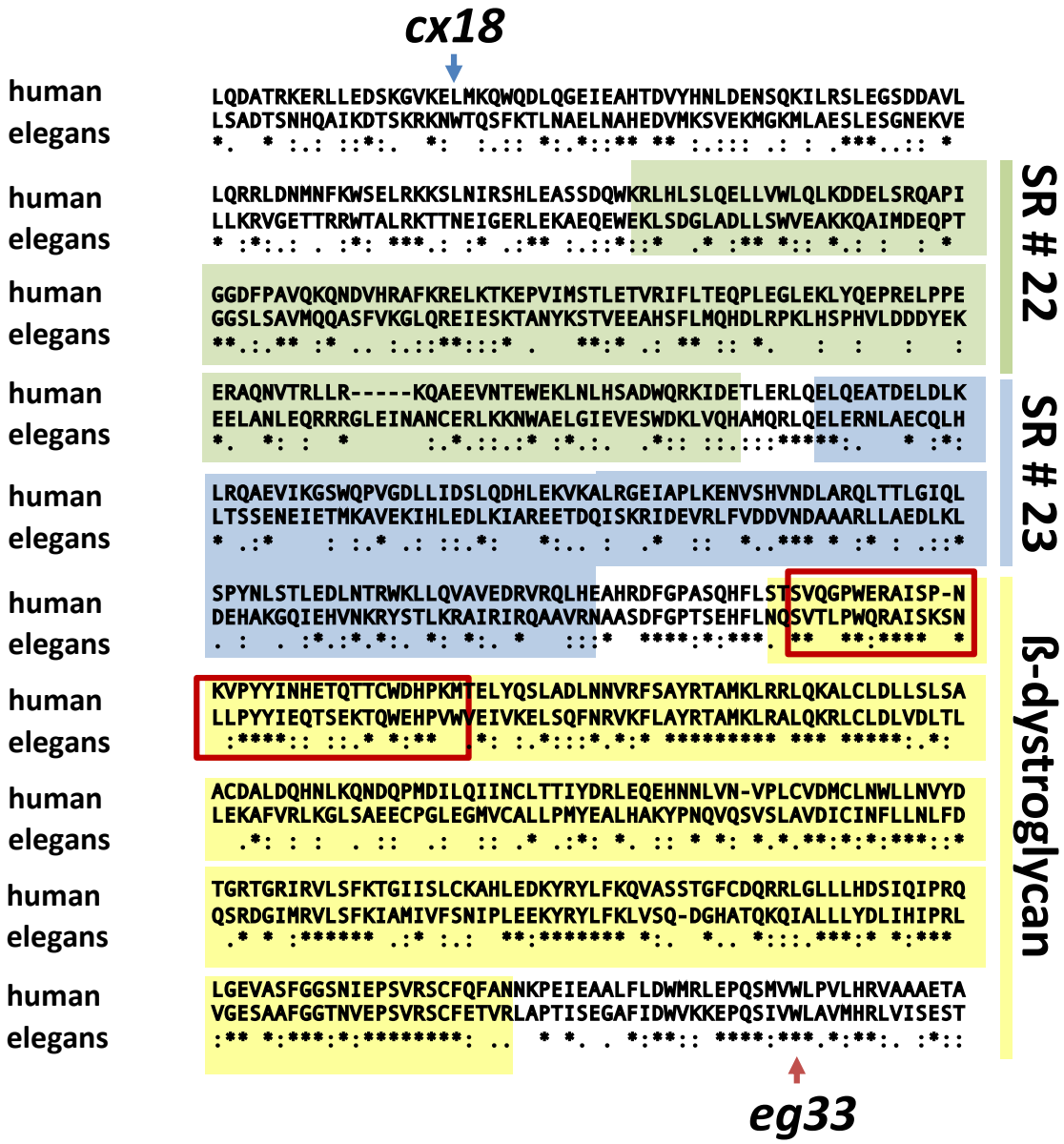

Figure 3.22: Alignment of essential functional domains within the C-terminal scaffolding region of human and *C. elegans* dystrophin protein The WW domain is outlined in red. The two mutations *eg33* and *cx18* are marked with an arrow. The final two spectrin repeats found in the rod region of the *C. elegans* ortholog of dystrophin are highlighted in green and blue respectively. The yellow highlighted region indicates the predicted region for binding ß-dystroglycan in the human dystrophin protein.

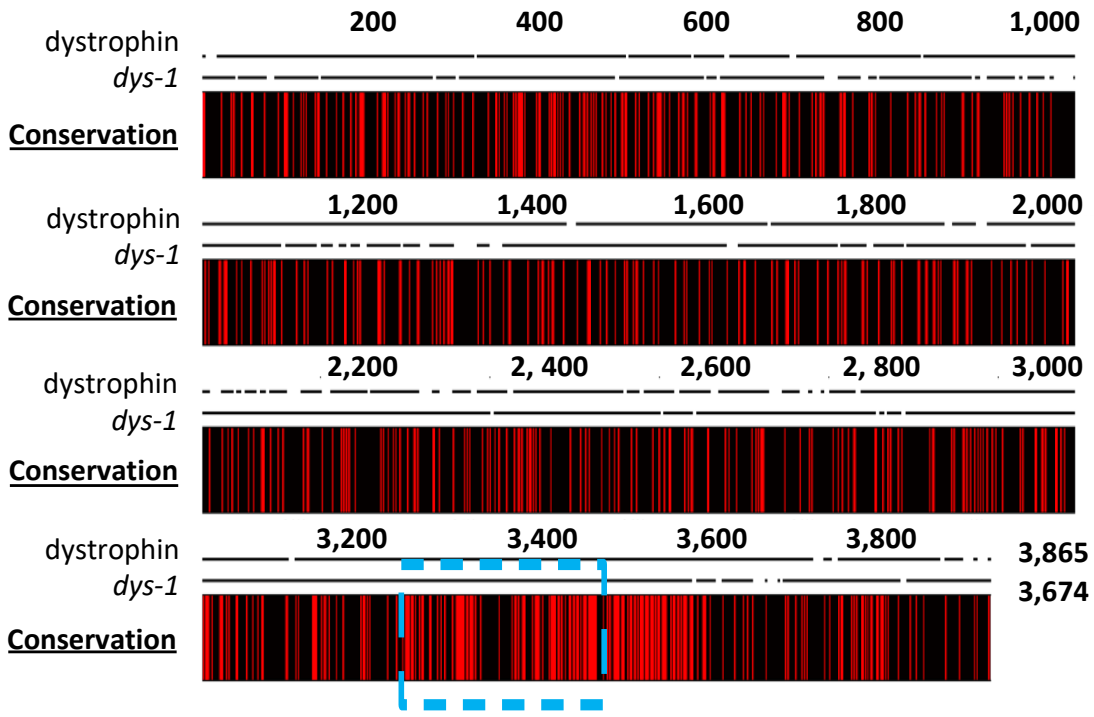

Figure 3.23: Map of sequence conservation between human and *C. elegans* orthologs of the dystrophin gene. The region containing β-dystroglycan binding domain is outlined in blue.

A novel synthetic screen to identify genetically linked dys-1 targets

Our muscle-specific transcriptome approach identified specific genes differentially regulated in both dystrophin-deficient samples across all replicates. Among several trends, we mapped an enrichment of genes involved in mitochondrial metabolism in our PRE dataset and genes involved in the establishment and maintenance of muscle structure and function in our POST dataset.

In order to validate and expand the biological significance of these results, we decided to perform a targeted RNAi knockdown genetic screen to test genes identified in our study for their ability to enhance muscle damage in dystrophin-deficient strains. We reasoned that if there were genetic compensatory mechanisms to increase gene expression,

perhaps to counteract decline in muscle structure and function, the knockdown of these upregulated genes detected in our screen would lead to an increase of the impairment of muscle viability that would, in turn, suggest a genetic link between *dys-1* and the tested genes.

Unfortunately, the *dys-1* phenotype is subtle when compared to *wt* worms. For this reason, we decided to use a previously established *dys-1* mutant strain *dys-1(cx18); hlh-1(cc561ts)* that uses a background mutation to enhance *dys-1* symptoms to create a more definitive and scorable phenotype.

It has been previously shown that combining dystrophin mutations with mutations in the transcription factor MyoD exacerbates dystrophic phenotypes in mice and that this combination has a similar effect in *dys-1* strains [196]. The temperature-sensitive strain *hlh-1(cc561ts)* contains a hypomorphic mutation in the *C. elegans* homolog of MyoD, *hlh-1*, which renders these strains viable at the permissive temperature 15°C and severely uncoordinated with defects in body muscle morphology at non-permissive temperatures above 20°C [197]. This strain has been already crossed with *dys-1*(*cx18*), producing a new strain named *dys-1(cx18); hlh-1(cc561ts)*, which showed a similar phenotype at non-permissive temperature.

In order to ameliorate the uncoordinated defects and lethality obtained at 20°C, we decided to decrease this temperature to 18°C (semi-permissive). At this temperature, ~75% of the single mutants, and ~50% of the double mutants are still viable (Figure 3.24).

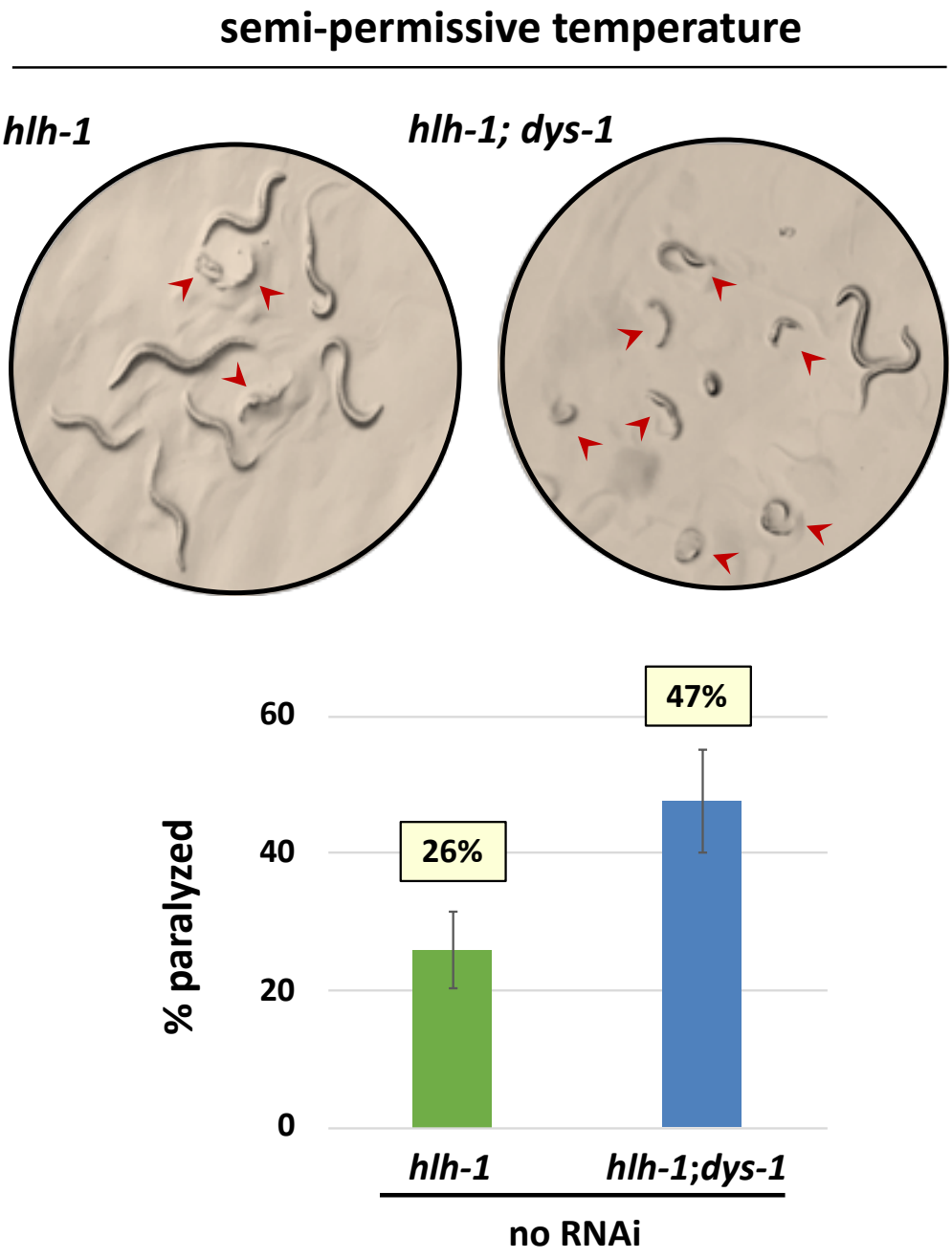

Figure 3.24: *hlh-1* single mutants and *hlh-1;dys-1(cx18)* double mutant strains exhibit differential incidence of morphological defects under semi-permissive conditions. Top panel: Single *(hlh-1)* or double *(hlh-1; dys-1)* mutants scored for paralysis at semi-permissive temperature (18°C). Red arrows indicate worms that were scored as paralyzed. Bottom panel: Quantification and comparison of the average incidence of paralysis for single vs. double mutant strains at semi-permissive temperature. The values above each bar chart represent the average score between all replicate plates for each respective strain (n=543).

Populations were synchronized and grown at 15°C (permissive) until they reached the L4 stage and were then moved to a semi-permissive temperature of 18°C and allowed to lay eggs for 24 hours (Figure 3.24, Figure 3.25). At semi-permissive temperature, the single mutant strains *hlh-1* gave rise to the progeny of which 26% developed with severe defects in body morphology and were almost completely paralyzed (Figure 3.24). Under the same conditions, the double mutant strains *hlh-1*; *dys-1* yielded a 47% of paralysis (21% increase), and the hatched larvae shown severe defects in body morphology (Figure 3.24).

We then selected a subset of representative upregulated genes identified by PAT-Seq. These genes were also chosen based on function, primarily because of their known roles in mitochondrial metabolism, muscle structure, and signaling function. We speculated that if these genes were indeed abundant in symptomatic *dys-1* worms as a compensatory mechanism to counteract paralysis, their depletion in the double mutant background would enhance paralysis when compared to the single mutant background.

The RNAi experiments were performed at the semi-permissive temperature of 18°C. Worms were scored for the incidence of morphological defects and resulting paralysis (Figure 3.25). The results between control and experimental strains were compared with each other, and then to the observed differences in semi-permissive experiments performed on single and double mutant strains in the absence of RNAi. As a control, we initially performed a knockdown of *dyb-1*, a known member of the nematode DAPC (Figure 3.26) [172]. We reasoned that *dyb-1* RNAi in the single *hlh-1* mutant background should increase the rate of paralysis but have no effect in the double mutant strain since in this strain *dys-1* function is absent and its interaction with *dyb-1* has been already severed.

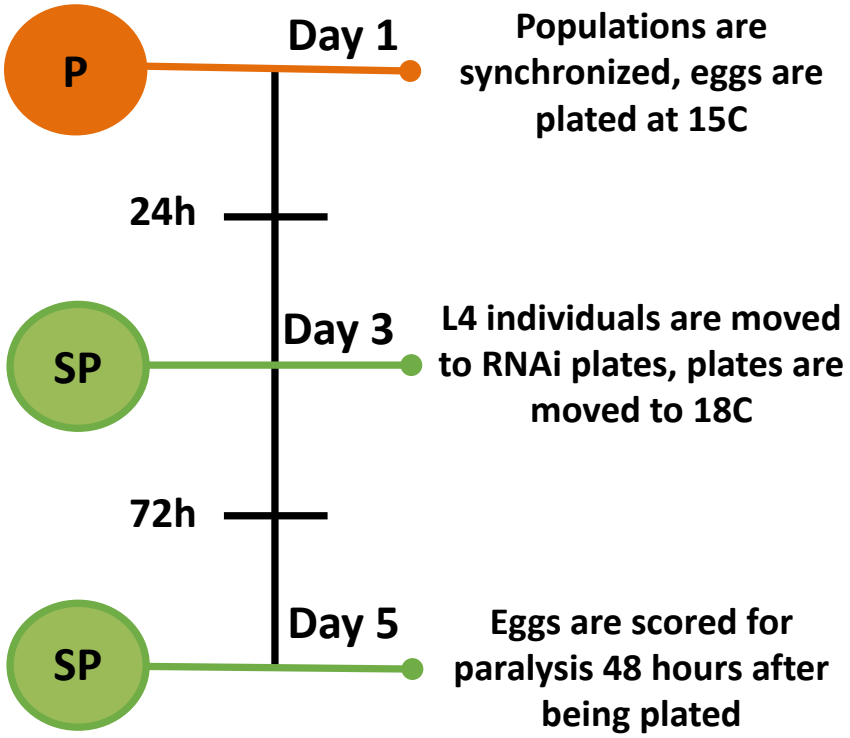

Figure 3.25: Experimental pipeline for semi permissive RNAi screen. P= permissive temperature (orange), SP= semi permissive temperature (green)

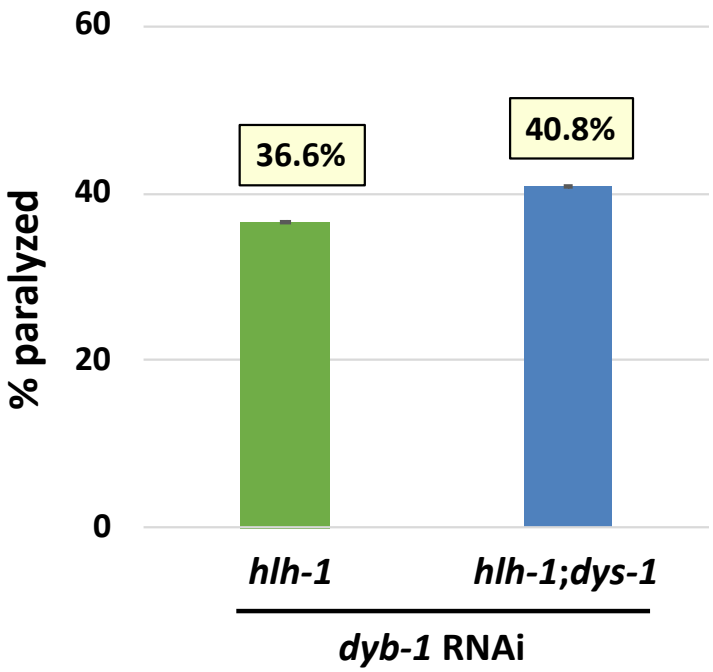

Figure 3.26: *dyb-1* knock-down increased incidence of paralysis in single mutants. Percentage of paralyzed worms following RNAi for *dyb-1,* with average percentage of paralysis of 5 replicate plates summarized above each bar (n=385).

As expected, the knockdown of *dyb-1* was able to increase the incidence of paralysis in the single mutant, which was comparable to the result obtained with the double mutant strain in semi permissive control experiments (Figure 3.26).

We then tested select genes from our muscle and signaling-related gene pools. Although some of the genes were synthetic lethal in combination with the *hlh-1* background mutation (*act-1*, *cmd-1*, *unc-27* and *unc-15*), and could not be tested further, the majority of genes tested were able to enhance paralysis, although to differing degrees (Figure 3.27).

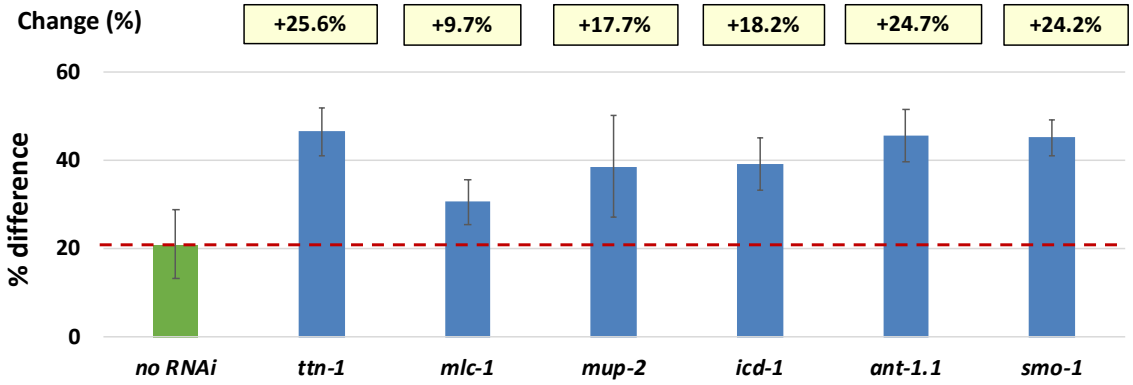

Figure 3.27: Synthetic paralysis RNAi assay to selected test genes found to be upregulated in this study. Each gene chosen for knockdown is displayed as the difference in paralysis observed between the *hlh-1* and *hlh-1;dys-1*(*cx18*) mutants and normalized to the difference of paralysis obtained from semi-permissive control screens described in Panel B (21%). Red dotted line marks the point of normalization for change in paralysis. The change in incidence of paralysis compared to the difference without RNAi (Panel B) is shown on top of each bar.

DISCUSSION

Here we have used the nematode *C. elegans* to study the cell-autonomous molecular events associated with the functional loss of the dystrophin gene, which leads to Duchenne muscular dystrophy in humans. We have performed genetic crosses to establish new transgenic strains that serve both as a model for DMD, and as a functional tool to perform high quality, muscle-specific RNA-IPs at a resolution that has not yet been achieved. Using these strains, we have isolated, sequenced and analyzed muscle-specific transcriptomes

during disease progression, and identified several differentially regulated pathways in the dystrophic nematode muscle.

We have also developed a novel, temperature-based genetic screen and performed a quantitative analysis to assess the functional significance of the dysregulated genes identified in our sequencing results, thus confirming their potential contribution towards DMD initiation and progression. This approach will further allow a direct evaluation of the role of specific genetic pathways in the clinical severity of DMD, which will be fruitful in developing drug targets for treating DMD patients. Our dystrophin-deficient strains DP1 and DP2 display altered molecular pathways that are very similar to those observed in *mdx* mice and DMD patients, strongly implying that this model system phenocopies many aspects of the disease at the molecular level [110,113,198].

These new strains recapitulate phenotypes previously characterized in the literature for *dys-1*(*cx18*) and *dys-1*(*eg33*), with shortened average and maximum lifespan, hyperactivity and excessive bending of the head [130,178] (Figure 3.3, Figure 3.4), suggesting that introducing the PAP cassette into the *dys-1* genetic background has not altered the *dys-1* phenotype.

The longevity curves obtained with our lifespan assay were somewhat shorter that those initially reported by Oh and Kim (2013) [178]. In their experiments, animals are placed on NGM plates containing FUDR at a concentration of 100 μg/ml, and they observed that the majority of their dystrophic worms survived until the day 20. In our experiments, 40% to 50% of the tested animals were still alive at the day 20. We have used a different lifespan assay protocol which adds less FUDR in the plates, to a final concentration of 50 μM, and this change could be in part responsible for our observed decrease in survival [199]. In

addition, our scoring method of lethality could have also accounted for these differences (see Experimental). Importantly, we observed consistency in lethality between the *dys-1*(*eg33*) and the *dys-1*(*cx18*) strains before and after the crosses with our *myo-3p*::GFP::*pab-1*::3xFLAG strain, suggesting consistency within our assay.

Our study uncovered ~ 2,000 muscle protein-coding genes with altered expression levels in the early and late-stage dystrophic muscle when compared to wild type muscle tissues. Among this group, ~500 genes showed at least 2-fold increase in both the PRE and the POST dataset, and across both biological replicates for each sample. In order to reduce background signal, we have applied a stringent bioinformatic filter to restrict our analysis to the top 30-40% of the total genes identified in this study (Figure 3.28), which may have in turn lowered the number of genes considered, but provided us with higher quality results (Figure 3.2**8**).

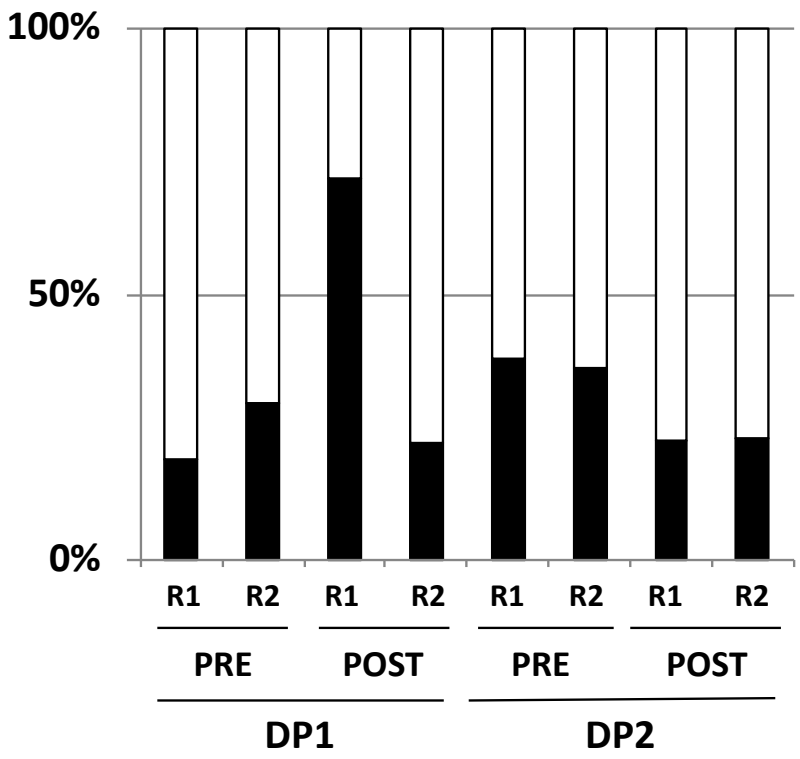

Figure 3.28: Bioinformatic filters have restricted analysis to the top 40% of genes identified by PAT-Seq results. Analysis of trends in gene expression was performed only on the top ~30-40% positive hits produced by Cufflinks. Black bars: % of reads used for each dataset in this study. White bars: % of reads discarded. R1 and R2: Replicate 1 and Replicate 2.

Our mapped reads from our POST datasets were consistent with our past studies across both biological replicates [181]. Of note, we obtained less than average mapped raw reads in all our PRE datasets (Table 3.1) which may have biased our results. The original PAT-Seq approach was optimized using mixed stage populations as the starting material for the immunoprecipitation steps [181,182], and it was never applied to isolate RNA from early stages such as embryos and L1/2 worms. The mechanical filtration steps we used to isolate these stages may have also introduced unwanted noise in our PRE dataset, which was

recovered from the flow-through of the strainers. The L3/L4 and adult worms in our POST datasets were instead retained by the strainers and isolated from the flow-through.

Although we obtained fewer mapped reads, it is important to note that the total number of unique genes we mapped in our PRE datasets is similar across all datasets (but with less coverage) (Table 3.2), suggesting that the distribution of our mapped reads in our PRE dataset for abundant genes is not biased. In addition, our PCA analysis shows that the genes and their abundance in both replicates in our PRE datasets are very similar to each other, also suggesting consistency (Figure 3.29). Of note, when compared to the top 250 genes identified in our past muscle-specific transcriptome from mixed stage worms [182], genes mapped in both our PRE datasets show a similar trend to those mapped in our POST datasets, further suggesting that the genes identified in our PRE dataset are not random, but are the direct result of our immunoprecipitation approach (Figure 3.8).

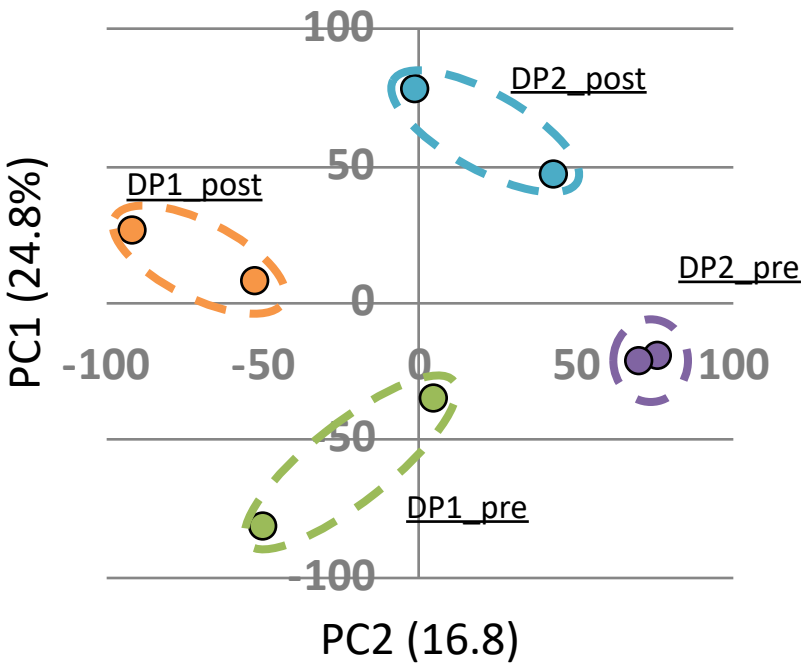

Figure 3.29: Principal Component Analysis (PCA) shows a high correlation among each duplicate within our datasets.

Despite the differences in mapped reads between PRE and POST datasets after filtration, the reads obtained are not likely to have been biased by the size selection method itself. It has been previously shown that although there are measurable differences in strength between wild-type and *dys-1(eg33)* and *dys-1(cx18)*, which cannot be attributed to differences in worm diameter [170], and our filtration control experiment in (Figure 3.30) confirmed that there are no significant differences in stage enrichment in PRE and POST populations in the *dys-1* strains (Figure 3.30).

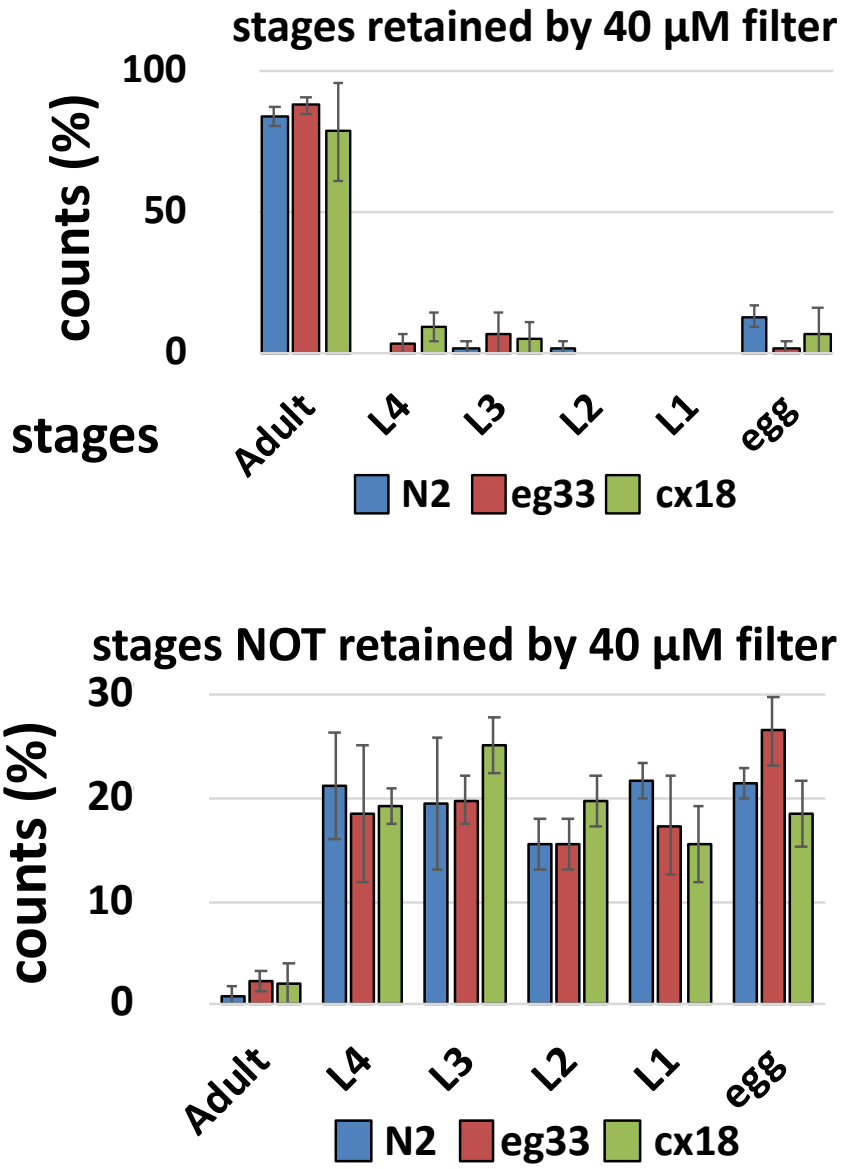

Figure 3.30: A similar number of N2, *dys-1(eg33)*, *dys-1(cx18)* worm strains in each developmental stage were able to pass through 40 µM filters. The left graph indicates the quantity of each strain and their respective developmental stage retained by the filter (n=190). Right panel indicates the quantity of each strain and developmental stage that passed through the filter (n=676).

Our study revealed two distinct sets of genes that contribute to the DMD phenotype in *C. elegans*. The first set is primarily activated early in development and is composed of genes involved in mitochondrial homeostasis, cell death and protein degradation signaling in the muscle (Figure 3.10). The second set is activated during the final half of the developmental cycle, continues through adulthood, and is involved in the establishment and maintenance of muscle structure (Figure 3.10).

There are currently a number of studies in *mdx* mice reporting the involvement of both pathways in DMD progression [130,169,200], but prior to this study it was unclear how these two pathways were intertwined with each other, and in what order these events occurred. This question is important, as impaired mitochondria metabolism has been already observed in *mdx* myoblast in which a functional DAPC has not yet been assembled [97].

Our results suggest that these two pathways do not occur simultaneously; the mitochondrial dysfunction is detected early in disease progression, in accordance with previous findings [169], either before symptoms are initiated or while they are still mild.

In the PRE dataset, we detected the differential regulation of numerous mitochondrial genes associated with the glycolysis pathway and ATP/ADP transport such as *ant-1.1*, *nduo-2*, *nduo-3* and *atp-3* (Figure 3.10, Figure 3.12). Proteomics studies in *mdx* mice also support these results [169]. Muscle contraction is dependent upon ATP production and usage, and its abundance is tightly regulated in healthy muscles.

The aberrant mitochondrial activity has been previously reported in DMD patients and animal models of DMD [168,170,201–204], even prior to dystrophin assembly at the sarcolemma [97]. Furthermore, previous studies in *C. elegans* have characterized the functional relationship between DYS-1 and surrounding members of the DAPC and have

found that *dys-1* mutations lead to the mislocalization of the Ca^{2+}-gated K^{+} channel protein SLO-1 resulting in altered intracellular calcium levels [97]. We also detect a decrease of mitochondrial localization in the muscle of *dys-1* worms (Figure 3.12), which is consistent with these results. Our RNAi experiments in Figure 3.15 also confirmed the importance of the DAPC in relation to mitochondria localization, because the selective knockdown of four members of this complex caused a decrease of mitochondria localization to the body muscle. Taken together, our results validate these studies and highlight an important signaling role for *dys-1*, which evidently functions outside of its accepted role as a scaffolding protein in the DAPC.

After the onset of symptoms in post-symptomatic samples, while mitochondrial dysfunction is still present (Figure 3.14, Figure 3.12), we detect a second pathway, which perhaps tries to actively compensate for the loss of muscle structure by overexpressing genes involved in muscle formation. We do not know if these transcripts are indeed carrying out a compensatory mechanism, and more experiments need to be performed to further validate this finding. Of note, many of them were able to enhance paralysis in our RNAi experiments in Figure 3.27**,** suggesting that they are functionally translated. The upregulation of a subset of these genes have also been validated in mammalian satellite cells, and it was shown that two key genes were similarly upregulated in the *mdx/utr*$^{-/-}$ mouse (Figure 3.17). This further supports the translational value of *C. elegans* as a model system for the initiation and progression of DMD in skeletal muscle, despite fundamental differences in the function of vertebrate and invertebrate striated muscle.

Our results have shown that *dys-1*(*eg33*) and *dys-1*(*cx18*) transcriptomes, while highly similar, are not identical (Figure 3.9, Figure 3.21). A previous study found *dys-1*(*eg33*) mutants

to be significantly weaker than *dys-1*(*cx18*) and their wild-type counterparts [170], but the molecular mechanisms driving these differences was not known. *dys-1*(*eg33*) possess a weaker thrashing score in liquid than *dys-1*(*cx18*) [170] and display stronger mitochondrial network fragmentation in the body wall muscles [170]. *dys-1*(*eg33*), but not *dys-1*(*cx18*), also responds to prednisone and melatonin, showing improved muscular strength, thrashing rate, and mitochondrial network integrity in response to treatment with these compounds [170]. Our results align with these findings, as we were able to show that *dys-1* mRNA is surprisingly transcribed in both strains with little detectable degradation (Figure 3.21), suggesting that two different DYS-1 truncated proteins are present in these two strains, and potentially act as hypomorphic alleles. We do not yet know why the nonsense mutations in the *dys-1* genes are not recognized and degraded by the nonsense mediated decay pathway.

The shorter *dys-1*(*cx18*) strain lacks both the DYS-1 WW domain and the β-dystroglycan binding domain, which in the human dystrophin gene are responsible for binding to β-dystroglycan and anchoring the protein to the sarcolemma. The lack of this element is perhaps able to induce the altered signaling pathways we have detected in the *dys-1*(*cx18)* strain, which in turn may be responsible for the differences in both phenotype and gene expression observed between these two strains. Alternatively, the presence of this element followed by a truncated c-terminal domain may induce muscle stress in burrowing experiments and allows for drug sensitivity. In support of this hypothesis, we detected a strong conservation in this region between the human and the worm dystrophin ortholog (Figure 3.23), which implies there is a lost functional role in the *dys-1*(*cx18*) strain. More experiments need to be performed to address this issue. Importantly, DGN-1, the worm ortholog of the β-dystroglycan gene, has been found to be located outside the muscle and

does not bind DYS-1 [144]. If correct, the loss of the β-dystroglycan binding site in the *dys-1*(*cx18*) mutant strain cannot be directly responsible for the functional differences observed between the *dys-1*(*cx18*) and the *dys-1*(*eg33*) strains. However, in contrast with this past study we have repeatedly identified *dgn-1* in our *C. elegans* muscle transcriptomes in this study and elsewhere [181,182], suggesting that perhaps there could be a small population of DGN-1 in muscle which is responsible for anchoring *dys-1* to the sarcolemma. This issue requires further studies to closely characterize the role of these two truncated versions of DYS-1 and how they may impact cellular signaling in the muscle.

Our results in Figure 3.19 found widespread splicing disorders in both our PRE and POST datasets. Our study identified thousands of aberrant splice junctions in the *dys-1*(*eg33*) mutant strain, which correlates with altered abundances of RNA splicing factors such as snRNPs and SR proteins. Disorders in mRNA splicing have been also observed in 120 transcriptomes from skeletal and heart muscle derived from healthy and dystrophic biopsies and autopsies [193]. In this context, *C. elegans* again phenocopy these defects and provides a more robust platform to study the genetic mechanisms caused by these lesions in the context of DMD. We do not know if the widespread aberrant splicing we detected is able to escape NMD or it is subjected to it. Of note, in our muscle datasets we scarcely detected genes involved in this process, suggesting that perhaps, if NMD occurs is not able to completely prevent their translation.

Our RNAi experiments in Figure 3.27 most effectively screen for genes that play a role in the muscle and work cooperatively with dystrophin beginning early in development. The effects of the RNAi knockdown are scored in the first hours after L1 animals hatch. In this light, the results of our semi permissive control experiments showed that the absence of

dystrophin was able to affect the early development of the embryos that ultimately hatched with severe muscle defects. This finding coincides with our sequencing results in our PRE datasets which suggested dystrophin may play an early role, both in development and in regulating mitochondrial function, and is not only a structural protein whose absence affects developed muscle after continuous contraction.

The changes in gene expression observed in our POST dataset suggest that many of the genes encoding structural proteins of the sarcomere are involved in the progression of dystrophin-induced muscle damage (Figure 3.10). Our RNAi experiments in Figure 3.27 confirmed that these genes act in a *dys-1* dependent manner and verify their role in a compensatory mechanism that may allow *C. elegans* to increase transcription of muscle-structure related genes in response to muscle damage.

mup-2, a gene that codes for the ortholog of muscle protein troponin, TTN-1 a titin-like protein, and *mlc-1*, an ortholog of myosin regulatory light chain were all able to increase the incidence of muscle defects and paralysis in the dystrophin-deficient strain *dys-1(cx18); hlh-1(cc561ts)*, without inducing the same effect on the control strain *hlh-1(cc561ts)* (Figure 3.27).

Taken together, these results suggest that *mup-2, ttn-1*, and *mlc-1* are all genetically connected to *dys-1* and are not only overexpressed as transcripts when visible symptoms begin, but are also expressed as proteins, as their dosage is necessary to increase paralysis in a *dys-1* dependent manner.

Outside this group of genes selected because of their role in muscle structure, we also studied upregulated genes essential in several signaling pathways. *icd-1* is the β-subunit of the nascent-polypeptide associated complex. *icd-1* was significantly upregulated in POST

symptomatic data sets. It mediates proteins transport to mitochondria and is necessary and sufficient to suppress apoptosis [205]. *icd-1* knockdown induces a two-fold increase of incidence of muscle defect and paralysis in *dys-1* dependent manner (Figure 3.27), suggesting that these two genes are also genetically connected.

These synthetic paralysis phenotypic experiments in Figure 3.27 are challenging to analyze. Unfortunately, *dys-1* mutations do not lead to a drastic muscle phenotype and aggravation of phenotypic severity using the *hlh-1* ts allele is needed in order to simplify scoring. Since *hlh-1* is involved in muscle development, these results may report a developmental arrest phenotype caused by disruption in muscle elongation during embryogenesis. Although this may be the case, our readout is the comparison of the incidence of lethality induced by a given RNAi experiment in worms with and without the *dys-1* mutations. Because of this, the scored variation in morphological defects mirrors the contribution of the loss of *dys-1* to the developmental arrest phenotype, which is induced at a much lower rate by *hlh-1* alone in all our RNAi experiments.

We opted to use this genetic background because it was previously published and successfully used in a similar approach [196]. In addition, while some groups have used approaches without modified genetic backgrounds to define impaired movement and muscle function, such as thrashing or tracking of movement, we elected to use this semi permissive assay because it is rapid, reveals readily scorable differences between single and double mutants, and is easily adaptable for future large-scale experimentation.

Another observed limitation in using our approach for RNAi screens was the incidence of synthetic lethality. When combined with background mutations in *hlh-1*, several genes involved in the development of muscle proved to be embryonic lethal when knocked

down. Because this synthetic lethality achieved the same penetrance in single and double mutant strains, it prevented the scoring of differences between the two strains. It is important to note that this did not occur in the bulk of our experiments that knocked down muscle-specific genes, meaning it is still feasible to use this method to screen the majority of genes in the genome, both muscle-specific and ubiquitously expressed.

In conclusion, our analysis of dystrophin deficient muscle transcriptomes has confirmed the signaling role of dystrophin in nematode muscle and allowed us to further study the consequences of dystrophin deficiencies in great detail.

EXPERIMENTAL

Preparation of nematode transgenic strains

Body muscle-specific PAP expressing transgenic lines (*wt* PAP) were obtained from a previous publication [181]. SJ4103 strains were obtained from the CGC, which is funded by NIH Office of Research Infrastructure Programs (P40 OD010440). Young adult *C. elegans* worms were isolated on nematode growth media (NGM) agar plates seeded with OP50-1 and incubated at 31°C for 3.5 hours. To prepare the crosses, Plates were then incubated for four days at 20°C and males were isolated from populations. Groups of five males were paired with 10 L4 hermaphrodites and incubated for 3 days at 20°C. Crosses between *wt* PAP and *dys-1*(*cx18*) and *dys-1*(*eg33*) strains, and crosses between SJ4103 and *dys-1(cx18)* strains were screened for GFP fluorescence using a Leica DM13000B microscope. Strains positive for fluorescent markers were subjected to Sanger sequencing for the verification of mutations in the dystrophin gene using the following primers: *dys-1*(*cx18*)_F: GGCTTAATATGAGCTGGACGAAG, *dys-1(cx18)*_R: CGCTGTCCATCTTCTTGTGG,

*dys-1(eg33)*_F: GGACGGTCATGCGACCC, *dys-1(eg33)*_R: TTTGCACACGTTGCATTTGG. In order to simplify the nomenclature, we have renamed the crossed strain *dys-1(eg33)*/PAP to DP1 and the crossed strain *dys-1(cx18)*/PAP to DP2 throughout this manuscript.

Preparation of PRE and POST symptomatic PAT-Seq strains for RNA immunoprecipitation

C. elegans strains were divided into pre-symptomatic (PRE) and post-symptomatic (POST) pools using mechanical filtration using pluriStrainer cell strainers (pluriSelect). Mixed-stage populations were harvested from nematode growth media (NGM) agar plates seeded with OP50-1 and pelleted at 1,500 rpm. Solid pellets of approximately 2ml were sequentially pipetted through 40 μm and 20 μm nylon cell strainers. The collected flow-through contained embryo/L1/L2 population, which we renamed PRE. Worms retained by both filters, which included L3/L4/Adult population, were then combined and renamed POST. During the filtration process, pellets were continuously resuspended in M9 buffer to prevent worms from being crushed or forced against mesh filters.

Mechanical filtration control experiments

N2, *dys-1(eg33)*, and *dys-1(cx18)* worm strains were grown on standard NGM plates as mixed-stage populations until 200 μl solid pellets were obtained for each strain. The entirety of this pellet was passed through a 40 μM cell strainer. The pellet was continuously resuspended in M9 during the filtration process. The retained populations and the flow through were both pelleted and resuspended in 500 μl of M9 buffer. From this resuspension, 25 μl samples

were taken both from the retained population and the flow through populations and each stage present in this aliquot was scored. 25 µl samples were taken in triplicate for each worm strain for both retained and flow through samples. Values for each stage were calculated as a percentage of the total number of worms in each 25 µl sample and then averaged across replicates. The results of this analysis are shown in Figure 3.30.

RNA immunoprecipitation

C. elegans strains used for RNA immunoprecipitations were maintained at 20°C on nematode growth media (NGM) agar plates seeded with OP50-1. Populations were passaged until a 1 ml pellet for mixed stage IPs and a 2 ml pellet for split stage IPs was obtained following centrifugation at 1,500 rpm. Following the isolation of PRE and POST symptomatic populations through mechanical filtration, worm strains were harvested, suspended and crosslinked in 0.5% paraformaldehyde solution for one hour at 4°C. Worms were then pelleted at 1,500 rpm, washed with M9 buffer, and flash-frozen in an ethanol-dry ice bath. Pellets were thawed on ice and suspended in 2 ml of lysis buffer (150 mM NaCl, 25 mM HEPES, pH 7.5, 0.2 mM dithiothreitol (DTT), 30% glycerol, 0.0625% RNAsin, 1% Triton X-100). Lysate was then subjected to sonication for five minutes at 4°C (amplitude 20%, 10 sec pulses, 50 sec rest between pulses) using a sonicator (Fisher Scientific), and centrifuged at 21,000 x g for 15 min at 4°C. 1 ml of supernatant was added per 100 µl of Anti-FLAG® M2 Magnetic Beads (Sigma-Aldrich) and incubated overnight at 4°C in a tube rotisserie rotator (Barnstead international). mRNA immunoprecipitations were carried out as previously described. Total precipitated RNA was extracted using Direct-zol RNA Miniprep Plus kit (R2070, Zymo Research), suspended in nuclease-free water and quantified with a

Nanodrop® 2000c spectrophotometer (Thermo-Fisher Scientific). Each RNA IP was performed in duplicate to produce two biological replicates for the following samples: DP1 PRE, DP2 PRE, DP1 POST, DP2 POST, *wt* PAP PRE and *wt* PAP POST.

cDNA library preparation and sequencing

We prepared a total of 16 cDNA libraries from *dys-1(eg33)* mixed stage, DP1 mixed stage, DP1 PRE1, DP1 PRE2, DP1 POST1, DP1 POST2, DP2 mixed stages, DP2 PRE1, DP2 PRE2, DP2 POST1, DP2 POST2, *wt* PAP mixed stages, *wt* PAP PRE1, *wt* PAP PRE2, *wt* PAP POST1 and *wt* PAP POST2. Each cDNA library was prepared using 100 ng of precipitated RNAs. cDNA library preparation was performed using the SPIA (Single Primer Isothermal Amplification) technology (IntegenX and NuGEN, San Carlos, CA) as previously described [181,182]. cDNA was then sheared using a Covaris S220 system (Covaris, Woburn, MA), and sample-specific barcodes were sequenced using the HiSeq platform (Illumina, San Diego, CA). We obtained ~60-90M mappable reads (1x75) each dataset.

Bioinformatics analysis

Raw Reads Mapping: The raw reads were demultiplexed using their unique tissue-specific barcodes and converted to FASTQ files. Unique datasets were then mapped to the *C. elegans* gene model WS250 using the Bowtie 2 algorithm with the following parameters: --local -D 20 -R 3 -L 11 -N 1 -p 40 --gbar 1 -mp 3. Mapped reads were further converted into a bam format and sorted using SAMtools software using generic parameters [206].

Cufflinks/Cuffdiff Analysis: Expression levels of individual transcripts were estimated from the bam files by using Cufflinks software [207]. We calculated the fragment per kilobase per million bases (FPKM) number obtained in each experiment and performed a pairwise with other tissues using the Cuffdiff algorithm [207]. We then used the median FPKM value >=1 between each replicate as a threshold to define positive gene expression levels. The results are shown in **Additional File 1: Tables S1-S3**. **Additional File 1: Table S4** was compiled using scores produced by the Cuffdiff algorithm [207] and plot using the CummeRbund package.

RT-PCR experiment for detection of dys-1 transcripts in dys-1 strains

N2, *dys-1(eg33)*, and *dys-1(cx18)* strains were grown on NGM plates as mixed populations until 200 µl pellets were obtained for each strain. These pellets were subjected to total RNA extraction and DNAse I treatment using the Direct-zol RNA Mini-Prep Plus kit (Zymo Irvine, CA #R2051) according the protocol for tissue samples detailed in the product literature. 1.5µl of the RNA obtained was used in cDNA synthesis. 1µl of synthesized DNA was used from each cDNA sample to perform PCRs to amplify regions of the *dys-1* gene from N2, *dys-1(eg33)*, and *dys-1(cx18)* samples. The following primer sequences were used to detect the presence or absence of *dys-1* transcripts and as a PCR control respectively: *dys*-1_F: CGGCAAGAAGACAATTGCTCAAA, *dys*-1_R: TCCTCATGAGCATTCAGCTCCG, *myo-2*_F: GGAGTGCTACCGATTGGTTGCCG, *myo-2*_R: CTTGTTCACCCATTCGTTTCCGACC. PCR products were subjected to Sanger sequencing using the following primer: *dys*-1_F: CGGCAAGAAGACAATTGCTCAAA. The primers used for the RT-PCR overlap the exon containing the cx18 mutation.

Kaplan-Meier survival curve assays

Survival curves were performed as previously described [199,208]. Briefly, we prepared NGM plates each containing 330 µl of 150 mM FUDR (Sigma Life Sciences, Darmstadt, Germany). These plates were seeded with OP50-1 that was UV inactivated prior to plating worms to minimize contamination. All worm strains used in survival curves were synchronized with bleach. We plated 25 L4 worms from each strain per plate, each across 3 replicates, and stored in 18°C incubators for the duration of the experiment. For each time point, the plates were recovered, and worms were visually inspected and counted directly in the plate using a dissection stereomicroscope (Leica S6E) and a cell counter. The strains were scored for survival every 48 hours, with survival being defined as pharyngeal pumping or the ability to move the head in response to prodding by a worm pick. Each plate was anonymized and scored twice.

RNAi feeding screens at semi-permissive temperatures

RNAi plates were made by adding IPTG to NGM plates to a final concentration of 1mM. Plates were allowed to dry at room temperature for 5 days before seeding with bacteria. The desired HT115 bacterial cultures were inoculated from glycerol stocks sourced from the Ahringer library [209] and grown in 3 ml LB cultures containing ampicillin (10µg/ml) and tetracyline (12.5 µg/ml) and grown at 37°C for 16 hrs. Dry NGM plates containing IPTG were then seeded with 75 µl of bacterial culture and left at room temperature to induce dsRNA production overnight for 16 hrs. RNAi feeding experiments were performed using the temperature-sensitive strains PD4605 *(hlh-1(cc561))* and LS587 *(hlh-1(cc561); dys-1(cx18))*.

Strains were synchronized with bleach as previously described [210] and eggs were incubated at permissive temperature (15°C) until populations reached the L4 stage. Young adults were then plated on NGM plates seeded with the desired RNAi clone and containing 1mM IPTG, with 5 worms per plate, and incubated at semi-permissive temperature (18°C) for 24 hours to allow young adults to lay eggs. Plates were then recovered, and adult worms were removed, and plates containing eggs were returned to semi-permissive temperature to incubate for 24 hours on RNAi plates. Plates were then scored for gross defects in body morphology and resulting paralysis. We scored approximately 100 worms per plate across 5 replicate plates for each strain and each gene tested [209]. Each plate was scored twice. The RNAi clone overlap the Exon 20 of the F15D3.1a gene.

Preparation of the dyb-1 clone

The following primers were used to add SacII and SpeI cut sites to the ORF of *dyb-1*:

dyb-1 F: TCTTCTACTAGTATGTTGTGGTCAAATGGTGG

dyb-1 R: CATCATCCGCGGGAAGCCATTGATTGTTACGCC

The generated PCR fragment was ligated into pDONR221 (Invitrogen) containing the sequence for GFP at the 3'end. The *dyb-1::GFP* transgene was then moved into the second position of the destination vector pCFJ150 [186], which also containing the *myo-3* promoter and *unc-54* 3'UTR in first and third positions respectively.

RNAi feeding screens on SJ4103 and SJ4103;cx18 strains

RNAi plates were made by adding IPTG to NGM plates to a final concentration of 1mM. Plates were allowed to dry at room temperature for 5 days before seeding with bacteria. The

desired HT115 bacterial cultures were inoculated from glycerol stocks sourced from the Ahringer library [209] and grown in 3ml LB cultures containing ampicillin (10μg/ml) and tetracyline (12.5 μg/ml) and grown at 37°C for 16 hrs [211]. Dry NGM plates containing IPTG were then seeded with 75μl of bacterial culture and left at room temperature to induce dsRNA overnight for 16 hrs. SJ4103 and *SJ4103;cx18* strains were synchronized with bleach as previously described [210] and eggs were incubated at room temperature until both populations reached the L4 stage. L4 worms were then moved to IPTG plates seeded with the appropriate RNAi clone. Plates were stored at room temperature until F1 worms reached the young adult stage and were then isolated for fluorescent imaging.

Fluorescent imaging and analysis of SJ4103 strains

The SJ4103 and SJ4103;*cx18* fluorescent strains were cultured on standard NGM plates at room temperature. To obtain worms at distinct developmental stages, SJ4103 and SJ4103;*cx18* strains were synchronized with bleach. Worms subjected to RNAi feeding were selected for imaging as young adults. Worms were placed on 2% agarose pads and immobilized in 1mM levamisole. Fluorescent images were taken using a Leica DM13000B microscope and analyzed using ImageJ software (developed by Wayne Rasband at the National Institutes of Health, available at http://rsbweb.nih.gov/ij/).

Satellite cell culture and differentiation

mdx/utr$^{-/-}$ and *wt* BL10 satellite cells were seeded in 6 well plates at a starting density of 160,000 and incubated at 37ºC in 30% growth medium . After reaching 80% confluency, growth medium was exchanged for differentiation media (DMEM, 2% HS, 100 μg/mL

Primocin. Differentiation media was replaced once every 24 hours for five days. Differentiation media was removed and RNA extractions were performed on the fifth day.

RNA Extraction and Real-time Quantitative qPCR (RT-qPCR)

Total RNA was extracted from *mdx/utr-/-* and BL10 satellite cells using the Direct-zol RNA Miniprep Plus kit according to the manufacturer's instructions (R2070, Zymo Research), suspended in nuclease-free water and quantified with a Nanodrop® 2000c spectrophotometer (Thermo-Fisher Scientific). 200 ng of total RNA for each sample was used as a template for cDNA synthesis using Reverse Transcriptase III (Invitrogen, Carlsbad, CA) and a polyDT primer. RT-qPCR reactions were performed using SYBRgreen (Eurogentec, Freemont, CA) on an ABI 7900 HT thermocycler. qPCR data were normalized using GAPDH primers GAPDH_FWD 5': CCGCATCTTCTTGTGCAGT-3', GAPDH_REV: 5'-GAATTTGCCGTGAGTGGAGT-3'. The following primers were used to detect troponin T (TNNT2), myosin light chain (MYLPF), and α-actin (ACTA1): TNNT2_F: 5'-CGAGCAGCAGCGTATTCGC-3' TNNT2_R: 5'-CAGCCTTCCTCCTGTTCTCCTC-3', MYLPF_F: 5'-TTTCCATCTGGAGCTACTGC-3' MYLPF_R: 5'-ATAATGCCATCCCTGTTCTG-3', ACTA1_F: 5'-CGTGGCTATTCCTTCGTGAC-3', ACTA1_R: AACGCTCATTGCCGATGGT. Change in mRNA expression was calculated using the ΔΔCt method. Two biological replicates and three technical replicates per biological replicate were included.

CHAPTER 4

CONCLUSION

Dystrophin is highly conserved throughout metazoans

Conservation of the dystrophin gene and a number of its binding partners in most metazoans suggests it is likely there is a conserved functional role as well, and that dystrophin plays a fundamental role in nearly all muscle biology [129,143]. Although the degree of conservation of the dystrophin protein as a whole drops drastically when switching from comparisons between human dystrophin and other vertebrates to comparisons of invertebrate orthologs, the higher degree of conservation within each functional domain of the invertebrate dystrophin-like proteins found in drosophila, zebrafish, and nematodes again reinforces the notion that despite differences in sequence, the fundamental role of dystrophin is consistent throughout metazoans (Table 2.1) [141,174]. Furthermore, the conservation of numerous binding partners both in and around the DAPC in invertebrates suggests that dystrophin associates similarly with this protein complex to carry out both a structural and signaling role in the muscle in the same manner as human dystrophin [129,141,143].

Conservation of the overall structure of each of the four major functional domains of dystrophin gene from humans to *C. elegans* highlights the potential of *C. elegans* as an informative model system for the study of DMD. The presence of a dystrobrevin homologue (*dyb-1*) whose knockout induces a *dys-1* like head bending phenotype provides promising evidence that dystrophin forms a stabilizing connection with the invertebrate DAPC through dystrobrevin in the same manner that dystrophin connects to ß-dystroglycan in human muscle.

Although *C. elegans* have proven to be a valuable model system for the study of DMD in that past two decades, it has not been adopted by the DMD community to the same extent as the *mdx* mouse and the GRMD dog. The number of studies using *C, elegans* is low, and a number of these studies include supporting experiments done in mammalian systems. While this is likely due to a number of reasons, an important factor is the apparent difference between vertebrate and invertebrate muscle. Fundamental differences in the structure and function of muscle between the two species certainly place some limitations on the use of *C. elegans* to model human muscular dystrophy. However, performing a phylogenetic analysis on the dystrophin protein, its individual functional domains, and its surrounding binding partners further emphasizes that dystrophin plays a fundamental role in muscle biology that is maintained between vertebrates and invertebrates. The functional similarities between the human and *C. elegans* version of dystrophin and the DAPC are reflected on both the sequence and protein level, and characterizing these similarities will ideally result in the adoption of *C. elegans* as a mainstream model system for the condition, which will in turn improve the rate of discovery and diversity of information available on the initiation and progression of DMD.

Signaling pathways altered in early and late stages of DMD progression

We have found that there are signaling consequences that occur in dystrophin deficient muscle that are in fact independent from both the inflammatory response and muscle regeneration related processes. Our results indicate that dystrophin plays an essential signaling role in the muscle that begins early in development, and is involved in nearly all basic functions of the body muscle.

Many of the outstanding questions in the DMD field relate to the ambiguity surrounding the initiation of the disease at the cellular level. The downstream effects of dystrophin deficiencies are clear, but the order in which these phenotypes arise is still up for debate. Some of the earliest phenotypes of DMD actually precede the incidence of contraction-induced lesions at the sarcolemma [79,212,213]. The use of *C. elegans* has allowed for the characterization of the signaling events occurring early in development in the absence of inflammation and regeneration. This allows the community to move closer to a true definition of the very first changes that occur in dystrophic muscle, and the order in which these changes arise. To our knowledge, this is the first instance in which transcriptomes for dystrophic muscle have been isolated from *C. elegans* muscle tissue that is both stage specific and free from contaminating tissue types, inflammation, and muscle regeneration.

There are a number of interesting trends identified in our results that have not yet been explored and would provide essential information about the timeline of DMD initiation and progression. Performing a gene ontology analysis to identify the genes that were differentially regulated between the two dystrophin-deficient transcriptomes *(dys-1(eg33)* and *(dys-1(cx18))* uncovered a number of intriguing pathways that were not explored within the context of this study. Specifically, pathways like MAPK, Wnt, and endocytosis related pathways were significantly altered in the *dys-1(cx18)* transcriptomes, while remaining unaltered in the *dys1(eg33)* transcriptomes. While all of these processes have been implicated in some manner in conditions related to muscle damage, cell regeneration, and membrane repair, their role in Duchenne muscular dystrophy is not explicitly clear. Furthermore, the fact that these pathways appear dysregulated in an animal model that lacks muscle regeneration is surprising, and raises a number of questions about the direct relationship

between the dystrophin protein itself and these cellular processes. It is certainly possible that the effects of dystrophin deficiencies on assembly of transmembrane proteins extends beyond the components of the DGC. Typically, the Wnt signaling pathways is associated with wound healing and fibrogenesis in the context of conditions like muscular dystrophy [195,214]. Furthermore, the treatment of DMD using the drug Celecoxib has shown to increase utrophin expression through the activation of the MAPK pathway [215]. Although the research relating these pathways back to their involvement in DMD is still sparse, their widespread involvement in cellular division, commitment of stem cell fates, and activation of repair pathways makes the Wnt, MAPK, and endocytosis related pathways make them likely candidates in the search for therapeutic targets for the treatment of DMD. The fact that these pathways are significantly altered in *C. elegans* further suggests that their involvement is not limited to a response to muscle injury but may be directly interacting with the dystrophin protein in some manner. Furthermore, the fact that these pathways are differentially altered between the two *dys-1* transcriptomes suggests that it is possible that these pathways could somehow be affected by the presence or absence of certain components within the C-terminal binding domain of the dystrophin protein, in nematodes and potentially in mammals as well.

There are also a number of trends within these *dys-1* transcriptomes that have been identified but have not yet been explored in detail within the context of this work. Previous studies using transcriptome data from human dystrophic muscle have focused on the fact that individual changes in gene expression to not necessarily provide information on the genetic partners of these differentially regulated genes, and information about interconnected genes would show in greater detail which pathways are most affected by dystrophin's absence [216]. One particular study has used differential co-expression analysis

(DCEA) to address this exact issue, and using microarray gene expression data, they have uncovered in greater detail the relationship between certain transcription factors and their targets as they are implicated in DMD progression [216]. It is certainly feasible to use data like this to determine whether or not any of the nematode orthologs of these identified targets are also dysregulated in *dys-1* transcriptomes, and whether or not these same signaling pathways are affected in nematode muscle. This would ideally serve as even further confirmation that invertebrate muscle is a powerful tool to uncover relevant changes in signaling related to the human version of DMD.

It is true that like several other model systems for DMD, phenotypes in dystrophin deficient *C. elegans* are mild compared to the human version of the condition. An approach that is gaining popularity in other muscle-focused studies performed in *C. elegans* is to alter the stress conditions under which populations are cultured in order to exacerbate the mechanical stress placed on the body muscle, so that it more closely reflects the nature of mechanical stress placed on human muscle [191,217]. It would be interesting to repeat this study after culturing dystrophin nematode strains under increased stress conditions like burrowing or swimming, to then evaluate changes in gene expression that are more representative of those associated with true paralysis in human DMD muscle. Another outstanding question regarding the use of *C. elegans* as a model system for the study of DMD refers to the most notable symptom associated with dystrophin deficiencies: aberrant head bending. Despite the fact that this is the characteristic symptom of all *dys-1* mutants and is used as a screening method for binding partners of DYS-1, like DYB-1, the underlying cause of this phenotype remains unknown. It has not yet been determined if this is a behavioral phenotype, if it is the result of some underling structural deficiency, or even why the head,

rather than some other portion of the organism's anatomy exhibits this symptom. It is interesting to consider that the point at which the head bends during movement corresponds closely to the location of the nerve ring. During early stages of *C. elegans* development, the pharynx grows through a ring of neurons at the base of the head known as the nerve ring, which can be considered to be the nematode version of the mammalian brain [218]. In humans, tissue specific isoforms of dystrophin are expressed in the neurons and the brain, and it would be interesting to further explore whether or not there is a connection between the head bending phenotype observed in *dys-1* mutants, and the proximity of the bend in the head to the location of the nerve ring. Experiments clarifying this connection could also provide more insight about which *dys-1* phenotypes are behavioral, rather than the result of impaired muscle function.

The consistent presence of *dys-1* transcripts in the *dys-1(cx18)* and *dys-1(eg33)* strains also raises a number of questions about the characterization of these two strains as truly dystrophin deficient. It is possible that truncated versions of this protein are translated, and retain partial function. This could potentially explain the phenotypic differences between the two strains, which possess mutations in two difference functional domains of the dystrophin protein. It is possibly to address these outstanding questions by establishing a novel dystrophic *C. elegans* strain that has had the *dys-1* gene deleted from the genome, in order to generate a true knockout strain. Performing muscle-specific transcriptomic studies on this hypothetical strain could resolve any outstanding questions regarding the potential hypomorphic function of truncated DYS-1 protein in these two strains.

Signaling changes in dystrophic muscle may be independent drivers of disease progression

We originally hypothesized that the changes in gene expression identified by our PAT-Seq experiments would identify signaling events that were not necessarily the consequence of long-term dystrophin deficiency, but were instead contributing to disease progression. The validation of our sequencing results holds translational value for a number of reasons. Despite a lack of inflammation, regeneration, or fibrosis in the muscle, dystrophin deficient *C. elegans* strains are not asymptomatic, and the changes in gene expression identified in this study reflect some of those seen in human and *mdx* mouse muscle.

As previously mentioned, *C. elegans* do not possess a human satellite cell equivalent, and as a result do not have muscle regeneration occurring in response to any form of muscle injury. Despite this, we observe an upregulation of genes involved in the maintenance and repair of muscle in human and mouse. This further supports the hypothesis that dystrophin deficiencies alone can induce signaling cascades in the muscle that alter its physiology, even without muscle injury to trigger these signaling events. The upregulation of these genes may also help to partially explain the mild phenotype observed in *dys-1 C. elegans* strains. The upregulation of these muscle structure related genes may represent a compensatory mechanism that is activated in dystrophin's absence to stave off muscle damage. The worsening of paralysis in double mutant strains after knocking down these upregulated genes supports this notion and opens a number of interesting questions regarding the exact mechanisms behind the upregulation of these genes in response to dystrophin absence. It would be interesting to systematically tag some of the most significantly upregulated genes in

our results to observe their expression at the protein level in both *dys-1* strains. While the phenotypes observed following the knockdown of some of these upregulated genes using RNAi suggests that these genes are functionally translated, ideally this upregulation should be confirmed at the protein level. Furthermore, it would be valuable to generate additional double knockout strains with null mutations in both *dys-1* and in significantly upregulated genes from our datasets that would confirm the need for compensatory upregulation of these genes in the absence of dystrophin.

The verification of the overexpression of some of our most significant hits in mammalian satellite cells from *mdx/utr*$^{-/-}$ mice provides encouraging evidence that *C. elegans* are a powerful tool for the study of DMD, and that our PAT-Seq results can potentially provide insight about the cell autonomous changes in gene expression occurring in human muscle as well. This can perhaps be used to identify additional therapeutic targets to alleviate symptoms of DMD.

We believe that our identification of splicing defects in the *dys-1(eg33)* genetic background are novel and may provide a new perspective on disease progression. However, more experiments need to be performed in order to first confirm these splicing defects, and then to define how dystrophin deficiencies can bring about splicing defects in the muscle.

Overall, the analysis of some of the outstanding trends in our PAT-Seq results has confirmed the biological significance of these altered signaling evens in dystrophin deficient *C. elegans* muscle, and has supported the hypothesis that these signaling events are not necessarily consequences of muscle damage in late stage DMD progression, but are in fact independent drivers of early disease progression.

REFERENCES

1 Hoffman, E. P., Brown, R. H. & Kunkel, L. M. Dystrophin: The protein product of the duchenne muscular dystrophy locus. *Cell* **51,** 919–928 (1987).

2 Yiu, E. M. & Kornberg, A. J. Duchenne muscular dystrophy. *J. Paediatr. Child Health* **51,** 759–764 (2015).

3 Landfeldt, E. *et al.* Life expectancy at birth in Duchenne muscular dystrophy: a systematic review and meta-analysis. *Eur. J. Epidemiol.* (2020). doi:10.1007/s10654-020-00613-8

4 Ervasti, J. M. & Campbell, K. P. Membrane organization of the dystrophin-glycoprotein complex. *Cell* **66,** 1121–1131 (1991).

5 Ohlendieck, K., Ervasti, J. M., Snook, J. B. & Campbell, K. P. Dystrophin-glycoprotein complex is highly enriched in isolated skeletal muscle sarcolemma. *J. Cell Biol.* **112,** 135–148 (1991).

6 Yoshida, M. & Ozawa, E. Glycoprotein complex anchoring dystrophin to sarcolemma. *J. Biochem.* **108,** 748–752 (1990).

7 Allen, D. G., Whitehead, N. P. & Froehner, S. C. Absence of Dystrophin Disrupts Skeletal Muscle Signaling: Roles of Ca2+, Reactive Oxygen Species, and Nitric Oxide in the Development of Muscular Dystrophy. *Physiol. Rev.* **96,** 253–305 (2016).

8 Flanigan, K. M. Duchenne and becker muscular dystrophies. *Neurologic Clinics* **32,** 671–688 (2014).

9 Yucel, N., Chang, A. C., Day, J. W., Rosenthal, N. & Blau, H. M. Humanizing the mdx mouse model of DMD: the long and the short of it. *npj Regen. Med.* **3,** 4 (2018).

10 Daoud, F. *et al.* Role of Mental Retardation-Associated Dystrophin-Gene Product Dp71 in Excitatory Synapse Organization, Synaptic Plasticity and Behavioral Functions. *PLoS One* **4,** e6574 (2009).

11 Rae, M. G. & O'Malley, D. Cognitive dysfunction in Duchenne muscular dystrophy: a possible role for neuromodulatory immune molecules. *J. Neurophysiol.* **116,** 1304–1315 (2016).

12 Anand, A. *et al.* Dystrophin induced cognitive impairment: Mechanisms, models and therapeutic strategies. *Ann. Neurosci.* **22,** 108–118 (2015).

13 Ricotti, V. *et al.* The NorthStar Ambulatory Assessment in Duchenne muscular dystrophy: Considerations for the design of clinical trials. *J. Neurol. Neurosurg. Psychiatry* **87,** 149–155 (2016).

14 Kang, P. B. Beyond the gowers sign: Measuring outcomes in duchenne muscular dystrophy. *Muscle and Nerve* **48,** 315–317 (2013).

15 Zatz, M. *et al.* Serum creatine-kinase (CK) and pyruvate-kinase (PK) activities in Duchenne (DMD) as compared with Becker (BMD) muscular dystrophy. *J. Neurol. Sci.* **102,** 190–196 (1991).

16 Fridén, J. & Lieber, R. L. Serum creatine kinase level is a poor predictor of muscle function after injury. *Scand. J. Med. Sci. Sport.* **11,** 126–127 (2001).

17 Flanigan, K. M. *et al.* Mutational spectrum of DMD mutations in dystrophinopathy patients: Application of modern diagnostic techniques to a large cohort. *Hum. Mutat.* **30,** 1657–1666 (2009).

18 Echigoya, Y., Lim, K. R. Q., Nakamura, A. & Yokota, T. Multiple exon skipping in the duchenne muscular dystrophy hot spots: Prospects and challenges. *Journal of Personalized Medicine* **8,** (2018).

19 Koenig, M. *et al.* The molecular basis for Duchenne versus Becker muscular dystrophy: correlation of severity with type of deletion. *Am. J. Hum. Genet.* **45,** 498–506 (1989).

20 Ginjaar, I. B. *et al.* Dystrophin nonsense mutation induces different levels of exon 29 skipping and leads to variable phenotypes within one BMD Family. *Eur. J. Hum. Genet.* **8,** 793–796 (2000).

21 Wein, N., Alfano, L. & Flanigan, K. M. Genetics and Emerging Treatments for Duchenne and Becker Muscular Dystrophy. *Pediatric Clinics of North America* **62,** 723–742 (2015).

22 Flanigan, K. M. *et al.* Mutational spectrum of DMD mutations in dystrophinopathy patients: Application of modern diagnostic techniques to a large cohort. *Hum. Mutat.* **30,** 1657–1666 (2009).

23 Aartsma-Rus, A., Ginjaar, I. B. & Bushby, K. The importance of genetic diagnosis for Duchenne muscular dystrophy. *J. Med. Genet.* **53,** 145–151 (2016).

24 Griggs, R. C. *et al.* Efficacy and safety of deflazacort vs prednisone and placebo for Duchenne muscular dystrophy. *Neurology* **87,** 2123–2131 (2016).

25 Takeuchi, F. *et al.* Trends in steroid therapy for Duchenne muscular dystrophy in Japan. *Muscle Nerve* **54,** 673–680 (2016).

26 McDonald, C. M. *et al.* Long-term effects of glucocorticoids on function, quality of life, and survival in patients with Duchenne muscular dystrophy: a prospective cohort study. *Lancet* **391,** 451–461 (2018).

27 Tangsrud, S. E., Petersen, I. L., LØdrup Carlsen, K. C. & Carlsen, K. H. Lung function in children with Duchenne's muscular dystrophy. *Respir. Med.* **95,** 898–903 (2001).

28 Matsumura, T. Beta-blockers in Children with Duchenne Cardiomyopathy. *Rev. Recent Clin. Trials* **9,** 76–81 (2014).

29 Dittrich, S. *et al.* Effect and safety of treatment with ACE-inhibitor Enalapril and β-blocker metoprolol on the onset of left ventricular dysfunction in Duchenne muscular dystrophy - A randomized, double-blind, placebo-controlled trial. *Orphanet J. Rare Dis.* **14,** 105 (2019).

30 Zhang, Y. *et al.* Enhanced CRISPR-Cas9 correction of Duchenne muscular dystrophy in mice by a self-complementary AAV delivery system. *Sci. Adv.* **6,** eaay6812 (2020).

31 Hakim, C. H. *et al.* AAV CRISPR editing rescues cardiac and muscle function for 18 months in dystrophic mice. *JCI insight* **3,** (2018).

32 Xu, L., Lau, Y. S., Gao, Y., Li, H. & Han, R. Life-Long AAV-Mediated CRISPR Genome Editing in Dystrophic Heart Improves Cardiomyopathy without Causing Serious Lesions in mdx Mice. *Mol. Ther.* **27,** 1407–1414 (2019).

33 López, S. M. *et al.* Challenges associated with homologous directed repair using CRISPR-Cas9 and TALEN to edit the DMD genetic mutation in canine Duchenne muscular dystrophy. *PLoS One* **15,** (2020).

34 Jacinto, F. V., Link, W. & Ferreira, B. I. CRISPR/Cas9-mediated genome editing: From basic research to translational medicine. *J. Cell. Mol. Med.* jcmm.14916 (2020). doi:10.1111/jcmm.14916

35 Mendell, J. R. *et al.* Dystrophin immunity in Duchenne's muscular dystrophy. *N. Engl. J. Med.* **363,** 1429–1437 (2010).

36 Lim, K. R. Q., Maruyama, R. & Yokota, T. Eteplirsen in the treatment of Duchenne muscular dystrophy. *Drug Design, Development and Therapy* **11,** 533–545 (2017).

37 Syed, Y. Y. Eteplirsen: First Global Approval. *Drugs* **76,** 1699–1704 (2016).

38 Eteplirsen (Exondys 51) for duchenne muscular dystrophy. *Medical Letter on Drugs and Therapeutics* **58,** 145–146 (2016).

39 Aartsma-Rus, A. & Krieg, A. M. FDA Approves Eteplirsen for Duchenne Muscular Dystrophy: The Next Chapter in the Eteplirsen Saga. *Nucleic Acid Therapeutics* **27,** 1–3 (2017).

40 Boehler, J. F. *et al.* Membrane recruitment of nNOSμ in microdystrophin gene transfer to enhance durability. *Neuromuscular Disorders* **29,** 735–741 (2019).

41 Romero, N. B. *et al.* Phase I study of dystrophin plasmid-based gene therapy in Duchenne/Becker muscular dystrophy. *Hum. Gene Ther.* **15,** 1065–1076 (2004).

42 Mendell, J. R. Safety Study of Mini-dystrophin Gene to Treat Duchenne Muscular Dystrophy - Full Text View - ClinicalTrials.gov. (2006). Available at: https://clinicaltrials.gov/ct2/show/NCT00428935. (Accessed: 12th March 2020)

43 Okada, T. & Takeda, S. Current challenges and future Directions in recombinant AAV-mediated gene therapy of duchenne muscular dystrophy. *Pharmaceuticals* **6,** 813–836 (2013).

44 Mandel, J. L. The gene and its product. *Nature* **339,** 584–586 (1989).

45 Koenig, M. *et al.* Complete cloning of the duchenne muscular dystrophy (DMD) cDNA and preliminary genomic organization of the DMD gene in normal and affected individuals. *Cell* **50,** 509–517 (1987).

46 Fealey, M. E. *et al.* Dynamics of Dystrophin's Actin-Binding Domain. *Biophys. J.* **115,** 445–454 (2018).

47 Stone, M. R. *et al.* Absence of keratin 19 in mice causes skeletal myopathy with mitochondrial and sarcolemmal reorganization. *J. Cell Sci.* **120,** 3999–4008 (2007).

48 Le, S. *et al.* Dystrophin As a Molecular Shock Absorber. *ACS Nano* **12,** 12140–12148 (2018).

49 Amann, K. J., Renley, B. A. & Ervasti, J. M. A cluster of basic repeats in the dystrophin rod domain binds F-actin through an electrostatic interaction. *J. Biol. Chem.* **273,** 28419–28423 (1998).

50 Rybakova, I. N., Amann, K. J. & Ervasti, J. M. A new model for the interaction of dystrophin with F-actin. *J. Cell Biol.* **135,** 661–672 (1996).

51 Prins, K. W. *et al.* Dystrophin is a microtubule-associated protein. *J. Cell Biol.* **186,** 363–369 (2009).

52 Belanto, J. J. *et al.* Microtubule binding distinguishes dystrophin from utrophin. *Proc. Natl. Acad. Sci. U. S. A.* **111,** 5723–5728 (2014).

53 Bork, P. & Sudol, M. The WW domain: a signalling site in dystrophin? *Trends Biochem. Sci.* **19,** 531–533 (1994).

54 Ponting, C. P., Blake, D. J., Davies, K. E., Kendrick-Jones, J. & Winder, S. J. ZZ and TAZ: new putative zinc fingers in dystrophin and other proteins. *Trends Biochem. Sci.* **21,** 11–13 (1996).

55 Koenig, M., Monaco, A. P. & Kunkel, L. M. The complete sequence of dystrophin predicts a rod-shaped cytoskeletal protein. *Cell* **53,** 219–228 (1988).

56 Wagner, K. R., Cohen, J. B. & Huganir, R. L. The 87K postsynaptic membrane protein from Torpedo is a protein-tyrosine kinase substrate homologous to dystrophin. *Neuron* **10,** 511–22 (1993).

57 Kameya, S. *et al.* α1-Syntrophin gene disruption results in the absence of neuronal-type nitric-oxide synthase at the sarcolemma but does not induce muscle degeneration. *J. Biol. Chem.* **274,** 2193–2200 (1999).

58 Ramaswamy, K. S. *et al.* Lateral transmission of force is impaired in skeletal muscles of dystrophic mice and very old rats. *J. Physiol.* **589,** 1195–1208 (2011).

59 Peter, A. K., Cheng, H., Ross, R. S., Knowlton, K. U. & Chen, J. The costamere bridges sarcomeres to the sarcolemma in striated muscle. *Prog. Pediatr. Cardiol.* **31,** 83–88 (2011).

60 Church, J. E. *et al.* Alterations in Notch signalling in skeletal muscles from mdx and dko dystrophic mice and patients with Duchenne muscular dystrophy. *Exp. Physiol.* **99,** 675–687 (2014).

61 Vieira, N. M. *et al.* Jagged 1 Rescues the Duchenne Muscular Dystrophy Phenotype. *Cell* **163,** 1204–1213 (2015).

62 Khairallah, R. J. *et al.* Microtubules underlie dysfunction in duchenne muscular dystrophy. *Sci. Signal.* **5,** ra56 (2012).

63 Bansal, D. *et al.* Defective membrane repair in dysferlin-deficient muscular dystrophy. *Nature* **423,** 168–172 (2003).

64 Morikawa, Y. *et al.* Actin cytoskeletal remodeling with protrusion formation is essential for heart regeneration in Hippo-deficient mice. *Sci. Signal.* **8,** (2015).

65 Alexander, M. S. *et al.* MicroRNA-199a is induced in dystrophic muscle and affects WNT signaling, cell proliferation, and myogenic differentiation. *Cell Death Differ.* **20,** 1194–1208 (2013).

66 Fuenzalida, M. *et al.* Wnt signaling pathway improves central inhibitory synaptic transmission in a mouse model of Duchenne muscular dystrophy. *Neurobiol. Dis.* **86,** 109–120 (2016).

67 Culligan, K., Banville, N., Dowling, P. & Ohlendieck, K. Drastic reduction of calsequestrin-like proteins and impaired calcium binding in dystrophic mdx muscle. *J. Appl. Physiol.* **92,** 435–445 (2002).

68 Ibraghimov-Beskrovnaya, O. *et al.* Primary structure of dystrophin-associated glycoproteins linking dystrophin to the extracellular matrix. *Nature* **355,** 696–702 (1992).

69 Chang, W. J. *et al.* Neuronal nitric oxide synthase and dystrophin-deficient muscular dystrophy. *Proc. Natl. Acad. Sci. U. S. A.* **93,** 9142–9147 (1996).

70 Ohlendieck, K. & Campbell, K. P. Dystrophin-associated proteins are greatly reduced in skeletal muscle from mdx mice. *J. Cell Biol.* **115,** 1685–1694 (1991).

71 Langenbach, K. J. & Rando, T. A. Inhibition of dystroglycan binding to laminin disrupts the PI3K/AKT pathway and survival signaling in muscle cells. *Muscle and Nerve* **26,** 644–653 (2002).

72 Takeda, S. [Gene therapy for muscular dystrophy]. *No To Hattatsu.* **36,** 117–23 (2004).

73 Gardner, K. L., Kearney, J. A., Edwards, J. D. & Rafael-Fortney, J. A. Restoration of all dystrophin protein interactions by functional domains in trans does not rescue dystrophy. *Gene Ther.* **13,** 744–751 (2006).

74 Madhavan, R., Massom, L. R. & Jarrett, H. W. Calmodulin specifically binds three proteins of the dystrophin-glycoprotein complex. *Biochem. Biophys. Res. Commun.* **185,** 753–9 (1992).

75 Madhavan, R. & Jarrett, H. W. Phosphorylation of dystrophin and alpha-syntrophin by Ca(2+)-calmodulin dependent protein kinase II. *Biochim. Biophys. Acta* **1434,** 260–74 (1999).

76 Newbell, B. J., Anderson, J. T. & Jarrett, H. W. Ca2+-calmodulin binding to mouse α1 syntrophin: Syntrophin is also a Ca2+-binding protein. *Biochemistry* **36,** 1295–1305 (1997).

77 Luise, M. *et al.* Dystrophin is phosphorylated by endogenous protein kinases. *Biochem. J.* **293,** 243–247 (1993).

78 Madhavan, R. & Jarrett, H. W. Calmodulin-Activated Phosphorylation of Dystrophin. *Biochemistry* **33,** 5797–5804 (1994).

79 Niebroj-Dobosz, I., Kornguth, S., Schutta, H. S. & Siegel, F. L. Elevated calmodulin levels and reduced calmodulin-stimulated calcium-ATPase in Duchenne progressive muscular dystrophy. *Neurology* **39,** 1610–1614 (1989).

80 Yang, B. *et al.* SH3 domain-mediated interaction of dystroglycan and Grb2. *J. Biol. Chem.* **270,** 11711–11714 (1995).

81 Oak, S. A., Russo, K., Petrucci, T. C. & Jarrett, H. W. Mouse α1-syntrophin binding to Grb2: Further evidence of a role for syntrophin in cell signaling. *Biochemistry* **40,** 11270–11278 (2001).

82 Oak, S. A., Zhou, Y. W. & Jarrett, H. W. Skeletal muscle signaling pathway through the dystrophin glycoprotein complex and Rac1. *J. Biol. Chem.* **278,** 39287–39295 (2003).

83 Ervasti, J. M., Ohlendieck, K., Kahl, S. D., Gaver, M. G. & Campbell, K. P. Deficiency of a glycoprotein component of the dystrophin complex in dystrophic muscle. *Nature* **345,** 315–319 (1990).

84 Cirak, S. *et al.* Restoration of the dystrophin-associated glycoprotein complex after exon skipping therapy in duchenne muscular dystrophy. *Mol. Ther.* **20,** 462–467 (2012).

85 Rando, T. A. The dystrophin-glycoprotein complex, cellular signaling, and the regulation of cell survival in the muscular dystrophies. *Muscle and Nerve* **24,** 1575–1594 (2001).

86 Prosser, B. L., Khairallah, R. J., Ziman, A. P., Ward, C. W. & Lederer, W. J. X-ROS signaling in the heart and skeletal muscle: Stretch-dependent local ROS regulates [Ca2+]i. *Journal of Molecular and Cellular Cardiology* **58,** 172–181 (2013).

87 Brenman, J. E., Chao, D. S., Xia, H., Aldape, K. & Bredt, D. S. Nitric Oxide Synthase Complexed with Dystrophin and Absent from Skeletal Muscle Sarcolemma in Duchenne Muscular Dystrophy. *Cell* **82,** 743–752 (1995).

88 Adams, M. E., Odom, G. L., Kim, M. J., Chamberlain, J. S. & Froehner, S. C. Syntrophin binds directly to multiple spectrin-like repeats in dystrophin and mediates binding of nNOS to repeats 16-17. *Hum. Mol. Genet.* **27,** 2978–2985 (2018).

89 Ito, N., Ruegg, U. T., Kudo, A., Miyagoe-Suzuki, Y. & Takeda, S. Activation of calcium signaling through Trpv1 by nNOS and peroxynitrite as a key trigger of skeletal muscle hypertrophy. *Nat. Med.* **19,** 101–106 (2013).

90 Moon, Y. *et al.* Nitric Oxide Regulates Skeletal Muscle Fatigue, Fiber Type, Microtubule Organization, and Mitochondrial ATP Synthesis Efficiency Through cGMP-Dependent Mechanisms. *Antioxidants Redox Signal.* **26,** 966–985 (2017).

91 Zhao, J. *et al.* Dystrophin R16/17 protein therapy restores sarcolemmal nNOS in trans and improves muscle perfusion and function. *Mol. Med.* **25,** 31 (2019).

92 Patel, A. *et al.* Dystrophin R16/17-syntrophin PDZ fusion protein restores sarcolemmal nNOSμ. *Skelet. Muscle* **8,** 36 (2018).

93 Yamashita, K. *et al.* The 8th and 9th tandem spectrin-like repeats of utrophin cooperatively form a functional unit to interact with polarity-regulating kinase PAR-1b. *Biochem. Biophys. Res. Commun.* **391,** 812–817 (2010).

94 Sancar, F. *et al.* The dystrophin-associated protein complex maintains muscle excitability by regulating Ca 2+-dependent K + (BK) channel localization. *J. Biol. Chem.* **286,** 33501–33510 (2011).

95 Marchand, E. *et al.* Improvement of calcium handling and changes in calcium-release properties after mini- or full-length dystrophin forced expression in cultured skeletal myotubes. *Exp. Cell Res.* **297,** 363–379 (2004).

96 Addinsall, A. B. *et al.* Treatment of Dystrophic mdx Mice with an ADAMTS-5 Specific Monoclonal Antibody Increases the Ex Vivo Strength of Isolated Fast Twitch Hindlimb Muscles. *Biomolecules* **10,** 416 (2020).

97 Onopiuk, M. *et al.* Mutation in dystrophin-encoding gene affects energy metabolism in mouse myoblasts. *Biochem. Biophys. Res. Commun.* **386,** 463–466 (2009).

98 Rosenberg, A. S. *et al.* Immune-mediated pathology in Duchenne muscular dystrophy. *Science Translational Medicine* **7,** 299rv4 (2015).

99 De Paepe, B. & De Bleecker, J. L. Cytokines and chemokines as regulators of skeletal muscle inflammation: presenting the case of Duchenne muscular dystrophy. *Mediators Inflamm.* **2013,** 540370 (2013).

100 De Paepe, B., Creus, K. K., Martin, J. J. & De Bleecker, J. L. Upregulation of chemokines and their receptors in duchenne muscular dystrophy: Potential for attenuation of myofiber necrosis. *Muscle and Nerve* **46,** 917–925 (2012).

101 Confalonieri, P. *et al.* Muscle inflammation and MHC class I up-regulation in muscular dystrophy with lack of dysferlin: an immunopathological study. *J. Neuroimmunol.* **142,** 130–6 (2003).

102 Evans, N. P., Misyak, S. A., Robertson, J. L., Bassaganya-Riera, J. & Grange, R. W. Immune-Mediated Mechanisms Potentially Regulate the Disease Time-Course of Duchenne Muscular Dystrophy and Provide Targets for Therapeutic Intervention. *PM and R* **1,** 755–768 (2009).

103 Villalta, S. A., Nguyen, H. X., Deng, B., Gotoh, T. & Tidball, J. G. Shifts in macrophage phenotypes and macrophage competition for arginine metabolism affect the severity of muscle pathology in muscular dystrophy. *Hum. Mol. Genet.* **18,** 482–96 (2009).

104 Mann, C. J. *et al.* Aberrant repair and fibrosis development in skeletal muscle. *Skeletal Muscle* **1,** 21 (2011).

105 Arnold, L. *et al.* Inflammatory monocytes recruited after skeletal muscle injury switch into antiinflammatory macrophages to support myogenesis. *J. Exp. Med.* **204,** 1057–1069 (2007).

106 Ardite, E. *et al.* PAI-1-regulated miR-21 defines a novel age-associated fibrogenic pathway in muscular dystrophy. *J. Cell Biol.* **196,** 163–175 (2012).

107 Vidal, B. *et al.* Fibrinogen drives dystrophic muscle fibrosis via a TGFβ/alternative macrophage activation pathway. *Genes Dev.* **22,** 1747–1752 (2008).

108 Wehling, M., Spencer, M. J. & Tidball, J. G. A nitric oxide synthase transgene ameliorates muscular dystrophy in mdx mice. *J. Cell Biol.* **155,** 123–131 (2001).

109 Spencer, M. J., Montecino-Rodriguez, E., Dorshkind, K. & Tidball, J. G. Helper (CD4+) and cytotoxic (CD8+) T cells promote the pathology of dystrophin-deficient muscle. *Clin. Immunol.* **98,** 235–243 (2001).

110 Bakay, M., Zhao, P., Chen, J. & Hoffman, E. P. A web-accessible complete transcriptome of normal human and DMD muscle.

111 Kastenschmidt, J. M., Avetyan, I. & Armando Villalta, S. Characterization of the inflammatory response in dystrophic muscle using flow cytometry. in *Methods in Molecular Biology* **1687,** 43–56 (Humana Press Inc., 2018).

112 L., D. P. *et al.* Increased muscle expression of interleukin-17 in Duchenne muscular dystrophy. *Neurology* **78,** 1309–1314 (2012).

113 Almeida, C. F., Martins, P. C. M. & Vainzof, M. Comparative transcriptome analysis of muscular dystrophy models Largemyd, DMDmdx /Largemyd and DMDmdx: What makes them different? *Eur. J. Hum. Genet.* **24,** 1301–1309 (2016).

114 Sicinski, P. *et al.* The molecular basis of muscular dystrophy in the mdx mouse: A point mutation. *Science (80-.).* **244,** 1578–1580 (1989).

115 Nguyen, T. M., Le, T. T., Blake, D. J., Davies, K. E. & Morris, G. E. Utrophin, the autosomal homologue of dystrophin, is widely-expressed and membrane-associated in cultured cell lines. *FEBS Lett.* **313,** 19–22 (1992).

116 Khurana, T. S., Watkins, S. C. & Kunkel, L. M. The subcellular distribution of chromosome 6-encoded dystrophin-related protein in the brain. *J. Cell Biol.* **119,** 357–366 (1992).

117 Romero, N. B., Mezmezian, M. & Fidziańska, A. Main steps of skeletal muscle development in the human. Morphological analysis and ultrastructural characteristics of developing human muscle. in *Handbook of Clinical Neurology* **113,** 1299–1310 (Elsevier B.V., 2013).

118 Clerk, A., Morris, G. E., Dubowitz, V., Davies, K. E. & Sewry, C. A. Dystrophin-related protein, utrophin, in normal and dystrophic human fetal skeletal muscle. *Histochem. J.* **25,** 554–561 (1993).

119 Vainzof, M., Passos-Bueno, M. R., Nguyen Thi Man & Zatz, M. Absence of correlation between utrophin localization and quantity and the clinical severity in Duchenne/Becker dystrophies. *Am. J. Med. Genet.* **58,** 305–309 (1995).

120 Takemitsu, M. *et al.* Dystrophin-related protein in the fetal and denervated skeletal muscles of normal and mdx mice. *Biochem. Biophys. Res. Commun.* **180,** 1179–86 (1991).

121 Passaquin, A. C., Metzinger, L., Léger, J. J., Warter, J. -M & Poindron, P. Prednisolone enhances myogenesis and dystrophin-related protein in skeletal muscle cell cultures from mdx mouse. *J. Neurosci. Res.* **35,** 363–372 (1993).

122 Law, D. J., Allen, D. L. & Tidball, J. G. Talin, vinculin and DRP (utrophin) concentrations are increased at mdx myotendinous junctions following onset of necrosis. *J. Cell Sci.* **107,** 1477–1483 (1994).

123 Perkins, K. J. & Davies, K. E. Alternative utrophin mRNAs contribute to phenotypic differences between dystrophin-deficient mice and Duchenne muscular dystrophy. *FEBS Letters* **592,** 1856–1869 (2018).

124 Tinsley, J. M. *et al.* Amelioration of the dystrophic phenotype of mdx mice using a truncated utrophin transgene. *Nature* **384,** 349–353 (1996).

125 Deconinck, A. E. *et al.* Utrophin-dystrophin-deficient mice as a model for Duchenne muscular dystrophy. *Cell* **90,** 717–727 (1997).

126 *Breeding Strategies for Maintaining Colonies of Laboratory Mice A Jackson Laboratory Resource Manual Cover Photos*.

127 Kornegay, J. N. The golden retriever model of Duchenne muscular dystrophy. *Skeletal Muscle* **7,** 9 (2017).

128 Sharp, N. J. H. *et al.* An error in dystrophin mRNA processing in golden retriever muscular dystrophy, an animal homologue of Duchenne muscular dystrophy. *Genomics* **13,** 115–121 (1992).

129 Roberts, R. G. & Bobrow, M. Dystrophins in vertebrates and invertebrates. *Hum. Mol. Genet.* **7,** 589–95 (1998).

130 Bessou, C., Giugia, J.-B., Franks, C. J., Holden-Dye, L. & Ségalat, L. Mutations in the Caenorhabditis elegans dystrophin-like gene dys-1 lead to hyperactivity and suggest a link with cholinergic transmission. *Neurogenetics* **2,** 61–72 (1998).

131 Lecroisey, C. *et al.* DYC-1, a Protein Functionally Linked to Dystrophin in *Caenorhabditis elegans* Is Associated with the Dense Body, Where It Interacts with the Muscle LIM Domain Protein ZYX-1. *Mol. Biol. Cell* **19,** 785–796 (2008).

132 Ségalat, L. Dystrophin and functionally related proteins in the nematode Caenorhabditis elegans. *Neuromuscul. Disord.* **12,** S105–S109 (2002).

133 Mariol, M. C. *et al.* Muscular degeneration in the absence of dystrophin is a calcium-dependent process. *Curr. Biol.* **11,** 1691–4 (2001).

134 Brouilly, N. *et al.* Ultra-structural time-course study in the *C. elegans* model for Duchenne muscular dystrophy highlights a crucial role for sarcomere-anchoring structures and sarcolemma integrity in the earliest steps of the muscle degeneration process. *Hum. Mol. Genet.* **24,** 6428–6445 (2015).

135 Gieseler, K. Development, structure, and maintenance of C. elegans body wall muscle. *WormBook* **2017,** 1–59 (2017).

136 Bessou, C. *et al.* Mutations in the Caenorhabditis elegans dystrophin-like gene dys-1 lead to hyperactivity and suggest a link with cholinergic transmission. *Neurogenetics* **2,** 61–72 (1998).

137 Kim, H., Rogers, M. J., Richmond, J. E. & McIntire, S. L. SNF-6 is an acetylcholine transporter interacting with the dystrophin complex in Caenorhabditis elegans. *Nature* **430,** 891–896 (2004).

138 Hosono, R., Mitsui, Y., Sato, Y., Aizawa, S. & Miwa, J. Life span of the wild and mutant nematode Caenorhabditis elegans. Effects of Sex, Sterilization, and Temperature. *Exp. Gerontol.* **17,** 163–172 (1982).

139 Gaud, A. *et al.* Prednisone reduces muscle degeneration in dystrophin-deficient Caenorhabditis elegans. *Neuromuscul. Disord.* **14,** 365–370 (2004).

140 Pozzoli, U. *et al.* Comparative analysis of vertebrate dystrophin loci indicate intron gigantism as a common feature. *Genome Res.* **13,** 764–772 (2003).

141 Greener, M. J. & Roberts, R. G. Conservation of components of the dystrophin complex in Drosophila. *FEBS Lett.* **482,** 13–8 (2000).

142 Pilgram, G. S. K., Potikanond, S., Baines, R. A., Fradkin, L. G. & Noordermeer, J. N. The roles of the dystrophin-associated glycoprotein complex at the synapse. *Molecular Neurobiology* **41,** 1–21 (2010).

143 Adams, J. C. & Brancaccio, A. The evolution of the dystroglycan complex, a major mediator of muscle integrity. *Biol. Open* **4,** 1163–1179 (2015).

144 Johnson, R. P., Kang, S. H. & Kramer, J. M. C. elegans dystroglycan DGN-1 functions in epithelia and neurons, but not muscle, and independently of dystrophin. *Development* **133,** (2006).

145 Trzebiatowska, A., Topf, U., Sauder, U., Drabikowski, K. & Chiquet-Ehrismann, R. Caenorhabditis elegans teneurin, ten-1, is required for gonadal and pharyngeal basement membrane integrity and acts redundantly with integrin ina-1 and dystroglycan dgn-1. *Mol. Biol. Cell* **19,** 3898–908 (2008).

146 Johnson, R. P. & Kramer, J. M. C. elegans dystroglycan coordinates responsiveness of follower axons to dorsal/ventral and anterior/posterior guidance cues. *Dev. Neurobiol.* **72,** 1498–1515 (2012).

147 Johnson, R. P. & Kramer, J. M. Neural maintenance roles for the matrix receptor dystroglycan and the nuclear anchorage complex in caenorhabditis elegans. *Genetics* **190,** 1365–1377 (2012).

148 Deyst, K. A., Bowe, M. A., Leszyk, J. D. & Fallon, J. R. The α-dystroglycan-β-dystroglycan complex: Membrane organization and relationship to an agrin receptor. *J. Biol. Chem.* **270,** 25956–25959 (1995).

149 Nakamura, A. *et al.* Up-regulation of the brain and Purkinje-cell forms of dystrophin transcripts, in Becker muscular dystrophy. *Am. J. Hum. Genet.* **60,** 1555–8 (1997).

150 Hugnot, J. P. *et al.* Distal transcript of the dystrophin gene initiated from an alternative first exon and encoding a 75-kDa protein widely distributed in nonmuscle tissues. *Proc. Natl. Acad. Sci. U. S. A.* **89,** 7506–7510 (1992).

151 Doorenweerd, N. *et al.* Timing and localization of human dystrophin isoform expression provide insights into the cognitive phenotype of Duchenne muscular dystrophy. *Sci. Rep.* **7,** (2017).

152 Roberts, R. G. & Bohm, S. V. Expression of Members of the Dystrophin, Dystrobrevin, and Dystrotelin Superfamily. *Crit. Rev. Eukaryot. Gene Expr.* **19,** 89–108 (2009).

153 Lidov, H. G. W., Selig, S. & Kunkel, L. M. Dp140: A novel 140 kDa CNS transcript from the dystrophin locus. *Hum. Mol. Genet.* **4,** 329–335 (1995).

154 Byers, T. J., Lidov, H. G. W. & Kunkel, L. M. An alternative dystrophin transcript specific to peripheral nerve. *Nat. Genet.* **4,** 77–81 (1993).

155 Chelly, J. *et al.* Dystrophin gene transcribed from different promoters in neuronal and glial cells. *Nature* **344,** 64–65 (1990).

156 D'souza, V. N. *et al.* A novel dystrophin isoform is required for normal retinal electrophysiology. *Hum. Mol. Genet.* **4,** 837–842 (1995).

157 Zubrzycka-Gaarn, E. E. *et al.* The Duchenne muscular dystrophy gene product is localized in sarcolemma of human skeletal muscle. *Nature* **333,** 466–469 (1988).

158 Gawor, M. & Proszynski, T. J. The molecular cross talk of the dystrophin-glycoprotein complex. *Ann N Y Acad Sci* **1412,** 62–72 (2018).

159 Lai, Y. *et al.* Dystrophins carrying spectrin-like repeats 16 and 17 anchor nNOS to the sarcolemma and enhance exercise performance in a mouse model of muscular dystrophy. *J Clin Invest* **119,** 624–635 (2009).

160 Guilbaud, M. *et al.* miR-708-5p and miR-34c-5p are involved in nNOS regulation in dystrophic context. *Skelet Muscle* **8,** 15 (2018).

161 Perry, M. M. & Muntoni, F. Noncoding RNAs and Duchenne muscular dystrophy. *Epigenomics* **8,** 1527–1537 (2016).

162 Vita, G. L. *et al.* Hippo signaling pathway is altered in Duchenne muscular dystrophy. *PLoS One* **13,** e0205514 (2018).

163 Bridges, L. R. The association of cardiac muscle necrosis and inflammation with the degenerative and persistent myopathy of MDX mice. *J Neurol Sci* **72,** 147–157 (1986).

164 Whitehead, N. P., Yeung, E. W. & Allen, D. G. Muscle damage in mdx (dystrophic) mice: role of calcium and reactive oxygen species. *Clin Exp Pharmacol Physiol* **33,** 657–662 (2006).

165 Banks, G. B. & Chamberlain, J. S. The value of mammalian models for duchenne muscular dystrophy in developing therapeutic strategies. *Curr Top Dev Biol* **84,** 431–453 (2008).

166 Giacomotto, J. *et al.* Chemical genetics unveils a key role of mitochondrial dynamics, cytochrome c release and IP3R activity in muscular dystrophy. *Hum Mol Genet* **22,** 4562–4578 (2013).

167 Rybalka, E., Timpani, C. A., Cooke, M. B., Williams, A. D. & Hayes, A. Defects in mitochondrial ATP synthesis in dystrophin-deficient mdx skeletal muscles may be caused by complex I insufficiency. *PLoS One* **9,** e115763 (2014).

168 Ryu, D. *et al.* NAD+ repletion improves muscle function in muscular dystrophy and counters global PARylation. *Sci Transl Med* **8,** 361ra139 (2016).

169 Vila, M. C. *et al.* Mitochondria mediate cell membrane repair and contribute to Duchenne muscular dystrophy. *Cell Death Differ* **24,** 330–342 (2017).

170 Hewitt, J. E. *et al.* Muscle strength deficiency and mitochondrial dysfunction in a muscular dystrophy model of Caenorhabditis elegans and its functional response to drugs. *Dis Model Mech* **11,** (2018).

171 Timpani, C. A., Hayes, A. & Rybalka, E. Revisiting the dystrophin-ATP connection: How half a century of research still implicates mitochondrial dysfunction in Duchenne Muscular Dystrophy aetiology. *Med. Hypotheses* **85,** 1021–1033 (2015).

172 Gieseler, K., Bessou, C. & Segalat, L. Dystrobrevin- and dystrophin-like mutants display similar phenotypes in the nematode Caenorhabditis elegans. *Neurogenetics* **2,** 87–90 (1999).

173 Grisoni, K. *et al.* The stn-1 syntrophin gene of C.elegans is functionally related to dystrophin and dystrobrevin. *J Mol Biol* **332,** 1037–1046 (2003).

174 Grisoni, K., Martin, E., Gieseler, K., Mariol, M. C. & Segalat, L. Genetic evidence for a dystrophin-glycoprotein complex (DGC) in Caenorhabditis elegans. *Gene* **294,** 77–86 (2002).

175 Oh, K. H. & Kim, H. Reduced IGF signaling prevents muscle cell death in a Caenorhabditis elegans model of muscular dystrophy. *Proc. Natl. Acad. Sci.* **110,** 19024–19029 (2013).

176 Hammarlund, M., Hobert, O., Miller 3rd, D. M. & Sestan, N. The CeNGEN Project: The Complete Gene Expression Map of an Entire Nervous System. *Neuron* **99,** 430–433 (2018).

177 Beron, C. *et al.* The burrowing behavior of the nematode Caenorhabditis elegans: a new assay for the study of neuromuscular disorders. *Genes. Brain. Behav.* **14,** 357–68 (2015).

178 Oh, K. H. & Kim, H. Reduced IGF signaling prevents muscle cell death in a Caenorhabditis elegans model of muscular dystrophy. *Proc. Natl. Acad. Sci. U. S. A.* **110,** 19024–9 (2013).

179 Marsh, E. K. & May, R. C. Caenorhabditis elegans, a model organism for investigating immunity. *Appl Env. Microbiol* **78,** 2075–2081 (2012).

180 Roy, P. J., Stuart, J. M., Lund, J. & Kim, S. K. Chromosomal clustering of muscle-expressed genes in Caenorhabditis elegans. *Nature* **418,** 975–979 (2002).

181 Blazie, S. M. *et al.* Comparative RNA-Seq analysis reveals pervasive tissue-specific alternative polyadenylation in Caenorhabditis elegans intestine and muscles. *BMC Biol* **13,** 4 (2015).

182 Blazie, S. M. *et al.* Alternative Polyadenylation Directs Tissue-Specific miRNA Targeting in Caenorhabditis elegans Somatic Tissues. *Genetics* **206,** 757–774 (2017).

183 Khraiwesh, B. & Salehi-Ashtiani, K. Alternative Poly(A) Tails Meet miRNA Targeting in Caenorhabditis elegans. *Genetics* **206,** 755–756 (2017).

184 Yang, Z., Edenberg, H. J. & Davis, R. L. Isolation of mRNA from specific tissues of Drosophila by mRNA tagging. *Nucleic Acids Res* **33,** e148 (2005).

185 Lemay, J. F., Lemieux, C., St-Andre, O. & Bachand, F. Crossing the borders: poly(A)-binding proteins working on both sides of the fence. *RNA Biol* **7,** 291–295 (2010).

186 Frokjaer-Jensen, C. Transposon-Assisted Genetic Engineering with Mos1-Mediated Single-Copy Insertion (MosSCI). *Methods Mol Biol* **1327,** 49–58 (2015).

187 Kim, W., Underwood, R. S., Greenwald, I. & Shaye, D. D. OrthoList 2: A New Comparative Genomic Analysis of Human and Caenorhabditis elegans Genes. *Genetics* **210,** 445–461 (2018).

188 Shen, Q. *et al.* Adenine nucleotide translocator cooperates with core cell death machinery to promote apoptosis in Caenorhabditis elegans. *Mol Cell Biol* **29,** 3881–3893 (2009).

189 Farina, F. *et al.* Differential expression pattern of the four mitochondrial adenine nucleotide transporter ant genes and their roles during the development of Caenorhabditis elegans. *Dev Dyn* **237,** 1668–1681 (2008).

190 Benedetti, C., Haynes, C. M., Yang, Y., Harding, H. P. & Ron, D. Ubiquitin-like protein 5 positively regulates chaperone gene expression in the mitochondrial unfolded protein response. *Genetics* **174,** 229–239 (2006).

191 Hughes, K. J. *et al.* Physical exertion exacerbates decline in the musculature of an animal model of Duchenne muscular dystrophy. *Proc Natl Acad Sci U S A* **116,** 3508–3517 (2019).

192 Benian, G. M., Kiff, J. E., Neckelmann, N., Moerman, D. G. & Waterston, R. H. Sequence of an unusually large protein implicated in regulation of myosin activity in C. elegans. *Nature* **342,** 45–50 (1989).

193 Wang, E. T. *et al.* Transcriptome alterations in myotonic dystrophy skeletal muscle and heart. *Hum Mol Genet* **28,** 1312–1321 (2019).

194 Kotagama, K., Schorr, A. L., Steber, H. S. & Mangone, M. ALG-1 Influences Accurate mRNA Splicing Patterns in the Caenorhabditis elegans Intestine and Body Muscle Tissues by Modulating Splicing Factor Activities. *Genetics* **212,** 931–951 (2019).

195 Girardi, F. & Le Grand, F. Wnt Signaling in Skeletal Muscle Development and Regeneration. *Prog Mol Biol Transl Sci* **153,** 157–179 (2018).

196 Gieseler, K., Grisoni, K. & Segalat, L. Genetic suppression of phenotypes arising from mutations in dystrophin-related genes in Caenorhabditis elegans. *Curr Biol* **10,** 1092–1097 (2000).

197 Harfe, B. D., Branda, C. S., Krause, M., Stern, M. J. & Fire, A. MyoD and the specification of muscle and non-muscle fates during postembryonic development of the C. elegans mesoderm. *Development* **125,** 2479–2488 (1998).

198 Tkatchenko, A. V, Le Cam, G., Leger, J. J. & Dechesne, C. A. Large-scale analysis of differential gene expression in the hindlimb muscles and diaphragm of mdx mouse. *Biochim Biophys Acta* **1500,** 17–30 (2000).

199 Sutphin, G. L. & Kaeberlein, M. Measuring Caenorhabditis elegans life span on solid media. *J Vis Exp* (2009). doi:10.3791/1152

200 Porter, J. D. *et al.* Temporal gene expression profiling of dystrophin-deficient (mdx) mouse diaphragm identifies conserved and muscle group-specific mechanisms in the pathogenesis of muscular dystrophy. *Hum Mol Genet* **13,** 257–269 (2004).

201 Cole, M. A. *et al.* A quantitative study of bioenergetics in skeletal muscle lacking utrophin and dystrophin. *Neuromuscul Disord* **12,** 247–257 (2002).

202 Even, P. C., Decrouy, A. & Chinet, A. Defective regulation of energy metabolism in mdx-mouse skeletal muscles. *Biochem J* **304 (Pt 2,** 649–654 (1994).

203 Kuznetsov, A. V *et al.* Impaired mitochondrial oxidative phosphorylation in skeletal muscle of the dystrophin-deficient mdx mouse. *Mol Cell Biochem* **183,** 87–96 (1998).

204 Passaquin, A. C. *et al.* Creatine supplementation reduces skeletal muscle degeneration and enhances mitochondrial function in mdx mice. *Neuromuscul Disord* **12,** 174–182 (2002).

205 Bloss, T. A., Witze, E. S. & Rothman, J. H. Suppression of CED-3-independent apoptosis by mitochondrial betaNAC in Caenorhabditis elegans. *Nature* **424,** 1066–1071 (2003).

206 Li, H. *et al.* The Sequence Alignment/Map format and SAMtools. *Bioinformatics* **25,** 2078–2079 (2009).

207 Trapnell, C. *et al.* Transcript assembly and quantification by RNA-Seq reveals unannotated transcripts and isoform switching during cell differentiation. *Nat Biotechnol* **28,** 511–515 (2010).

208 Park, H. H., Jung, Y. & Lee, S. V. Survival assays using Caenorhabditis elegans. *Mol Cells* **40,** 90–99 (2017).

209 Fraser, A. G. *et al.* Functional genomic analysis of C. elegans chromosome I by systematic RNA interference. *Nature* **408,** 325–330 (2000).

210 Stiernagle, T. Maintenance of C. elegans. *WormBook* 1–11 (2006). doi:10.1895/wormbook.1.101.1

211 Kamath, R. S. & Ahringer, J. Genome-wide RNAi screening in Caenorhabditis elegans. *Methods* **30,** 313–321 (2003).

212 Iwańczak, F., Stawarski, A., Potyrała, M., Siedlecka-Dawidko, J. & Agrawal, G. S. Early symptoms of Duchenne muscular dystrophy--description of cases of an 18-month-old and an 8-year-old patient. *Med. Sci. Monit.* **6,** 592–5

213 Lozanoska-Ochser, B. *et al.* Targeting early PKCθ-dependent T-cell infiltration of dystrophic muscle reduces disease severity in a mouse model of muscular dystrophy. *J. Pathol.* **244,** 323–333 (2018).

214 Liu, F. *et al.* Activation of the wnt/β-catenin signaling pathway in polymyositis, dermatomyositis and duchenne muscular dystrophy. *J. Clin. Neurol.* **12,** 351–360 (2016).

215 Péladeau, C., Adam, N. J. & Jasmin, B. J. Celecoxib treatment improves muscle function in mdx mice and increases utrophin A expression. *FASEB J.* **32,** 5090–5103 (2018).

216 Tian, L. *et al.* Unveiling transcription factor regulation and differential co-expression genes in Duchenne muscular dystrophy. *Diagn. Pathol.* **9,** 210 (2014).

217 Beron, C. *et al.* The burrowing behavior of the nematode *Caenorhabditis elegans* : a new assay for the study of neuromuscular disorders. *Genes, Brain Behav.* **14,** 357–368 (2015).

218 Altun, Z.F. 2017. Nervous system in the embryo, development of the nerve ring. In *WormAtlas*. doi:10.3908/wormatlas.4.2)